

Development of Environment-Responsive Hydrogels for the Delivery of Therapeutic Agents

by

Junbin Shi

A Thesis submitted to the Faculty of Graduate Studies of
The University of Manitoba
in partial fulfilment of the requirements of the degree of

MASTER OF SCIENCE

Department of Textile Sciences
University of Manitoba
Winnipeg

Copyright © 2012 by Junbin Shi

Contents

Abstract	I
Acknowledgments.....	II
List of Tables	III
List of Figures	IV
1 Introduction.....	1
1.1 Tissue Engineering Scaffolds.....	1
1.2 Anti-Cancer Drug Carriers	3
2 Literature review	5
2.1 Background	5
2.1.1 Hydrogels in TE.....	5
2.1.2 Hydrogels in smart drug delivery	6
2.2 Preparation and characterization of Hydrogels	7
2.2.1 Materials for hydrogels	7
2.2.2 Formation of Cross-links	17
2.2.3 Properties and Characterization of hydrogels	20
2.3 Osteogenetic differentiation	29

2.4	Smart Drug Delivery by pH response	32
3	Materials and Methods.....	33
3.1	Materials.....	33
3.2	Synthesis.....	33
3.2.1	PAA crosslinker	33
3.2.2	Oxidized alginate (O-alg)	34
3.2.3	Succinated chitosan (S-chi).....	35
3.3	Preparation of hydrogels.....	35
3.3.1	Hydrogel for bone regeneration	35
3.3.2	Hydrogel for cancer therapy	36
3.4	Characterization of hydrogels	37
3.4.1	Fourier transform infrared (FTIR) spectroscopy	37
3.4.2	Swelling test.....	37
3.4.3	<i>In vitro</i> degradation of hydrogel	38
3.4.4	<i>In vivo</i> degradation of hydrogels.....	39
3.4.5	Morphology of hydrogel	40
3.4.6	Mechanical properties of hydrogels determined by texture analyzer	41
3.4.7	Mechanical property of OS and D-OS hydrogels	41
3.4.8	<i>In Vitro</i> drug release from D-OS	41

3.5	Biological experiments of hydrogels for bone regeneration	42
3.5.1	Cell culture.....	42
3.5.2	Cell growth on hydrogels.....	42
3.5.3	Cell Viability of hydrogels.....	43
3.5.4	Cell morphology investigation.....	44
3.5.5	Quantitative Real-time PCR analysis.....	44
3.5.6	Calcium deposits of cells cultured on hydrogels	45
3.6	Biological experiments of hydrogels for cancer therapy	46
3.6.1	Cell culture.....	46
3.6.2	<i>In Vitro</i> cytotoxicity of OS and D-OS	47
3.6.3	Cell morphology on OS and cellular uptake of DOX from D-OS.....	48
3.7	Statistical analysis	49
4	Result and discussion.....	49
4.1	Hydrogel for bone regeneration	49
4.1.1	Synthesis and characterization of PAA crosslinker and hydrogel	49
4.1.2	Swelling test.....	53
4.1.3	Degradation profile of hydrogels	55
4.1.4	Analysis of mechanical properties of hydrogels.....	67
4.1.5	Cell Viability.....	70

4.1.6	Cell Morphology on hydrogels.	79
4.1.7	Osteogenic differentiation of BMSCs.....	94
4.2	Hydrogel for cancer therapy.....	103
4.2.1	Chemical structure of polysaccharide derivatives and hydrogels.....	103
4.2.2	Morphology and structure of hydrogel	104
4.2.3	Rheological Properties of hydrogels.....	106
4.2.4	In Vitro DOX release from the D-OS hydrogel.....	108
4.2.5	Cell morphology and intercellular distribution of DOX.....	109
4.2.6	Cytotoxicity of OS and D-OS hydrogel.....	120
5	Conclusion	125
5.1	TE.....	125
5.2	Cancer therapy.....	126
6	Reference	126

Abstract

This thesis includes two parts related to hydrogels as therapeutically useful constructs: a biomimetic hydrogel carrying stem cells for bone regeneration and an acid-sensitive hydrogel carrying drugs for cancer therapy.

In tissue engineering, one of the biggest difficulties is the control of stem cell fate on scaffolds. A biodegradable and cell attachable cross-linker was synthesized by one-step Michael addition reaction, and was used to fabricate a novel hydrogel to control the stem cell fate. For anti-cancer therapy, releasing drug on tumor cells or organs while having low effects on health cells under physiological conditions is a critical requirement. Two nature polymers are modified to achieve loading anti-cancer drug while forming hydrogels which can selectively release the drug in tumor environment by acid-sensitive linkages.

Acknowledgments

I would like to appreciate my supervisors, Dr Wen Zhong and Dr Malcolm Xing, for their giving me the motivation to investigate on new biomaterials and their encouragement of independent thinking. I'd like to thank other members of my committee as well for helping me improving the research, and sparing time on attending my final defense.

I would also like to thank Dr.Cenkowski for his help on stiffness measurement performed at the Department of Biosystems Engineering.

Finally, I would like to thank the NSERC Discovery Grant and NSERC RTI Grant, Manitoba Children's Foundation and Manitoba Research Council for their financial support on this study.

List of Tables

Table 3.1 Formulations of hydrogels	36
Table 3.2 Sequences of primers for the RT-PCR.....	45

List of Figures

Figure 4.1 Schematic illustration of preparation of G1 hydrogel ; Disulfide group (blue ellipse) can be cleaved under reductive environment and then make the hydrogel degradable; Argmatine group (yellow pentagon) and carboxyl group (green quadrangle) can form RGD mimicking repeat units.	51
Figure 4.2 Synthesis and characterization of cell-adhesive and bio-reducible PAA crosslinker	51
Figure 4.3 ¹ H NMR spectrum of PAA crosslinker	52
Figure 4.4 FTIR spectrum of (a) Hydrogel G2-b and (b) hydrogel G1-b	53
Figure 4.5 Swelling ratio of hydrogels at different precursor solution concentrations; G2 hydrogels are served as control groups (containing no crosslinker) at same concentration. (n=3) “*” means p<0.05 vs the control group.....	54
Figure 4.6 Photographs of hydrogel G1'-b underwent degradation with 10 mM DTT over (a) 1 hr, (b) 2 days, (c) 5 days, (d) 10 days. (Scale bar is 3mm).....	58
Figure 4.7 Cryosection images of partially degraded hydrogels G1'-b underwent degradation over 10 days in (a) 0.1 mM DTT and (b) 10 mM DTT. Scale bars represent 200µm for both images	59

Figure 4.8 <i>In vitro</i> reductive degradation profile of G1-b (Dash line) and G1'-b (Solid lines) hydrogel incubated in 0.1 mM (triangles) and 10 mM (cubes) DTT (n=3).....	60
Figure 4.9 <i>In vivo</i> reductive degradation profile of G1-b and G1'-b hydrogel (n=6).....	61
Figure 4.10 H&E staining of fibrous tissue surrounding hydrogel G1-b after 7 days; scale bars represent 200 μm	62
Figure 4.11 H&E staining of fibrous tissue surrounding hydrogel G1-b after 14 days; scale bars represent 200 μm	63
Figure 4.12 H&E staining of fibrous tissue surrounding G1-b after 21 days; scale bars represent 200 μm	64
Figure 4.13 H&E staining of fibrous tissue surrounding hydrogel G'-1-b after 7 days; scale bars represent 200 μm	65
Figure 4.14 H&E staining of fibrous tissue surrounding hydrogel G1'-b after 14 days; scale bars represent 200 μm	66
Figure 4.15 H&E staining of fibrous tissue surrounding G1'-b after 21 days; scale bars represent 200 μm	67
Figure 4.16 Typical Force–distance curves of hydrogels at different precursor solution concentrations.	69
Figure 4.17 Stiffness of hydrogels at at different precursor solution concentrations; and hydrogels G2 were control group; (n=3)	70
Figure 4.18 Cell viability of POB on hydrogel after 2days culture based on MTT assay (absorbance is normalized to 1 for TCPs control sample); (n=6).....	72

Figure 4.19 Cell viability of POB on hydrogel after 7days culture based on MTT assay (absorbance is normalized to 1 for TCPs control sample); (n=6).....	73
Figure 4.20 Live/Dead assay of BMSCs cultured on hydrogel G1-a for 7days Green for live cells, Red for dead cells (scale bar corresponding to 100um)	74
Figure 4.21 Live/Dead assay of BMSCs cultured on hydrogel G1-a for 14days Green for live cells, Red for dead cells (scale bar corresponding to 100um)	75
Figure 4.22 Live/Dead assay of BMSCs cultured on hydrogel G1-a for 28days Green for live cells, Red for dead cells (scale bar corresponding to 100um)	76
Figure 4.23 Live/Dead assay of BMSCs cultured on hydrogel G1-b for 7days Green for live cells, Red for dead cells (scale bar corresponding to 100um)	77
Figure 4.24 Live/Dead assay of BMSCs cultured on hydrogel G1-b for 14days Green for live cells, Red for dead cells (scale bar corresponding to 100um)	78
Figure 4.25 Live/Dead assay of BMSCs cultured on hydrogel G1-b for 28days Green for live cells, Red for dead cells (scale bar corresponding to 100um)	79
Figure 4.26 Morphology of C2C12 cells on hydrogel G1-b for 1 day. Green is cytoskeleton, and red is cell nucleus for all immunostaining images unless otherwise noted.....	81
Figure 4.27 Morphology of C2C12 cells on hydrogel G2-b for 1 day	82
Figure 4.28 Morphology of C2C12 cells on TCPs for 1 day.....	83
Figure 4.29 Morphology of HDF-2 cells on hydrogel G1-b for 1 day	84
Figure 4.30 Morphology of HDF-2 cells on hydrogel G2-b for 1 day	85
Figure 4.31 Morphology of HDF-2 cells on hydrogel TCPs for 1 day.....	86

Figure 4.32 Morphology of POB cells on hydrogel G1-b for 1 day	87
Figure 4.33 Morphology of POB cells on hydrogel G2-b for 1 day	88
Figure 4.34 Morphology of POB cells on TCPs for 1 day	89
Figure 4.35 Morphology of BMSCs on G1-a for 1 day; scale bar is 50um.....	90
Figure 4.36 3D ingrowths of BMSCs in G1-a gel for 1 day; scale bar is 20um.....	90
Figure 4.37 Morphology of BMSCs on G1-a for 7 days; scale bar is 50um.	91
Figure 4.38 3D ingrowths of BMSCs in G1-a gel for 7 days; scale bar is 50um	91
Figure 4.39 Morphology of BMSCs on G1-b for 1 day; scale bar is 50um.....	92
Figure 4.40 3D ingrowths of BMSCs in G1-b gel for 1 day; scale bar is 20um.....	92
Figure 4.41 Morphology of BMSCs on G1-b for 7 days; scale bar is 50um.	93
Figure 4.42 Depth scanning of BMSCs in G1-b gel for 7 days; scale bar is 50um.....	93
Figure 4.43 BSP expression profiling of mouse BMSCs cultured on hydrogels G1 with different stiffness for different times (a, b,c corresponding to different stiffness respectively from soft, medium, to stiff). Data values are expressed as mean±SE (n=3). “*” means p<0.05 vs the TCPs group	97
Figure 4.44 OC expression profiling of mouse BMSCs cultured on hydrogels G1 with different stiffness for different times. Data values are expressed as mean±SE (n=3). “*” means p<0.05 vs the TCPs group	98
Figure 4.45 OPN expression profiling of mouse BMSCs cultured on hydrogels G1 with different stiffness for different times. Data values are expressed as mean±SE (n=3). “*” means p<0.05 vs the TCPs group	99

Figure 4.46 ALP expression profiling of mouse BMSCs cultured on hydrogels G1 with different stiffness for different times. Data values are expressed as mean±SE (n=3). “*” means p<0.05 vs the TCPs group	100
Figure 4.47 von Kossa staining of Pre-Osteoblast cultured on hydrogel G1-a for 4 weeks.	100
Figure 4.48 von Kossa staining of Pre-Osteoblast cultured on hydrogel G1-b for 4 weeks.	101
Figure 4.49 von Kossa staining of Pre-Osteoblast cultured on hydrogel G1-c for 4 weeks.	102
Figure 4.50 FTIR spectrum of (a) Alginate (b) O-alg (c) Chitosan (d) S-Chi (e) OS hydrogel (f) D-OS hydrogel	104
Figure 4.51 Morphology of OS and D-OS hydrogel. (a) Photographs of OS and D-OS hydrogels the scale bar in is 0.5 cm. (b) A SEM image shows the freeze-dried morphology of OS hydrogels and the scale bar is 50 um. (c) A CLSM image shows the DOX (Red) in D-OS hydrogels and the scale bar is 100 um. (d -f) Scheme illustration of chemical structure of (d) OS and (e) D-OS hydrogel and (f) drug release from the hydrogel main body; O-alg in blue line, S-chi in green line, acid-sensitive linker in gray dot, and DOX in red pentagon.	105
Figure 4.52 Zero-shear viscosities of hydrogels OS and D-OS; orange line is D-OS and blue line is OS	107
Figure 4.53 Storage/loss modulus of hydrogels OS and D-OS; orange dots are D-OS, and blue dots are OS	108

Figure 4.54 DOX release from D-OS hydrogel in PBS buffers at different pH values. 109

Figure 4.55 Confocal microscopy images of MCF-7 cultured on TCPs without D-OS hydrogels at pH 7.4 medium for 24 hrs. F-actin showing green color corresponding to cytoskeleton and blue color to Topro-3 stained nucleus; scale bar is 100 um..... 111

Figure 4.56 Confocal microscopy images of MCF-7 cultured on TCPs with D-OS hydrogels at pH 7.4 medium for 24 hrs. F-actin showing green color corresponding to cytoskeleton and blue color to Topro-3 stained nucleus; scale bar is 100 um..... 112

Figure 4.57 Confocal microscopy images of MCF-7 cultured on TCPs without D-OS hydrogels at pH 6.8 medium for 24 hrs. F-actin showing green color corresponding to cytoskeleton and blue color to Topro-3 stained nucleus; scale bar is 100 um..... 113

Figure 4.58 Confocal microscopy images of cytoskeleton of MCF-7 cultured on TCPs with D-OS hydrogels at pH 6.8 medium for 24 hrs; scale bar is 100 um. 114

Figure 4.59 Confocal microscopy images of nucleus of MCF-7 cultured on TCPs with D-OS hydrogels at pH 6.8 medium for 24 hrs; scale bar is 100 um. The color is changed by the software from red to blue to differentiate from the DOX red fluorescence. 115

Figure 4.60 Confocal microscopy images of DOX distribution when MCF-7 cultured on TCPs with D-OS hydrogels at pH 6.8 medium for 24 hrs; scale bar is 100 um. 116

Figure 4.61 The overlays images of nuclear and cytoskeleton of MCF-7 cultured on TCPs with D-OS hydrogels at pH 6.8 medium for 24 hrs; scale bar is 100 um. Green color corresponds to cytoskeleton and blue color to nucleus. 117

Figure 4.62 The overlays images of nuclear of MCF-7 cultured on TCPs with D-OS hydrogels at pH 6.8 medium for 24 hrs and DOX distribution in them; scale bar is 100

um. Blue color corresponds to nucleus, red color to DOX, and purple to DOX distribution area in nucleus.....	118
Figure 4.63 The overlays images of cytoskeleton, nuclear of MCF-7 cultured on TCPs with D-OS hydrogels at pH 6.8 medium for 24 hrs and intercellular distribution of DOX; scale bar is 100 um. Green color corresponds to cytoskeleton, blue to nucleus, red color to DOX, and purple to DOX distribution area in nucleus,.....	119
Figure 4.64 Cell viability at pH 7.4 culture environment for 24 hrs based on MTT assay (absorbance is normalized to 1 for TCPS control sample) (n=6)	121
Figure 4.65 Cell viability at pH 6.8 culture environment for 2 hrs, 24 hrs and 48 hrs based on MTT assay (absorbance is normalized to 1 for TCPS control sample) (n=6) .	122
Figure 4.66 Live/Dead assay of MCF-7 cells cultured with hydrogel D-OS for 24 hrs at pH 7.4 culture environment; Green for live cells, Red for both dead cells and DOX; scale bars are 200 um.	123
Figure 4.67 Live/Dead assay of MCF-7 cells cultured with hydrogel D-OS for 24 hrs at pH 6.8 culture environment; Green for live cells, Red for both dead cells and DOX; scale bars are 200 um.	124

1 Introduction

Hydrogels are a form of polymeric materials that swell in water and retain a significant fraction of water within the three dimensional network (cross-linked structures) without dissolving [1, 2]. Since the first synthetic hydrogels as contact lens by Wichterle and Lim in 1954 [3], hydrogels have widely been applied on biomedicine, especially concerning such aspects as tissue engineering, and drug delivery [1, 2, 4, 5]. Hydrogels are versatile carriers for various types of biomedical cargoes, like cells in tissue engineering and drugs in cancer therapy. The overall theme of the thesis is presenting the versatility of hydrogels for biomedical application. The versatility of hydrogels focused on how to control the physical and chemical of developed hydrogels; how hydrogels interact with cells, as well as how cells responded to the hydrogel environments; and the contribution of developed hydrogels on bone regeneration and cancer therapy. Therefore, two novel hydrogels are developed to improve bone regeneration and smart cancer therapy respectively.

1.1 Tissue Engineering Scaffolds

Tissue engineering (TE), as a therapeutically cutting-edge method, is to recover the functionality of diseased tissues or organs by using living cells and biomimetic extracellular matrices (ECM) [6]. In native tissue, ECM is a dynamic structure, and

provides structural and anchoring support to the cells to improve tissue architecture while the ECM is also constantly remodeled by cells [7].

Scaffolds used in TE mimic the natural ECM and provide support for cell adhesion, migration, proliferation, and differentiation [4]. Hydrogels are such kinds of scaffolds, possessing tissue-like properties as they have been successfully used to culture various types of cells and mimic ECM environment [8].

Stem cells are one types of living cells widely used in TE, which are capable of self-renewal as well as differentiation towards specialized cell type. Therefore, they are the most versatile and promising cell source for TE [9]. In vitro control of tissue development is one of the main aspects of TE which involves control of stem cell fate [10]. Thus, there is an increasing need for regulation of stem cells and further evidence reveals that physical interaction between cells and scaffolds contributes to the stem cell activity and cell fate in addition to the genetic and molecular mediators (e.g., growth factors, transcription factors) [11]. Consequently, researchers try to control stem cell fate by controlling the physical properties of scaffolds. It has been reported that the local matrix stiffness on cell state has important implications for development, differentiation, disease, and regeneration[12]. Mooney et al [13] used alginate hydrogel to research the stiffness effect on stem cells and demonstrated the phenomenon that mesenchymal stem cell occurs osteogenesis (bone differentiation) at 11–30 kPa which is the rigidity of three-dimensional microenvironments [13].

However, successful tissue regeneration is still not easy because some other requirements for scaffolds are essential as well, such as biocompatibility, biodegradability, injectability for clinical usage, and cell-attachability [14, 15].

The overall purpose of the first part is the successful regulation of stem cell fate towards bone cell differentiation (osteogenesis) by designing a biodegradable hydrogel with tunable mechanical properties, low cytotoxicity, and good cell adhesion. Based on this purpose, we hypothesis that bone marrow Mesenchymal Stem Cells cultured on stiffer bio-reducible hydrogel will have more osteogenic differentiation than soft one. The overall purpose requires a bio-hydrogel mimicking native tissues both in physical properties and chemical properties; thus three objectives were set: 1) for synthesizing a hydrogel which is biocompatible (low-cytotoxicity) and biodegradable; 2) for mimicking physical properties of human tissues, hydrogels have tunable stiffness because of the fact that different native tissues have different stiffness; for mimicking chemical properties of extracellular matrix, we prepare hydrogels with ability to support for cell adhesion by incorporating cell detectable ligand; 3) for bone regeneration, bone marrow mesenchymal stem cells (BMSCs) cultured on hydrogel have osteogenesis.

1.2 Anti-Cancer Drug Carriers

Surgery, radiotherapy and chemotherapy are three main treatment methods for cancer therapy [16]. Chemotherapy, using of agents to kill fast-growing cells, is a most widely

used method for cancer treatment [17]. However, cells, proliferating in a similarly manner to cancer cells under normal physiological conditions, will also be killed by those agents without specific. Due to this fact, drug carriers for cancer therapy are extensively developed to smartly release drug on targeted cancer cells or tumors while having low effects on health cells [18].

Drug carriers can be liposome, particle or hydrogels [19, 20]. Liposome and particle have shortcomings, like unclear health impact, control circulation times in blood and clearance by the renal and reticuloendothelial systems (RES) [21-26]. Bae et al [27] report micelles for intracellular drug delivery are firstly circulated in blood, and then go through endocytosis, and lastly release drugs. However, this releasing profile depended on blood circulation performance, and endocytosis, thus being much slower than DOX directly treating on tumour site. In situ gel-forming drug depot offers a solution as gels will stuck in tumour site physically and release drug directly to tumour tissue without requirement of endocytosis to achieve on demand local drug delivery, faster drug release, longer drug retention and larger drug accumulation in tumours [28-32].

The overall purpose of this project is developing an in-situ smart extracellular drug delivery system for cancer therapy. Based on aforementioned facts, there are two objectives: 1) to load anti-cancer drug doxorubicin (DOX) into a biocompatible in-situ formed hydrogel; 2) to release much higher amount of DOX from the hydrogel in tumor mimicking environment than normal physiological conditions;

2 Literature review

2.1 Background

2.1.1 Hydrogels in TE

Defining TE as “an interdisciplinary field that applies the principles of engineering and life sciences toward the development of biological substitutes that restore, maintain, or improve tissue function”, Langer and Vacanti identified three general strategies for TE, i.e. use of 1) isolated cells or cell substitutes, 2) tissue-inducing substances, and 3) cells placed on or within scaffolds [33]. They constitute the prevalent method of using biodegradable polymer scaffolds as a carrier for cell transplantation [34], whereby cell populations isolated from tissue are seeded on polymer scaffolds to generate cell/matrix constructs for in vivo implantation [35]. Thus biomaterials function as polymer scaffolds to help cell organization and growth and allow nutrients to be transported to the transplanted cells. That is, the TE strategies emphasize the basics of cell growth and differentiation, in vitro control of tissue development, in vivo synthesis of tissues, the use of biomaterials as scaffolds in TE, transplantation issues and applications in the cardiovascular system, the gastrointestinal system, the kidney, reconstruction of cornea and pancreas, growth of cartilage and bones, nervous tissue regeneration, and dental and skin applications [10].

Hydrogels as carriers for cells in TE are employed as multidimensional [two dimensional (hydrogel membrane) or three dimensional (hydrogel block)] cell culture scaffolds with the necessity that they respond to or control the cellular environment [36]. A hydrogel should be able to promote cell adhesion and tissue regeneration and to assist the exchange of metabolites (oxygen and nutrition) for a 3D cell culture. Hydrogels have been designed to be biodegradable so that they can be degraded within and ultimately absorbed by the body, all at the same time as tissue is “regenerated”. Hydrogels are typically biocompatible, neither provoking strong immune response nor causing serious inflammation. Efforts should also be made to ensure that materials for hydrogels are free from such problems as mechanical materials failure, materials-associated infection, and immunogenic reaction to implanted materials [8].

2.1.2 Hydrogels in smart drug delivery

Cancer is a type of diseases with uncontrolled cell division cause by mutation of genes, such as oncogenes.[37] The method of chemotherapy is killing cells with rapidly division. However, agents used in chemotherapy also kill normal cells with similar proliferation manner which is a major side effect for traditional chemotherapy administration. Once drug are delivered into blood, the drug concentration will have a peak, and then are sharply decreased. [38] The amount of drug delivered to tumor site is a few while most of them are distributed to the whole body. This usually caused a necessary to repeat the drug delivery followed with an enhanced side effect. [39]

To overcome these shortcomings, Smart drug delivery based on hydrogels is developed as an approach to achieve on demand local drug distribution with high concentration and long retention.[30] When hydrogels are served as carriers for anti-cancer drugs, they are designed to only target drugs to cancer cells or tumor.[40] The environment of tumors are quite different from normal tissues, so hydrogels used in smart drug delivery are environment sensitive; once the environment differentiated from normal which is caused by diseases, the drug would be massively released from the carriers in response.[41] These changes of environment can be pH[27], calcium balance[42], present of specific proteins[43] et al. After releasing the drug, the hydrogels themselves are preferred to be biodegraded with low toxicity to health cells or tissue.[19] In-situ forming hydrogels also achieve localized drug treatment in cancer therapy without the necessary of losing drug by entering unwanted sites.[16]

2.2 Preparation and characterization of Hydrogels

This section is about the various preparation and characterization processes for bio-hydrogels, i.e.: 1) what they are or are made from, what their chemical and physical properties are, and how these are related to the functions they are expected to perform, and 2) how we can come to know all these.

2.2.1 Materials for hydrogels

Biomaterials for hydrogels are used or designed to elicit specific cellular functions and to direct cell-cell interactions both in implants that are initially cell-free and may serve as

matrices to contribute to tissue regeneration, and in implants to support cell transplantation [44]. Materials for hydrogels can be classified according to their sources as natural and synthetic. Their biocompatibility, biodegradability and cell-attach ability are essential to their application in TE, and will therefore be given greater details.

2.2.1.1 Natural hydrogels

Naturally occurring biomaterials (collagen, chitosan, hyaluronic acid, fibrin, gelatine, etc.) are expected to most closely simulate the native cellular environment. Uses of these are limited, however, by such factors as large batch-to-batch variation upon isolation from biological tissues, strict requirements for specific biomechanical properties, and so on, not to mention that some of them are rather costly [8, 35].

2.2.1.1.1 Hyaluronic acid (HA)

Hyaluronic acid is part of the ECM [45], and a naturally occurring linear polysaccharide that is abundant in the vitreous and synovial fluid and plays important roles in wound healing [46], cell differentiation and cell motility [47]. Research on stem cell culture indicates that function of the HA is essential also to the control of self-renewal of human embryonic stem cells [48]. It is highly biocompatible, suitable for modification with drugs and other effector molecules [49]. HA and its derivatives have been used to compose drug delivery systems consisting of a wide variety of drugs and cell encapsulation [2, 49].

HA is composed of beta (1-4) linked 2-acetamide-2-deoxy-D-glucose and beta (1-3) linked D-glucuronic acid, and is known to be non-antigenic, noninflammatory and generally non-tissue reactive [50]. HA can be degraded by HAse in vivo, which is ubiquitous in cells and in serum [51]. For the purpose of in vitro HA hydrogel study, different methods have been developed for measuring the hydrogel degradation, by such means as monitoring the release of uronic acid (a degradation component of HA) from a matrix, or monitoring the loss of weight [52-54].

The crosslinkage of HA hydrogel can be formed as a result of polyvalent hydrazide cross-linking, disulfide cross-linking, photo-crosslinking, or enzymatical crosslinking [2, 49, 54, 55]. Pure HA hydrogel is a nonadhesive hydrogel for cells, and the promotion of cell adhesion can be achieved by mixing pure HA hydrogel with gelatin microparticle [56, 57].

2.2.1.1.2 Collagen (and gelatin)

Collagen is naturally occurring proteins in the form of elongated fibrils and found in mammals [58, 59]. It is the main component of connective tissues such as tendons, ligaments and skin, and is up to 35% of the body protein content, i.e. the most abundant protein in mammals [60]. Gelatin is collagen that has been hydrolyzed under basic and high temperature conditions [61].

Collagen or Gelatin can be degraded by enzyme collagenase in vivo [62]. The methods used to form the collagen or gelatin hydrogel are quite similar to those for HA, such as disulfide cross-linking, photo-crosslinking, and enzymatical crosslinking [15, 63, 64].

2.2.1.1.3 Alginate

Alginate is block polymer composed of (1-4)-linked b-D-mannuronic acid (M units) and a-L-guluronic acid (G units) monomers, the ratio varying between M and G units [65]. Alginate polysaccharides covalently modified with RGD-containing cell adhesion legends are widely used for the settlement and attachment of cells. And calcium alginate hydrogel surfaces coupled with GRGDY peptides can be fabricated to achieve cellular interaction [14]. They are well known for their uses in mineralized polymeric matrices, which justifies their application in bone tissue regeneration [66]. However, it is difficult to have alginate degraded in vivo and in a short time [13].

However, alginate is hard to be degraded in vivo, and in a short term, it can be deemed to be no-change on crosslinking network, weight, and gel mechanical property [13]. Whereas, its oxidized counterpart is biodegradable since the molecular weight of alginate is highly decreased after oxidation. At the same time, oxidized alginate (O-alg) can also be served as a crosslinker because of resultant aldehyde groups along polymer backbone.[67]

2.2.1.1.4 Chitosan

Another type of polysaccharide, chitosan has been widely used for biomedical applications, such as cell culture platforms [68, 69], drug carriers[70] and non-viral gene delivery [71]. Chitosan is derived from chitin with a linear structure, consisting of β -(1-4)-linked 2-amino-2-deoxy-D-glucose and 2-acetamido-2-deoxy-D-glucose units [72]. Chitosan can be easily modified, usually via primary amine groups [73]. However, Chitosan can only be dissolved in an acetic environment, which limits its applications in

injectable cell culture scaffolds. A common solution is to partially N-succinylate chitosan to make it dissolvable in a neutral solution [74]. Chitosan has excellent biodegradability as well [70]. Lysozyme is used to degrade chitosan for in vitro degradation evaluations [75]. Chitosan polymer chains can be crosslinked by glutaraldehyde or genipin to form chitosan hydrogel [76, 77]. Other methods have also been developed to form chitosan hydrogels, such as maleic chitosan [78]. However, chitosan can only be dissolved in acetic environment which limits its application on injectable cell culture scaffolds. Current common solution is to partially N-succinylate chitosan to make it neutrally dissolvable.[74]

2.2.1.2 Synthetic hydrogels

Synthetic biomaterials are favoured as scaffold materials because their physical and biologic properties can be modified and they can be reproduced in similar and large quantities. The major classes of synthetic biomaterials are the glycolic acid derivatives, lactic acid derivatives, and other polyester derivatives [8].

2.2.1.2.1 Polyethylene glycol (PEG)

Widely used in human medicine, PEG resists protein adsorption and is therefore endowed with the unique nonfouling properties because of its nonadhesivity towards proteins and cells [36, 79].

PEG is non-ionic and soluble in water. PEG diacrylate is produced as a result of the modification of PEG with acrylate to get carbon double bond which will serve as a

gelation functional group [78]. Application of PEG or its diacrylate derivative (PEGDA) to TE [79-82] is limited by their inability to support cell spreading due to their being non-adhesive to protein and the absence of cell adhesion ligand [79, 83].

Pure PEG (molecular weight < 20,000) is chemically stable under physiological conditions [13]. But after modification some polymers based on PEG can be biodegradable, as instanced by oligo(poly(ethylene glycol) fumarate) (molecular weight ~10,000) [84].

Heavily investigated are the many crosslinking methods for PEG hydrogels, such as the thermal radical initiation system [84] and disulfide crosslinking system [55], so that nowadays both chemical hydrogels and physical hydrogels are available [85].

2.2.1.2.2 Polyvinyl alcohol (PVA)

Similar to PEG, PVA is another type of hydrophilic synthetic material. Its excellent biocompatibility makes it one of the most popular materials in medical applications [86]. However, also alike PEG, PVA does not support cell spreading and adhesion. Modification therefore is required before its use in TE [87]. PVA hydrogel is not biodegradable, but its acrylate modified form is degradable [88]. Other methods, like incorporation of biodegradable crosslinkers into PVA hydrogel, is also developed [89].

2.2.1.2.3 Poly (2-hydroxyethyl methacrylate)

P(HEMA), the homo-polymer or co-polymer from 2-hydroxyethyl methacrylate (HEMA), has been used as implant materials for a long time [90]. The contact lens is of

the classic chemical cross-linking hydrogels developed by Wichterle and Lim as a result of the copolymerization of hydroxyethyl methacrylate (HEMA) [3].

The p(HEMA) hydrogel is non-biodegradable, a property that restricts its application in TE, but is advantageous for its micro porous structure (a preferable morphology for TE scaffold) as a result of the polymerization-induced phase separation polymerization [91].

2.2.1.2.4 Poly (amido-amine)

Poly (amido-amine)s (PAAs) are a class of polymers characterized by the presence of amido and tertiary amino groups regularly arranged along the macromolecular chain. The backbone of poly (amido-amine)s are usually synthesised by poly addition of primary monoamines, or bis(secondary amines), to bis-acrylamides.[92]

PAAs can be easily modified during synthesis by the introduction of functional co monomers [93]. For example, a new PAAs was synthesized to contain the disulfide linkage in the main chain by means of stepwise polyaddition of 2-methylpiperazine to N,N-bis(acryloyl)cystamine (BACy1) or N,N-bis(acryloyl)-(L)-cystine (BACy2). This kind of functionalized PAAs exhibit their good biodegradability when they are degraded by reduction of the disulfide group under physiological conditions. Another example is the biomimetic poly(amidoamine) hydrogels for cell culture that evolve from the incorporation of 4-aminobutylguanidine (agmatine) moieties to create RGD-mimicking repeating units for promoting cell adhesion.[93]

PAAs are synthetic polymers endowed with biologically interesting properties, such as being highly biocompatible, free from toxicity, and biodegradable. But when it is

positively charged because of the positive charge of tertiary amine group and the absent of negative charge group, this kind of PAAs will show cytotoxicity, which is partially dependent on its positive charge arrangement and ions density [94-96]. Most PAAs for biomedical application have carboxyl groups along the main chain to decrease cytotoxicity and form amphoteric PAAs [97].

2.2.1.2.5 PEO-PPO-PEO triblock copolymer

PEO-PPO-PEO is a triblock copolymer consisting of poly (ethylene oxide) (PEO) and poly (propylene oxide) (PPO). It attracts interests in biomedical applications as it forms a thermo-reversible gel that shows gelation at around the body temperature (37 °C) via PPO segments aggregation [98, 99] Furthermore, the block composition (PEO/PPO ratio) and the molecular weight can be used to control the final properties of the products so as to meet the specific application needs [100]. However, it has the same issues in biodegradation [101] and cell attachment[102] when it is applied in TE. The solutions to these issues are similar with those related to PEG or PVA.

2.2.1.3 Combinations of natural and synthetic polymers

Combination of natural and synthetic hydrogels has been utilized to overcome shortcomings of pure natural and synthetic materials. Biomaterials combined in different ways have been developed to generate hydrogels with biological properties (e.g.

hydrophilicity, cell-adhesiveness, degradability), biophysical properties (e.g. porosity, branched vasculature), and mechanical ones (e.g. stiffness, viscoelasticity) [7].

2.2.1.3.1 Cross linkable group modification

Modification of natural polymers for creating cross linkable functional groups is a basic step for hydrogel design and further application. Arylate is one of such functional groups for such modification. HA-acrylate can form a stable covalent crosslink hydrogel via a free-radical mechanism between carbon-carbon double bonds (a covalent bond where two pairs of electrons are shared between the atoms rather than one pair) converting the double to a single bond and forming single bonds to join the other monomers. One of such efforts is to modify HA with methacrylic anhydride by adding ethyl eosin and triethanolamine as initiator, to result in the synthesis of a photocrosslinked polysaccharide hydrogel by irradiating using an argon ion laser [2].

Enzyme induced crosslink is also widely used to form hydrogels because of its low cytotoxicity. This crosslink system requires modification of natural polymer with an enzyme catalytic group. In one instance hydroxyphenylpropionic (HPA) acid was treated with NHS/EDC to link it to gelatin by reacting with tyrosine residues of the gelatin. Those conjugates can be catalyzed by hydrogen peroxide (H₂O₂) and horseradish peroxidase (HDP), and then crosslinked with each other to form gels because phenols can be crosslinked through either a more common C–C linkage between the ortho-carbons of the aromatic ring or a C–O linkage between the ortho-carbon and the phenolic oxygen. The

stiffness of the hydrogels was readily tuned by varying the H₂O₂ or HDP concentration [15].

Other modification processes (e.g. disulfide linkage) can be affected by modifying a natural polymer with 3,3'-dithiobis(propionic hydrazide) (DTP) or cystine to form thiolated gelatin or HA macromer.[52, 103]

2.2.1.3.2 P (PEG-co-peptides) conjugate

Cell anchorage is a strict requirement for the survival of most cell types, and it orchestrates critical roles in many cellular functions including migration, proliferation, differentiation, and apoptosis. Cell interaction with biomaterials is mediated through transmembrane receptors which recognize adhesion molecules at the materials surface [14]

PEG is a cyto-nonadhesive hydrogel and needs to be modified with cell adhesive peptides if it is to be used as a cell culture platform. Arg-Gly-Asp (RGD), a component of cell binding protein targeting α_v -integrins, is widely used to promote cell adhesion[104, 105]. RGD peptides was [79] incorporated into PEG diacrylate hydrogel through aminolysis of the N-hydroxy succinimide ester of acrylic acid by the α -amine terminus of the peptide sequence to produce an amide linkage between the peptide and the acrylic group.

PEG modified with polylysine [106] which serves as a functional cell attachment group for micro-vessel scaffolds is developed by activating PEG with N,N'-carbonyldiimidazole

and then forming the gel by the reaction between free-amine groups in Poly-L-lysine hydrobromide [58].

2.2.2 Formation of Cross-links

After deciding on the materials for hydrogels, the approach used to form cross-linkage between monomers or macromer is the second step which is introduced in this subsection. Cross-links in hydrogels are formed by covalent or ionic bonds. Weaker forces such as van der Waals forces and hydrogen bonds can also serve as cross-links, to result in the formation of swollen networks that will behave as hydrogels. Finally, semicrystalline, uncross-linked hydrophilic polymers may form hydrogels upon swelling since the crystallites act as physical cross-links and do not dissolve in water [1]. They are called ‘physical’ or ‘reversible’ gels when the network is formed by molecular entanglement or by non-covalent force, and called ‘permanent’ or ‘chemical’ gels when a covalently cross-linking network is present [5].

2.2.2.1 Preparation by chemical cross-linking

Cross-links can be formed by means of chemical reaction initiated by heat, pressure, change in pH, or radiation[4]. As previously mentioned, the contact lens is a classic chemical cross-linking hydrogel developed by Wichterle and Lim, based on copolymerization of hydroxyethyl methacrylate (HEMA) with the crosslinker ethylene glycol dimethacrylate (EGDMA) [3]. This hydrogel is created by free radical chain polymerization which can be initiated by light, heat, or redox [5]

Reviewed here are the two major methods to initiate free radical chain polymerization for biomaterials: photo-initiated polymerization and radical-initiated polymerization for the preparation of hydrogels. The former is instanced by the modification of hyaluronic acid (HA) with methacrylate functional groups to result in the covalent cross-linking in the presence of a radical-initiated polymerization system. A concrete instance is the modification of HA with methacrylic anhydride to produce a synthetic, photocrosslinked hydrogel [2]. One more instance is the improvement of a polysaccharide hydrogel by using 2-Hydroxy-4'-(2-hydroxyethoxy)-2-methylpropiophenone (Irgacure 2959) as the ultra violet light-sensitive photoinitiator to decrease cytotoxicity, and as a result to encapsulate human embryonic stem cells and control cell proliferation and differentiation in 3D [48, 78]. Irgacure 2959 was reported to have minimal toxicity towards six cell lines used for cell encapsulation [107]. Upon absorption of UV light, Irgacure 2959, as the free-radical donor, was cleaved into 2 primary radicals which then react with the vinyl (C=C) groups of modified hyaluronic acid to initiate radical polymerization. [108]

Radical-initiated polymerization can be achieved by thermal radical initiation reactions. One instance is the design of an injectable glucose sensitive microbead hydrogel by using a host macromer with bi-functional reactive group (vinyl groups), and adding sodium persulfate (SPS) as an initiator and N,N,N',N'-tetramethylethylenediamine (TEMED) as a catalyst [109]. Now researchers have proved the feasibility of this initiation system for its negative cooperative effect to cytotoxicity in these injectable hydrogels [110]. They have also demonstrated the cytocompatibility of the initiator concentration used in the APS/TEMED initiation system for MSCs in OPF hydrogels [111].

Diverse approaches have been utilized to produce in situ hydrogels with tunable properties using different triggers such as pH, temperature, light, and targeting biomolecules, as instanced by this facile approach to the creation of a ‘living’ controlled in situ gelling system based on a thiol-disulfide exchange reaction by changes in the pH of the pre-gel solution[112]. Another example is the self-setting injectable hydrogels that can be triggered by a decreased pH. Silated macromolecules, such as silated hydroxyl propylmethylcellulose have been used for such purposes [113]. Silated macromolecules can be self-crosslinked by silanol condensation to form hydrogels [114].

2.2.2.2 Preparation by physical cross-linking

Physical hydrogels are not homogeneous, because clusters of molecular entanglements, or hydrophobically- or ionically-associated domains, can create inhomogeneities. Free chain ends or chain loops also represent transient network defects in physical gels [5].

Electrostatic between a polyelectrolyte and a multivalent ion of the opposite charge accounts for the formation of a physical hydrogel known as ‘ionotropic’ hydrogel [5]. For example, alginates are naturally derived anionic polysaccharides and used as hydrogels by adding calcium ions as the opposite charge [115]. Divalent cations like Ca^{2+} cooperatively bind between the G blocks of adjacent alginate chains, creating ionic interchain bridges which cause gelling of aqueous alginate solutions [14].

With the development of nanotechnology, supramolecular self-assembly has attained keen interest in science [116]. Trials have been made adding multivalent ions of the opposite charge to the heated and cooled peptide amphiphile solution to cover and weaken

the ionic force, thus breaking the balance between the hydrogen bond, ionic force or van der Waals forces, and to have monomers or macromers aggregated to form the gel [117]. This is instanced by the design of an injectable b-Hairpin peptide hydrogel, which can be triggered by shielding its ionic repulse force in a salt environment, and in which the peptides are capable of killing Methicillin-Resistant *Staphylococcus aureus* [118]. Besides the ionic trigger, enzymes also can serve as triggers to achieve biocatalytic self-assembly and gelation. A number of related precursors based on aromatic peptide amphiphiles were synthesized to self-assemble supramolecular hydrogel initiated by subtilisin, a hydrolytic enzyme from *Bacillus licheniformis*, which hydrolyses the methyl ester to form a peptide derivative that will cause a decrease in hydrophilic force. Recent research has shown that the structures can potentially be controlled by appropriate assembling conditions [119].

2.2.3 Properties and Characterization of hydrogels

The materials for hydrogels and gelation methods affect physical and chemical properties of the final products. Hydrogel hydrophilic networks have a high affinity for water but are prevented from dissolving due to their chemically or physically crosslinked network. The polymer network absorbs water molecules, resulting in the gradual swelling of the hydrogel [120]. Character of the water in a hydrogel will determine the overall permeation of nutrients and gas into and cellular products out of the gel [53].

When a dry hydrogel is immersed in an aqueous environment, the water uptake process consists of quite a few steps. At the beginning, the polar, hydrophilic group gets hydrated by water molecules to lead to the formation of “primary bound water”; hydrophobic

groups thus exposed interact with water molecules, leading to hydrophobically-bound water or “secondary bound water”; the swelled network will imbibe additional water due to the osmotic driving force of the network chains towards infinite dilution; this additional swelling is opposed by the covalent or physical crosslinks, leading to an elastic network retraction force; at last, the hydrogel will reach an equilibrium swelling level and begin to disintegrate and dissolve if the network chains or crosslinks are degradable. The additional swelling water is called ‘free water’ or ‘bulk water’, and is assumed to fill the space between the network chains, and/or the center of larger pores, macro-pores or voids. It is believed that a gel used as a TE matrix may never be dried, because the total water in the gel is comprised of both “bound” and “free” water. [5].

Before hydrogel formation, it is critical to monitor the rheological properties of the polymers, including the viscosity of the precursor solution, gelation time, hydrogel pore size, steady shear and dynamic oscillatory information [114].

After gelation, the most important parameters used to characterize the network structure of hydrogels are the polymer volume fraction in the swollen state, the molecular weight of the polymer chain between two neighboring crosslinking points, and the corresponding mesh size. Parameters relating performance of hydrogels are: swelling behavior, interior morphology, mechanical properties, biodegradation, cytotoxicity, and cell viability, as well as chemical properties, as discussed in the following.

2.2.3.1 Swelling behavior

The polymer volume fraction in the swollen state being a measure of the amount of fluid imbibed and retained by the hydrogel [4], the swelling property to some degree characterizes water thus held in hydrogels, as indicated in a 2010 study. A hydrogel was cast, soaked in ethanol for 48 hrs, and then allowed to air dry. When properly dried, the material was placed in a phosphate buffered saline (PBS) solution at 37 °C and allowed to swell for 16 hrs. Readings were taken every 30 mins for the first four hours, then every hour for the next four hours, then every two hours for the remaining eight hours. Gel fraction of each hydrogel sample was measured by determining the weight of the gel before and after soaking in the ethanol. After the initial 16 hrs of swelling the samples were monitored for degradation. Weights were taken every 24 hrs for the next 30 days. A fresh amount of PBS, previously equilibrated at 37 °C, was employed every 24 hrs during the time of measurement to replace the used ones [121].

The mass swelling percentage of the hydrogel was calculated from the following relation [122]:

$$\% S = [(m_t - m_0) / m_0] \times 100;$$

Where m_0 is the mass of the dry gel and m_t is the mass of swollen gel at time t .

The swelling rate constant of the hydrogel was calculated from the following relation:

$$\text{Percentage mass swelling} = k_s t^{0.5}$$

where k_s is the swelling rate.

The initial swelling data were fitted to the exponential heuristic eq.

$$F = M_t / M_\infty = kt^n$$

where F is the fractional uptake; M_t / M_∞ , when M_t is the amount of diffusant sorbed at time t, M_∞ is the maximum amount absorbed; k is a constant incorporating characteristics of macromolecular network system and the penetrant; n is the diffusional exponent, which is indicative of the transport mechanism. The equation is valid for the first 60% of the normalized solvent uptake. For Fickian kinetics in which the rate of penetrate diffusion is rate limiting, $n = 0.5$, whereas values of n between 0.5 and 1 indicate the contribution of non-Fickian processes such as polymer relaxation. Diffusion coefficients are important penetration parameters of some chemical species to polymeric systems. Using n and k, the diffusion coefficient (D) of the solvent in the matrix can be calculated using the following equation:

$$K = 4[D/\pi r^2]^n$$

$$4D^n = k(\pi r^2)^n$$

$$D^n = (k/4)(\pi r^2)^n$$

where D is the diffusion coefficient and r the radius of gel disc.

2.2.3.2 Gel or gel/cell construct morphology

The hydrogel is of a cross-linked network. A scanning electron microscope (SEM) is utilized by some researcher for the observation of gel morphology.[78, 91, 106, 123, 124] [125] The sample for SEM should, first, be frozen quickly to best keep the original

morphology upon the samples having reached their maximum swelling ratio in dd-water at room temperature after 24 h and then freeze dried in a Freeze Drier until all water is sublimed. The freeze-dried hydrogel specimens are then cut and fixed on aluminum stubs and then coated with gold for interior morphology observation with a scanning electron microscope [78].

Because dehydration for SEM to some degree leads to artifact in the highly water-saturated gels, their morphology can be better viewed by cryosectioning the gels followed by staining with fluorescein isothiocyanate (FITC), and visualized under fluorescence or confocal microscopy [106].

SEM can also show cell morphology attached to the hydrogel when it is applied to TE. The method of treating samples can be quite different because cell morphology is subject to changes when going through the freeze drying process. Accordingly, in some studies hydrogels seeded with cells were washed with PBS, fixed with 4% glutaraldehyde or 10% buffered formalin, and dehydrated by the use of graded ethanol followed by the addition of hexamethyldisilazane. Cellular constructs were sputter coated with gold and observed under the SEM [106, 126, 127].

Backscattered electron microscopy (BSE-SEM) is commonly used for characterizing repaired bone sections by showing the mineralized tissues at the implant-bone interface [128, 129]. Furthermore, BSE-SEM provides the mineralized composition and density of bone regenerated from non-autogenous grafts in bone TE.[130, 131]

2.2.3.3 Mechanical properties

The key structural parameter determining the material modulus and diffusional characteristics is the network crosslinking density. Many means are available for bulk or local gel mechanical measurement, such as the Dynamic Mechanical Analyzer for bulk gel mechanical measurement (DMA), atomic Force Microscopy (AFM) or Tracer Particle Microrheology (TPM) for the measurement of local gel and cell mechanical changes [36].

Researchers have been able to determine the compressive modulus of the various swollen hydrogels on a mechanical tester using a parallel plate apparatus and loading of 10% of the initial thickness per min (~200 mm/min). Samples for mechanical testing (n=5 per composition) are cylindrical (~2 mm height, ~7 mm diameter) and are compressed until failure or until 60% of the initial thickness was reached. The modulus is determined as the slope of the stress versus strain curve at low strains (<20%) [53].

Mechanical testing can also be performed on a DMA Q800 Dynamic Mechanical Analyzer in a “controlled force” mode, whereby the swollen hydrogel samples in the shape of a circular disc are submerged in distilled water and mounted between the movable compression and fluid cup; a compression force from 0.01 to 0.05 or 0.30 N (depending on the gel strength) at a rate of 0.02 or 0.05 N/min was applied at room temperature; the compression elastic modulus (E) of the swollen hydrogel can be extracted by plotting the compressional force versus strain [132].

In a self-assembly physical hydrogel, AFM is used for to show the gel nanostructure formation and nucleation and early-stage structure growth [119, 133].

2.2.3.4 Cytotoxicity and cell viability

When cells are seeded to gels in 2D, cytotoxicity is largely related to the chemical structure of the hydrogel; under three dimensional situations, that is, when the cells are encapsulated in the hydrogel, cell viability can also be affected by poor nutrient and gas exchange because of the inappropriate cross-linking density [53]. Assays generally used to measure hydrogel cytotoxicity and cell viability are described as follows.

MTT assay is a popular approach to evaluate cell viability on hydrogels [52, 56, 78]. MTT (3-(4,5-Dimethylthiazol-2-yl)-2,5-diphenyltetrazolium bromide, a yellow tetrazole) is reduced to purple formazan in living cells [134]. A solubilization solution (usually either dimethyl sulfoxide, an acidified ethanol solution, or a solution of the detergent sodium dodecyl sulfate in diluted hydrochloric acid) is added to dissolve the insoluble purple formazan product into a colored solution. The absorbance of this colored solution can be quantified by measuring at a certain wavelength (usually between 500 and 600 nm, an absorbance maximum at 490-500 nm in phosphate-buffered saline) by a spectrophotometer. The absorption maximum is dependent on the solvent employed [135].

Researchers have managed to assess the viability of photoencapsulated fibroblasts immediately after encapsulation and after 1 week of in vitro culture using a commercially available MTT viability assay (ATCC, 30-1010K). For this assay, 100 uL of the provided MTT reagent (tetrazolium salt solution) is added directly to the wells containing the constructs (n =3 per macromer solution) and placed in an incubator at 37 °C for 4 h. The purple formazan produced by active mitochondria is solubilized by construct

homogenization in 1 ml of the provided detergent solution and orbital shaking for 2 h. The absorbance of these solutions is then read at 570 nm (Molecular Devices SpectraMax 384) [53].

Live/Dead assays are cytotoxicity and viability assays too. Live/Dead fluorescent staining (Invitrogen) can be used to test osteoblasts for viability and proliferation at Day 1, 3 and 7. The live (green) and dead (red) cells are observed after 30 min incubation and sufficient PBS wash. For quantitative evaluation, WST-1 [5 Basel, Switzerland] colorimetric assay can be used. The incubation lasted for 2 h and the absorbance at 450 nm is measured with reference to 620 nm in a microplate reader [136].

2.2.3.5 Degradation analysis

Gels as TE scaffolds are mostly capable of degradation and ultimately absorbed in the body [8]. Gels can be degraded by some chemicals or enzymes. For example, DTT or GSH, reducing agents, can degrade hydrogels containing disulfide linkages. [52, 55, 137]. Disulfide linkages can maintain stable in normal physiological conditions but will be reductively degraded under reduction environment. [95, 137, 138] Prestwich et al found that crosslinker with disulfide bonds in hydrogels can be gradually degraded in a reductive environment and promote cell expansion [137]. Some hydrogels made from nature polymer can be generally degraded by corresponding enzymes, such as hyaluronidases for hyaluronic acid, [51] lysozyme for chitosan [75] and collagenase for collagen or gelatin [62]. Cells can also have effects on hydrogel degradation. For example,

alginate hydrogel can be partially degraded by fibroblasts encapsulated in it by showing a release of calcium ions from the construct.[139]

A lot of methods have been developed to do degradation analysis. After degraded, the weight of hydrogel main body will be reduced, so the degradation can be directly characterised by the changes of hydrogel weight.[121] Since some degradation components will also be released from the gel main body into the testing solution, another qualitative approach to characterise the gel degradation is showing the release profile of the degradation component by collecting the degradation component and then calculating the cumulative amount of this component. [140] For detecting local degradation in gel systems, some researchers use the incorporation of a fluorescence resonance energy transfer (FRET) based linker within the gel-forming macromers [36]. Once the gel is treated by degradation solution, the FRET based linker will generate strong fluorescence where the cells will subsequently extend the process and move within the degraded gel, leaving tracks of increased fluorescence. Upon local gel degradation by encapsulated fibroblasts, the increased fluorescence is observed, allowing visualization of the degradation tracks generated by the migrating cells degradable linker within the PEG-based gel [62].

2.2.3.6 Chemical properties

Characterization of chemical properties includes clarification of macromer molecular weight that can be measured by Gel permeation chromatography (GPC), analysis of chemical structure by NMR [78], and so on. Among these, gelation efficiency is the

important parameter that describes the capability of a hydrogel and can be expressed by the following equation:

$$Gf=Wd/Wp*100\%$$

where Wd is the weight of the dry hydrogel and Wp is the total feed weight of the two macromer precursors and the photo-initiator [132].

2.3 Osteogenetic differentiation

Many of research have focused the use of hydrogels as scaffolds to regulate and control cell proliferation and differentiation for the construction of artificial organs. This is especially the case of stem cells or some types of adult cells able to assist proliferation in tissues or organs. A clarification of such cases, and of the various approaches involved, may have to be stated in genetic terms, which are necessary especially for uninitiated students and new researchers. The following will be such a statement.

Take bone tissue regeneration as such an application. There are two main approaches for bone regeneration in TE: use of autogenetic (i.e. autogenetic bone grafts) and synthetic materials, that is, the cell-free and cell-based approaches (although none of them has translated to clinical practice [141]). Biomaterials for bone regeneration have developed from ceramic, metal materials to such TE materials as nanofiber and hydrogel [142, 143]. Most of them are based on a bone matrix component such as calcium phosphate, hydroxyapatite, silica, and collagen/gelatin, which provide the mechanical and

biochemical environment necessary for bone regeneration and can be fabricated with high structural resolution [143].

Natural hydrogels such as matrigel, alginate or agarose gel, gelatin/collagen, and synthetic hydrogels such as PEG and PLA/PGA containing cell attachable biotin have often been used for bone TE research [143, 144], but their clinic usage as bone regeneration biomaterials is still limited [141]. Currently the main problems in bone regeneration TE are those that relate fate regulation of stem cells, improvement of mechanical properties, vascularization, swelling after injection, and toxicity originating from unreacted constituents [141, 145-147].

For stem cell fate regulation, it has been reported that the local matrix stiffness on cell state has important implications for development, differentiation, disease, and regeneration [148]. In order to control stem cell fate, researchers have examined the stiffness effect on stem cells by comparing the cell/matrix interaction between 2D and 3D in alginate hydrogel. They demonstrate the commitment of mesenchymal stem-cell population's changes in response to the rigidity of three-dimensional microenvironments, with osteogenesis (bone differentiation) occurring predominantly at 11–30 kPa. Hydrogels for this study are conjugated with RGD to help cell settlement and attachment. The genes used for characterization of osteogenic differentiation are osteogenic biomarkers core binding factor 1 (Cbfa-1), osteopontin (OPN) and osteocalcin (OCN) [13].

2D surface properties regulating stem cells fate is another aspect commonly investigated, as more and more evidence shows spatial control based on surface

morphology could control stem cell differentiation. Some researchers tried controlling stem cell morphology and differentiation by hydrogel surface wrinkles, and found that cells attaching to the lamellar pattern will spread by taking the shape of the pattern, exhibiting high AR, and getting differentiated into an osteogenic phenotype. In contrast, cells attaching inside the hexagonal patterns remain rounded with low spreading before differentiating into an adipogenic phenotype [146]. But it is important to be aware of the highly strict requirement of experimental design to control the single variable in an experiment because there are too many variables which could affect the stem cell differentiation. Effects of other factors, such as materials surface wettability and cell adhesion composition, are still unclear [149].

Characterization methods for bone differentiation like Von Kossa-stained histological sections [150], Energy-dispersive X-ray (EDX) analysis of spherulitic minerals and rhombohedral minerals [66], Alizarin Red S staining and Alkaline phosphatase assay [151] are widely used.

The ultimate goal of bone TE is, very likely, to understand how chemical and physical environments regulate osteogenesis of stem cells, osteoblast, and osteoclasts. Using genetic approaches, more and more genes and their expression pathways may be researched, with increasing interest in the control of cell proliferation and differentiation by referring to hydrogel properties.

2.4 Smart Drug Delivery by pH response

Environment sensitive hydrogels, responding to stimuli, hold the potential as smart drug-delivery systems.[19, 32, 152]

The factors usually used to trigger drug release are redox potential, temperature, antibody, or pH et al.[31, 99, 153-158] pH is one of the most used trigger to design drug carriers owing to the fact that the tumour tissues show low pH environment.[154, 159-162] Extracellular pH ranges of tumour tissues are different according to different types of cancer. For example, extracellular pH range of Uterine Cancer is between 6.5 and 7.2, for Melanoma, it's 6.6 to 6.8, and for Astrocytoma, it's 5.8 to 7.1. [160] Once drug carriers are exposure to an extracellular tumour acidic environment, drug can be release via such as decreasing non-covalent interaction between drugs and their carriers because of protonation of drug like doxorubicin (DOX) [18, 163] or cleavage of acid-labile covalent linkage between drug and its carriers [164] Covalent conjugating drug to drug carriers through a simuli-sensitive bond have shown advantages, not only high drug loading efficiency but also excellent capability of controlled release of drug in an environmentally sensitive manner.[27, 159] Schiff base is one kind of such chemical bones used to covalent reversibly conjugate drug to drug carriers since they are biodegradable via hydrolysis, and the stability of these bonds decreases as the pH decreases (acid-sensitive linker).[165, 166]

3 Materials and Methods

3.1 Materials

All chemicals were purchased from Sigma-Aldrich without further purification unless otherwise noted. N,N'-cystaminebisacrylamide (CBA), and Von Kossa Method for Calcium Kit was purchased from Polysciences Inc. (Warrington, PA, USA), Poly(ethylene glycol) diacrylate (PEGDA, Mw=700), PBS 1X powder, Hoechst 33342, BODIPY® FL phalloidin, To-Pro-3 iodide, and Live-Cell staining kit were from Invitrogen. The 3- (4, 5-dimethyl thiazolyl-2)-2, 5-diphenyltetrazolium bromide (MTT) cell viability assay kits were from Biotium Inc. (Hayward, CA). . O.C.T compounds were purchased from V.W.R. Dialysis membrane (7 kDa MWCO) was from Fisher Scientific (Ottawa, ON, Canada).

3.2 Synthesis

3.2.1 PAA crosslinker

The poly (amidoamine)s crosslinkers (PAA) with guanidine as side chains and disulfide linkage in backbone were synthesized as follows: CBA (234 mg, 0.9 mmol) and agmatine (AS) (114 mg, 0.5 mmol) were dissolved in methanol/water (v/v=1/1) to make a final mass concentration 116 mg/ml. Then LiOH·H₂O (21 mg, 0.5 mmol) was added to the solution when a homogeneous solution was obtained. The reaction was carried out at 50

°C and kept dark for 48 hrs. After 48 hrs, the solvent was evaporated by a rotary-evaporator and freeze-dried for 2 days. The final product was stored at -20 °C for future use. ¹H NMR spectra of PAA were recorded on an Advance 300-MHz spectrometer. Samples of PAA (5 mg) were dissolved in 1 ml of D₂O/CD₃OD mixture. Chemical shifts (δ) were reported in parts per million (ppm). The molecular weight of PAA was calculated from ¹H NMR spectrum. ¹H NMR (ppm): δ, 1.40-1.60 (-CH₂(CH₂)₂CH₂-), 2.40-2.50 (-CH₂(C=O)NH-), 2.50-2.60 (-CH₂-N(CH₂)₂-), 2.80-2.90(-CH₂-N(CH₂)₂-, -CH₂-SS-CH₂-), 3.20-3.30 (-CH₂-NH(C=NH)NH₂), 3.40-3.60 (-(C=O)NH-CH₂-), 5.60-6.40 (CH₂=CH-(C=O)-).

3.2.2 Oxidized alginate (O-alg)

O-alg was prepared according to a reported procedure of Balakrishnan et al with slight modification.[67] Briefly, 2 g sodium alginate was dissolved in 10 ml ethanol, 1.3 g sodium metaperiodate in 10 ml water was added to the reaction mixture. The reaction was conducted at room temperature for 4 hr. The solution and precipitation was dialyzed against distilled water for 2 days to remove the byproduct and un-reacted sodium metaperiodate. Silver nitrate is used to detect the complete removal of sodium metaperiodate. The dialyzed solution is frozen at -80 °C overnight and then dehydrated by lyophilization and the final product was stored at -20 °C for future use.

3.2.3 Succinated chitosan (S-chi)

S-chi was synthesized based on Rogalsky's procedure with modification.[167] 2.0 g Chitoson was dissolved in acetic acid- ethanol mixture (100 ml 5 % acetic acid mixed with 120 ml ethanol). The solution is stirred at 40 °C, 400 rpm until chitosan was total dissolved. Four g Succinic anhydride in 40 ml acetone was added to the solution with thoroughly stirring. Then the reaction was allowed to be conducted at 40 °C for overnight. Afterwards, pH value of the mixture was adjusted to 11 by addition of 30 % sodium hydroxide, and the resultant viscous solution was dialyzed against distilled water for 2 days followed by freeze-drying to get white powder. The final product was stored at -20 °C for future use. The degree of succinylation[168] was calculated from ¹H NMR spectra of S-chi (6 mg) in 1 ml D₂O mixture. Chemical shifts (δ) were reported in parts per million (ppm).

3.3 Preparation of hdyrogels

3.3.1 Hydrogel for bone regeneration

PEGDA-PAA- poly (acrylic acid) hydrogels (G1) and Pure PEGDA hydrogels (G2) were all prepared in PBS solution (pH=7.4) initiated by APS (5.7 mg/ml) and catalyzed by addition of TEMED (2.9 mg/ml) at 37 °C for 5 min. G1 are hydrogels made by three monomers: PEGDA, PAA and Acrylic Acid, and G2 are hydrogels made by PEGDA, the only monomer, and served as controls without special notification. G1 with different

monomers' concentrations (62 mg/ml, 124 mg/ml, and 248 mg/ml) are designed to achieve various stiffness, swelling rate, and mechanical properties. G1 with different monomers' mass ratios are designed to achieve controllable degradation profiles (PEGDA: PAA: acrylic acid = 100:5:1 and 100:20:4). The formulation of hydrogels is shown in Table 3.1.

Table 3.1 Formulations of hydrogels

Total concentration of monomers Mass ratios of monomers (PEGDA: PAA: acrylic acid)	62	124	248
100:5:1	G1-a	G1-b	G1-c
100:20:4	G1'-a	G1'-b	G1'-c
100:0:0	G2-a	G2-b	G2-c

3.3.2 Hydrogel for cancer therapy

Blank hydrogel (OS) without drug are made of S-chi and O-alg. S-chi and O-alg were dissolved in PBS separately at a concentration of 2 wt% and 12 wt% respectively.

Hydrogels OS were made by straightly mixing the solutions of S-chi and O-alg at volume ratios of 1:1 at room temperature.

The procedure to prepare DOX-Loaded hydrogels (D-OS) are these, the water solution of doxorubicin was prepared at concentration of 0.2 mg/ml. Two wt% S-chi in PBS solution was firstly mixed with free DOX solution at volume ratio of 2:1. Secondly, 12 wt% O-alg in PBS solution was then added to the solution at a volume equal to DOX in water solution. The DOX-loaded gel precursor solutions was injected to a vial by pipetting at a rate which can allow all gel precursor solution completely be delivered to the substrate.

3.4 Characterization of hydrogels

3.4.1 Fourier transform infrared (FTIR) spectroscopy

FTIR was used to characterize the gel formation. It was carried out as follows: prepared hydrogels were immersed in methanol for 24 hrs, and then were dried at room temperature for one week. Dried hydrogel samples were ground to powder, mixed with KBr, and compressed into KBr pellets. FTIR spectra were then recorded with a *Thermo Scientific IR100 FT-IR Spectrometer*.

3.4.2 Swelling test

Dried hydrogels were weighed and immersed in vials containing PBS buffer (pH = 7.4) at room temperature. At predetermined time interval, the hydrogels were taken out from

solution, any visible surface moisture was wiped off, and the weight was recorded. Then the hydrogel was returned to the vial and the uptake of buffer was measured until the mass do not change within 24 hrs. The percentage amount of buffer absorbed was calculated using the following formula [78]:

$$\text{Water (\%)} = (W_t - W_0) / W_0 \times 100 \%,$$

Equation 3.1 The equation for calculation of hydrogel swelling ratio

Where W_t is the weight of hydrogels at weighing time and W_0 is the weight of dry hydrogel. All swelling ratio results were obtained from triplicate samples

3.4.3 *In vitro* degradation of hydrogel

The reductive degradation tests of hydrogels were conducted using the sample with its saturated water absorbance statue. Hydrogel G1'-b was selected as a typical samples. Hydrogels were cut to dish-like shape with diameter in 10 mm and thickness in 2 mm. Samples were blotted with filter papers to remove surface water, and immersed in PBS buffer (pH = 7.4) with 0.1 mM or 10 mM DTT at 37 °C. At each time interval, the hydrogels were taken out from buffer. Any visible surface moisture was wiped off, and then before weighting. Afterward, the hydrogel was returned to the vial. The percentage of weight remaining was calculated using the following formula [91]:

$$\text{Wet Weight remaining (\%)} = W_t / W_0 \times 100 \%$$

Equation 3.2 The equation for calculation of wet weight remaining of degraded hydrogels

Where W_t is the weight of hydrogels at weighing time and W_0 is the initial weight of hydrogel at maximum mass in water. All swelling ratio results were from three samples ($n=3$).

3.4.4 *In vivo* degradation of hydrogels

The G1 hydrogels were cut into 10×5mm (diameter × height) discs and were stored in PBS solution until subcutaneous implanted. 18 male Sprague Dawley rats (250±50 g body weight) were anaesthetized with intraperitoneal chloral hydrate (400 mg/kg), the dorsal surface were shaved, disinfected and prepared for surgery. The skin was incised, small pockets were created with blunt dissection, then filled with hydrogels (6 independent sites per animal), and skin was sutured. After periods of 1, 2 and 3 weeks of implantation rats were anaesthetized as previously described, the original wounds reopened and the remaining gels in the rat were taken out using forceps and scissors for analyses of weight and diameter. For H&E staining, hydrogels with the surrounding tissues were retrieved, fixed in 4% paraformaldehyde solution at 4 °C for 48 h, processed for paraffin sectioning, and stained with hematoxylin-eosin technique.

3.4.5 Morphology of hydrogel

The freeze-dried morphology of the hydrogel OS was examined under scanning electron microscopy (SEM, Cambridge Stereoscan 120) with accelerating voltage 20 kV. The swollen hydrogel samples at their maximum swelling ratio in distilled water were quickly frozen in liquid nitrogen and then freeze-dried for 3 days. The freeze-dried samples were treated with liquid nitrogen again[169] and were cut and mounted on metal stubs using a double-sided adhesive tape and vacuum-coated with a gold layer prior to examination.

For partially degraded hydrogel morphology (G1 and G2), cryosection technology is used. Before cryosection, the hydrogel was immersed in PBS overnight after 10 days in vitro degradation. Then, hydrogel was incubated in BODIPY® FL phalloidin solution for 1 hr at room temperature followed by three times of PBS wash. Embed stained hydrogel in half-filled cryomolds by O.C.T. compound, and then full fill the cryomolds by O.C.T. compound further. The cryomold was put under -20° C until O.C.T compounds became translucent, and then was transferred to -80° C for overnight. Remove the frozen block from the cryomold and mount it on the cryostat to collect the slides.[170]. Cryosection was used to visual hydrogel cross-section morphology as well.

3.4.6 Mechanical properties of hydrogels determined by texture analyzer

Stiffness of hydrogels (G1 and G2) was tested by TA.XT2i Texture Analyzer (Texture Technologies Corp.). Briefly, hydrogels were cut to dish-like shape for consistent size and geometry (diameter=5 mm and thickness=2 mm). The test speed was 0.5 mm/second. All measurements were carried out at room temperature. The stiffness of the swollen hydrogels was obtained from Analyzer software. Sample size of each group is 3 (n=3).

3.4.7 Mechanical property of OS and D-OS hydrogels

Hydrogel viscosity and storage\loss modulus were obtained from Advanced Rheology (AR 2000 TA Instruments) rheometer at room temperature. The storage\loss modulus was tested after viscosity test. The sample volume was 200ul in total.

3.4.8 *In Vitro* drug release from D-OS

A cylinder-shaped D-OS with size of 6 mm diameter × 10 mm length (~150 ul) was immersed in 15 ml PBS at pH 5, 6.8 or 7.4 at 37 °C in water bath without any shaking to mimic *in Vivo* drug release gel in-situ. At predetermined time intervals, 3 ml of incubation solution was taken out and 3 ml of fresh PBS was added to refill the incubation solution to 15 ml. UV absorbance of DOX released in PBS buffers was recorded with a Varian Cary-50 UV-vis spectrophotometer at wavelength of 480 nm. Based on the method provided

above to prepare D-OS hydrogel, all drugs was incorporated in to hydrogel, the Drug loading efficiency of D-OS was always 100% by default.

3.5 Biological experiments of hydrogels for bone regeneration

3.5.1 Cell culture

Human myoblasts C2C12 cells (gifted from Dr. K Wrogemann, University of Manitoba), human dermal fibroblasts (HDF-2 from ATCC), Mouse bone marrow stromal cells line (ATCC, USA) were cultured with Dulbecco's Modified Eagle's Medium (DMEM, GIBCO) supplemented with 10 % fetal bovine serum (FBS, GIBCO), 1.0×10^5 U/l penicillin (Sigma) and 100 mg/l streptomycin (Sigma) at 37 C in 5 % CO₂. Mouse pre-osteoblasts (POB from ATCC) were cultured in complete α -MEM medium containing 4 mM glutamine, supplemented with 10 % fetal bovine serum (FBS, GIBCO), 1.0×10^5 U/l penicillin (Sigma) and 100 mg/l streptomycin (Sigma) at 37 °C in 5 % CO₂.

3.5.2 Cell growth on hydrogels

Hydrogels (G1 and G2) for cell culture were made between two glass cover slips (22 mm \times 22 mm) by adding 70 ul gel precursor solution. After gelation under 37 °C for 5 mins, both cover slips were removed and then the gel was thoroughly washed with sterilized PBS solution for 3 times and cell culture medium for 3 times to remove

chemical residuals. Hydrogels were then irradiated under UV light in a bio-safety hood for 30 mins. Finally, the gels were placed in cell culture dishes (35 mm × 10 mm) whose bottom were coated with agarose gel to inhibit cell adhesion on dish surface.

3.5.3 Cell Viability of hydrogels

The gelation was first conducted in 96 well culture plates for 5 min at 37 °C. Pre-Osteoblast cells were used to test cell viability via MTT assay. Cells were first seeded onto the G1 hydrogels at a density of 1×10^4 cells/well in a 96-well culture plate. The culture media was changed every 2 days. At the designated time, 10ul MTT reagent was added to each well and further incubated for 4 hrs. Then the solution was removed from the well and formazan crystals were dissolved in 200 ul of DMSO and the absorbance was measured at 570 nm (n=3).

BMSCs cytotoxicity on hydrogel G1 with different stiffness were evaluated using Live/Dead staining according to protocol from Invitrogen Canada Inc. Hydrogel for cell culture was made between two cover slips according to the method described previously. BMSC Cell cultures were performed using G1 hydrogels for different time points before being stained. Cells with hydrogel were incubated in cell culture medium containing 2 μ M calcein AM and 4 μ M ethidium homodimer probes for 20 mins. Portions of disks were rinsed with PBS and imaged by a confocal laser scanning microscopy (CLSM) (Olympus FV1000, Japan).

3.5.4 Cell morphology investigation

The morphologies of C2C12, HDF-2, Pre-Osteoblast and BMSCs on hydrogels were investigated using CLSM. The hydrogels laden cells were fixed with 4 % paraformaldehyde solution at room temperature for 20 min. After washing with PBS, samples were permeabilized using 0.5 % Triton X-100 in PBS solution at room temperature for 5 min. They were then blocked in 1 % bovine serum albumin PBS solution at room temperature for 10 min. The sample was incubated in BODIPY® FL phalloidin solution for 20 mins at room temperature. The cell nuclei were stained with TO-PRO3.

3.5.5 Quantitative Real-time PCR analysis

One hundred microliter mouse bone marrow stromal cells(BMSCs) in medium at cell density of 2×10^6 cells/ml was seeded onto the hydrogels G1 with different stiffness and are allowed to settle for 2 hrs. Then, 2ml medium were added to the disk. After 2 days, cell-encapsulating hydrogels were transferred to FBS-supplemented DMEM containing a combination of osteogenic chemical supplements: 50ug/ml L-ascorbic acid 1-phosphate(Sigma), 10mM β -glycerophosphate(Sigma) and 100nM dexamethasone(Sigma). Gels with cells are return to incubator for various time points. The osteogenic medium were changed for every 2-3 days. At predetermined time intervals, the medium were aspirated with the unattached cells and the wells were washed with DPBS. Then, cells on hydrogels were treated by liquid nitrogen and smashed. In order to validate

the gene expression of osteogenic differentiation in all samples, total RNA isolation and cDNA synthesis were done by using TRIzol and Oligo dT (Invitrogen, USA), according to the standard procedures. Then quantitative Real-time PCR (qPCR) was performed by SYBER Green assays (Applied biosystems, USA). Amplification conditions were as follows: Hold in 95 °C for 10 mins, followed by 40 cycles at 15 seconds in 95 °C and 1 min in 60°C. Thermal cycling and fluorescence detection were done using the StepOnePlus™ Real-Time PCR System (Applied biosystems, USA). The mRNA expression levels were determined relative to the GAPDH by the Δ Ct method. Primer sequences were as synthesized as showed in Table 3.2.

Table 3.2 Sequences of primers for the RT-PCR

Gene	Forward primer sequence	Reverse primer sequence
BSP	5'-ccacactttccacactctcg-3'	5'-cgtcgctttccttcacttttg-3'
ALP	5'-ctccaaaagctcaacaccaatg-3'	5'-attgtccatctccagccg-3'
OC	5'-acactctaaaggggtgcac-3'	5'-tcccatgctgtgaccctctagagg-3'
OPN	5'-ctacgaccatgagattggcag-3'	5'-catgtggctataggatctggg -3'
GAPDH	5'-aggtcgggtgtaacggatttg-3'	5'-tntagaccatgtagttgaggtca-3'

OC osteocalcin, BSP bone sialoprotein, OPN osteopontin, ALP alkaline phosphatase, GAPDH glyceraldehyde-3-phosphate dehydrogenase; GAPDH was used as an internal control.

3.5.6 Calcium deposits of cells cultured on hydrogels

Von Kossa staining was used to evaluation of calcium deposits in BMSCs seeded hydrogel. Hydrogels for cell culture were made between two cover slips according to the

method described previously. Cell cultures were performed using hydrogels G1 for various time points before being stained using Von Kossa Staining Kit based on the protocol from Polysciences, Inc. Briefly, hydrogels with cells were fixed in 4% paraformaldehyde for 30min, and then rinsed in three times of distilled water. Three percent Silver Nitrate Solution was used to treated hydrogels under 30 mins UV light. The calcium minerals absorbing the silver nitrate solution present dark brown to black. Hydrogels were rinsed in three times of distilled water again before hydrogels were placed in 5 % sodium thiosulfate for 2 mins. And then hydrogels were counterstained in Nuclear Fast Red for 5 mins after rinsed in three times of distilled water. Samples were dehydrated with ethanol and mounted on slides.

3.6 Biological experiments of hydrogels for cancer

therapy

3.6.1 Cell culture

Human breast cancer cell line MCF-7 was cultured with Dulbecco's Modified Eagle's Medium (DMEM, GIBCO) supplemented with 10 % fetal bovine serum (FBS, GIBCO), 1.0×10^5 U/l penicillin (Sigma) and 100 mg/l streptomycin (Sigma) at 37 °C in 5 % CO₂.

3.6.2 *In Vitro* cytotoxicity of OS and D-OS

MCF-7 was firstly seeded on 96-well cell culture plates at a density of 5,000 cells/well for 2 hr to allow cell attachment. The culture media was changed after attachment using fresh medium (pH 6.8 or 7.4). For cytotoxicity of OS and D-OS in normal physiological environment, the pH of cell culture medium was set at 7.4, and for cytotoxicity of OS and D-OS in weakly acidic environment mimicking tumour tissue, the pH of cell culture medium was adjusted to 6.8 by adding acetic acid.[160] Free DOX, OS, or D-OS was added to the well for the designated time followed by 10 ul MTT reagent treatment to each well for 4 hrs incubation. Then the medium and hydrogel were removed from the well and the formazan crystals were dissolved in 200 ul of DMOS and the absorbance was measured at 570 nm (n=6).

Cell incubated with D-OS was also evaluated using Live/Dead staining according to protocol from Invitrogen Canada Inc. Hydrogel was made between two plastic cover slips by using 100 ul gel precursor solution. After gelation under 37 °C for 5 mins, both cover slips were removed and then the gel was thoroughly washed with sterilized PBS solution for 3 times and cell culture medium for 3 times to remove chemical residuals. Then, MCF-7 cells are seeded on the hydrogel surface at a density of 100,000 cells/ml. To inhibit cell adhesion on dish surface, agarose gel was coated on dish bottom first, and then the MCF-7 cells cultures were performed using hydrogels for 1 day before being stained. For staining, cells with hydrogel were incubated in cell culture medium containing 2 µM calcein AM

and 4 μM ethidium homodimer probes for 20 mins. Hydrogels with cells were rinsed with PBS, dried, mounted on slides and imaged by CLSM (Olympus FV1000, Japan).

3.6.3 Cell morphology on OS and cellular uptake of DOX from D-OS

The morphologies of MCF-7 cells incubated with hydrogels OS were investigated using CLSM. The hydrogels laden cells were fixed with 4 % paraformaldehyde solution at room temperature for 20 min. After washing with PBS, samples were permeabilized using 0.5 % Triton X-100 in PBS solution at room temperature for 5 min. They were then blocked in 1 % bovine serum albumin PBS solution at room temperature for 10 min. The sample was incubated in BODIPY® FL phalloidin solution for 20 mins at room temperature. The cell nuclei were stained with TO-PRO3.

CLSM was also employed to examine the cellular uptake of DOX. The MCF-7 cells were seeded in the culture dish with a cover slip at a density of 10,000 cells/dish and culture 24 hrs. D-OS was added to dishes for further incubation. After predetermined incubation time, the cover slip was washed with cold PBS for three times, and cells cytoskeleton, nucleus were stained according to the method described previously. The cover slip was set on microscope slide and examined by CLSM.

3.7 Statistical analysis

All experiments were repeated three or more times with triplicate samples. Significant differences between two groups were evaluated using a one way analysis of variance (ANOVA) with 95 % confidence interval. When $P < 0.05$, differences were considered to be statistically significant.

4 Result and discussion

4.1 Hydrogel for bone regeneration

4.1.1 Synthesis and characterization of PAA crosslinker and hydrogel

The reductively degradability, enhanced cell attachment and tunable stiffness of the hydrogel was endowed by the PAA crosslinker. This novel PAA crosslinker was designed to contain disulfide bonds in the backbone and guanidine in the side chains. It was synthesized from CBA and AS via Michael addition reaction. (Figure 4.1) Disulfide linkages (ellipses in Figure 4.1) render the hydrogel degradable under a reductive environment [138]. Peptide RGD can promote cell adhesion[171]. In this work, Agmatine, a guanidine pendant (pentagons in Figure 4.1) combined with an adjacent

carboxyl group (quadrangles in Figure 4.1) from an acrylic acid mimics RGD [93] to enhance cell adhesion.

The chemical structure of PAA (Figure 4.2) was confirmed by ^1H NMR spectra (Figure 4.3). The integral of peaks at 5.7 and 6.2 ppm represents the vinyl bonds residual in the polymers [172]. The molecular weight of PAA was calculated to be about 869 based on the integral of the peaks at 1.56 (attributed to methylene groups in agmatine), and 6.2 and 5.7 ppm (from the residual vinyl groups at the end of the synthesized PAA crosslinker). The vinyl residual as end group was involved in radical polymerization and served as a macromolecular crosslinker.

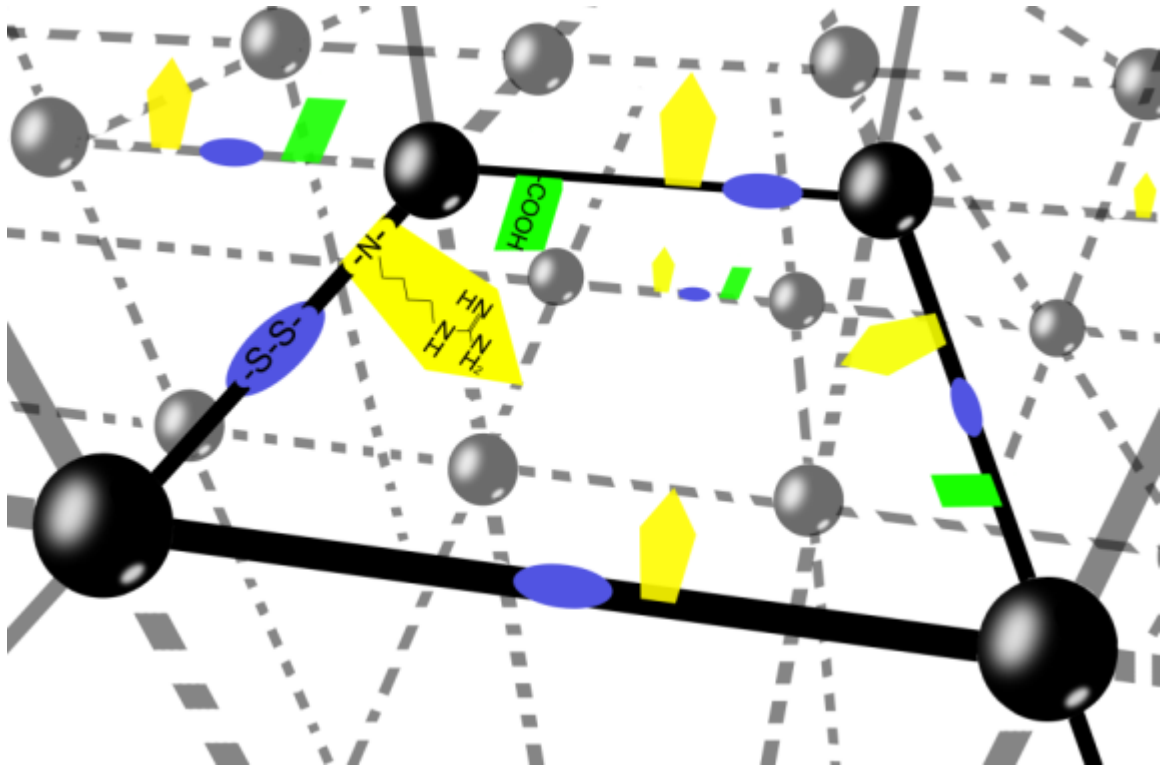


Figure 4.1 Schematic illustration of preparation of G1 hydrogel ; Disulfide group (blue ellipse) can be cleaved under reductive environment and then make the hydrogel degradable; Argmatine group (yellow pentagon) and carboxyl group (green quadrangle) can form RGD mimicking repeat units.

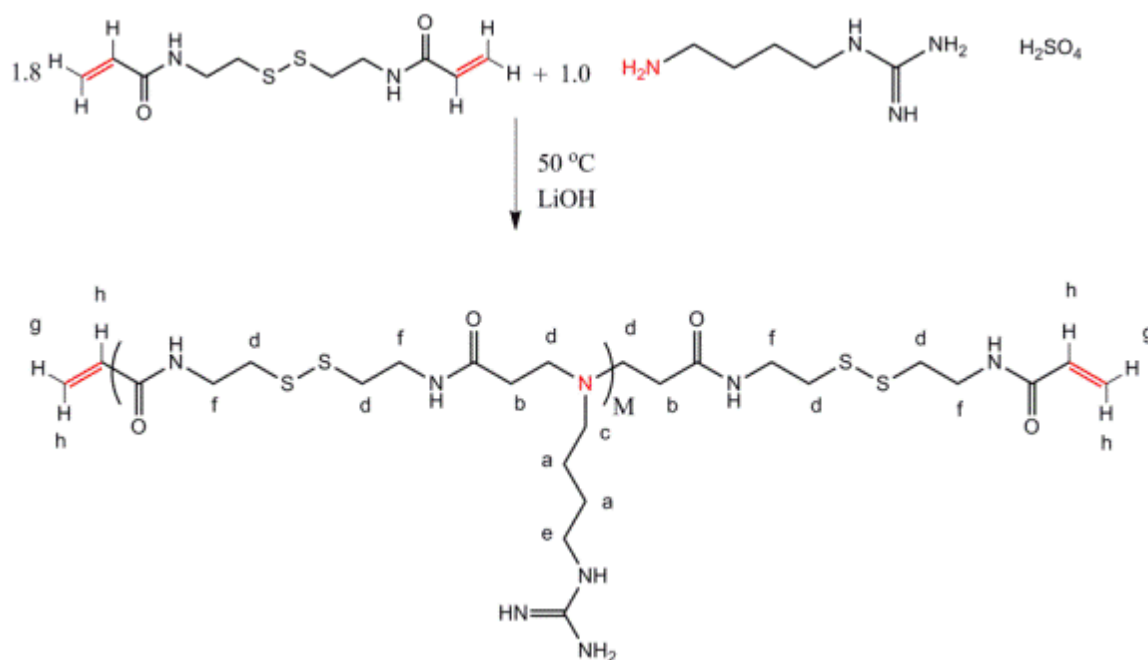


Figure 4.2 Synthesis and characterization of cell-adhesive and bio-reducible PAA crosslinker

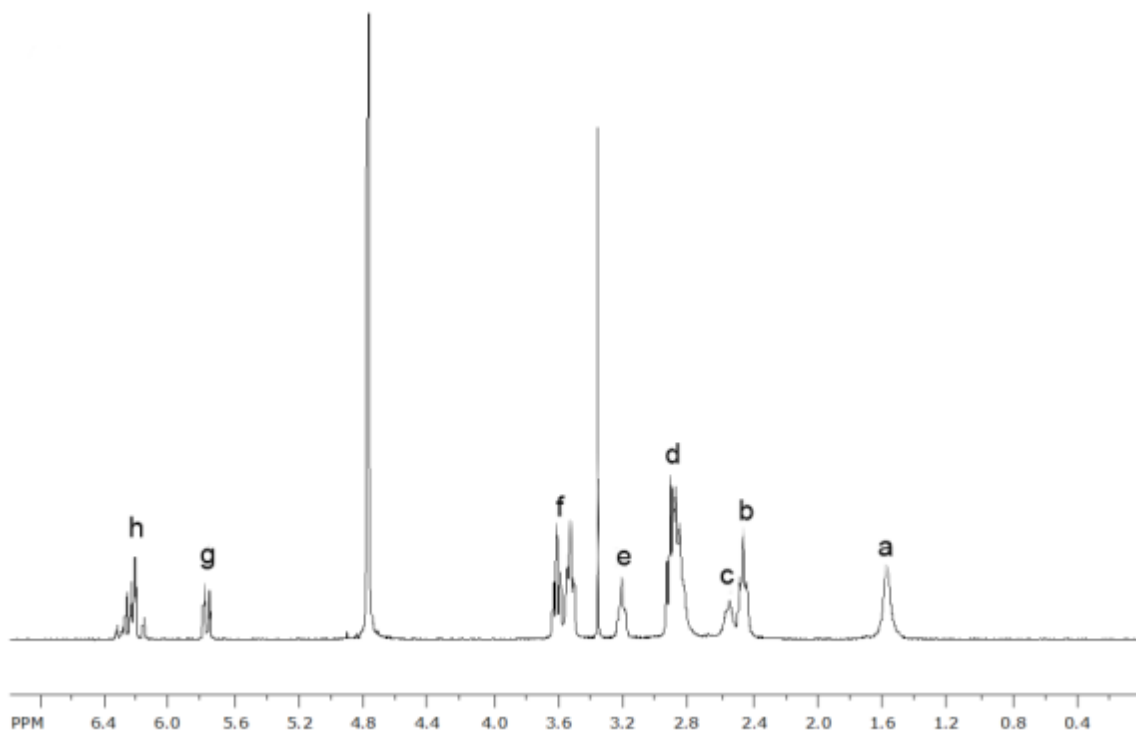


Figure 4.3 ^1H NMR spectrum of PAA crosslinker

Fourier transform infrared spectroscopy (FTIR) analysis was conducted on the prepared hydrogels to verify their structures. As shown in Figure 4.4, a strong band at $\sim 1730\text{ cm}^{-1}$ in the spectra of G2 and G1 hydrogel spectrum was attributed to the C=O stretching frequency from ester groups. However, for the G1 hydrogel (Figure 4.4 b), two new peaks appearance at $\sim 1660\text{ cm}^{-1}$ and $\sim 1544\text{ cm}^{-1}$ attributed to the C=O vibration of the conjugated amide groups (amide I and II bands respectively) in PAA crosslinker. The result shows the successful conjugation of PAA into hydrogel G1.

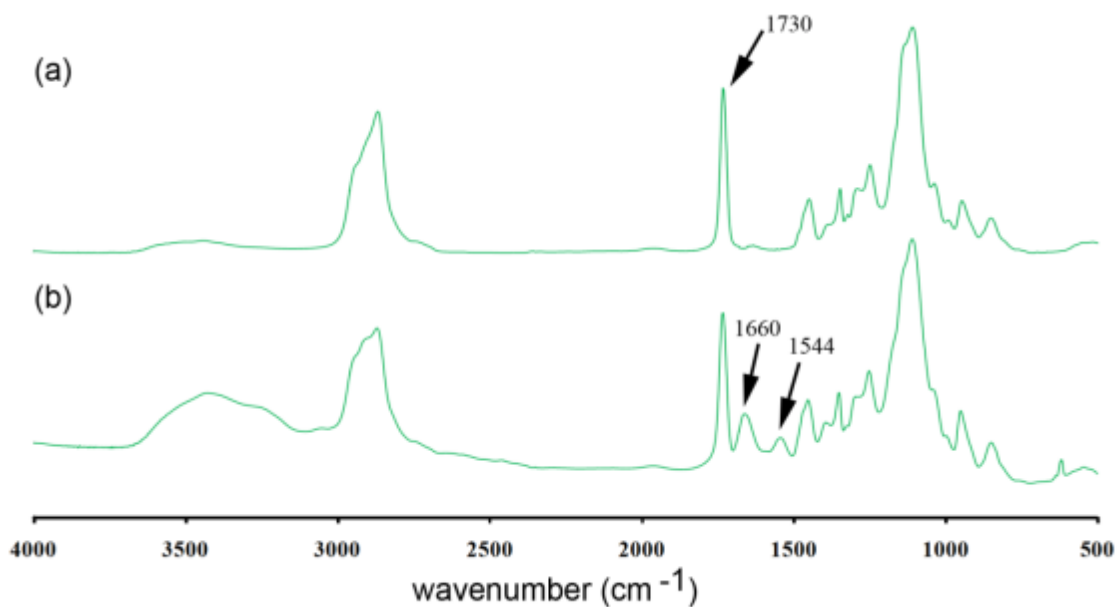


Figure 4.4 FTIR spectrum of (a) Hydrogel G2-b and (b) hydrogel G1-b

4.1.2 Swelling test

The capacity to present volume changes in response to external stimuli is a critical property of a hydrogel [173]. The swelling property of a hydrogel dramatically affects the cell viability in a synthetic hydrogel ECM by influencing the diffusion area of nutrients. [53]. The water holding capacity of a hydrogel is depicted as the ratio of the mass of water that has been absorbed by the hydrogel at a specified time to the mass of a dehydrated hydrogel using Equation 3.1 [78]. As shown in Figure 4.5, the swelling ratio of both G1 and G2 hydrogels decreased with the increase of the concentration of precursor solutions for preparing G1 and G2. This result is consistent with previous reports which suggested that a hydrogel with a lower crosslinking density has a better water storage efficacy than a

hydrogel with higher crosslinking density [1, 93]. Adding PAA crosslinkers into hydrogels does not affect gel swelling behavior significantly at low precursor solution concentration (62 mg/ml and 124 mg/ml). However, when the concentration is increased to 248 mg/ml, G1 hydrogels exhibited a better swelling behavior during four days observation. It may indicate the PAA crosslinkers have good hydrophilicity as the larger molecular weight resulted in the reduction of crosslinking density.

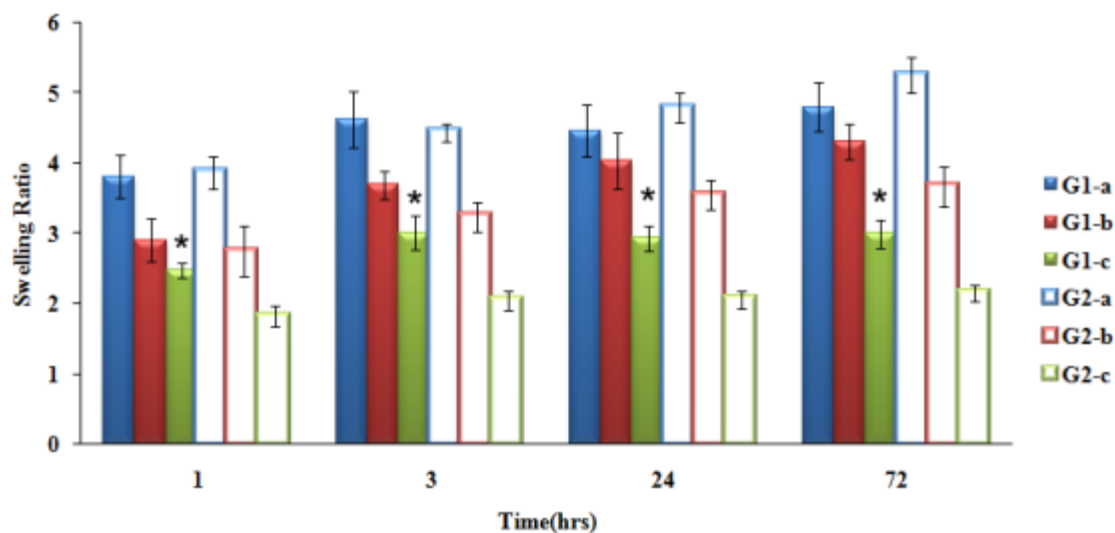


Figure 4.5 Swelling ratio of hydrogels at different precursor solution concentrations; G2 hydrogels are served as control groups (containing no crosslinker) at same concentration.

(n=3) “*” means $p < 0.05$ vs the control group

4.1.3 Degradation profile of hydrogels

Hydrogel as TE scaffold requires a controllable degradation to meet specific requirements for different tissues[174]. Disulfide bonds can be cleaved by endogenous thiols in a reducing environment [55] such as human plasma with a GSH level of about 10 μM , free reduced homocysteine level of about 0.1–0.35 μM , and with a free cysteine level of about 5 μM [172].

Concentrations of the reductive reagent GSH are known to be at the level of micromolars in the extracellular environment but at millimolars in the various subcellular organelles in cytoplasm. Recent reports also suggested the possibility of a large pool of reductive groups results on varieties of proteins in various types of cells[175]. Disulfide bonds in the network of a hydrogel are susceptible to be reductively degraded in a reducing intracellular environment, but remaining stable in a oxidizing environment. Glutathione (GSH) and dithiothreitol (DTT) are water-soluble reducing agents which have been used to degrade disulfide-containing polymers.[95, 176, 177] In this study, a PBS solution (pH 7.4) of dithiothreitol (DTT) was selected to mimic the reductive environment *in vivo* for the *in vitro* degradation study of the hydrogels. The amount of disulfide bonds in G1 hydrogels is controlled by varying the mass ratios of PAA to other monomers (PEGDA: PAA: acrylic-acid = 100:5:1 and 100:20:4). 0.1 mM and 10mM DTT solutions were utilized for degradation tests.

The degradation profiles of G1 hydrogels are illustrated in Figure 4.8 by plotting the remaining wet weight (%) vs. time. G1-b hydrogel (PEGDA: PAA: acrylic-acid =

100:5:1), showed no significant weight change during incubation with 0.1 mM and 10 mM DTT. However, G1'-b hydrogel (PEGDA: PAA: acrylic-acid = 100:20:4) displayed significant weight loss during its incubation with DTT. G1'-b hydrogel lost about 50 % of its wet weight (50 % wet weight remaining) during incubation in 10 mM DTT and lost about 15 % of its wet weight (85 % wet weight remaining) in 0.1 mM DTT over a period of 10 days. Four photos of degraded hydrogel G1'-b at different time points are taken to preliminarily show the morphology change while treated by 10 mM DTT. As shown Figure 4.6a, after 1 hr incubated in 10mM DTT, the hydrogel still have an even surface and almost complete gel block. After 2 days, the edges of gel started to be degraded, but the surface did not change much. (Figure 4.6b) On day 5, the edges of hydrogels kept being degraded, and the surface became rough and undulates. (Figure 4.6c) The distinct decreased volume of the hydrogel was observed on day 10 with the loss of mass (Figure 4.6d). As degradation proceeds, measurement and sample handling become increasingly difficult. So a degradation period of only 10 days was tested in which wet weight of hydrogel can still be measured without losing exactitude [91].

After being incubated in 0.1 mM and 10 mM DTT for 10 days, cryosection of G1'-b hydrogels were prepared to monitor hydrogel inner morphology. Different sizes of micro-scale porous structures were observed as shown in Figure 4.7. Such a structure was caused by the degradation that had been induced by the disulfide bond cleavage. This approach was first used by Chen *et. al.* to create a porous polyelectrolyte multilayered films. [176] Furthermore, the pore size of the hydrogel treated with 10 mM DTT is much larger than that of the hydrogel treated with 0.1 mM DTT. Therefore, the size of the pores created by

disulfide bond cleavage can be controlled by varying the concentration of the reductive agent. This micro-porous structure might be used to facilitate 3D ingrowths of cells in TE scaffolds.[178, 179]

In vivo degradation tests were further conducted in mice for up to 3 weeks. Figure 4.9 shows the time course of remaining hydrogel *in vivo*. About 80 % of the weight was retained in the implanted G1 hydrogel (PEGDA: PAA: acrylic-acid = 100:5:1) on day 21, and about 60% in G1 hydrogel (PEGDA: PAA: acrylic-acid = 100:20:4). At day 7, 14, and 21, H&E staining was used to monitor interactions between hydrogels and their surrounding tissues. As shown in Figure 4.10 to Figure 4.15, fibrous tissue can be found to form around the hydrogels, the thickness of the fibrous tissue encapsulation was different among G1 hydrogels with different PAA concentrations. The G1 hydrogel with higher PAA concentration was shown to promote cell expansion more efficiently. Compared to G1 hydrogel (PEGDA: PAA: acrylic-acid = 100:20:4), G1 hydrogel (PEGDA: PAA: acrylic-acid = 100:5:1) showed limited cell penetration and moderate extent of degradation, leaving behind a largely intact hydrogel. The extent of degradation and disintegration gradually diminished from the periphery towards the interior of the bulk hydrogel. The capsules surrounding both hydrogels contained little neutrophils, macrophages and mast cells, and no obvious inflammatory response was observed. The hydrogels are biocompatible within the mammalian subcutaneous environment.

It has been reported that the cleavage of disulfide bonds in polymers results in the formation of corresponding thiols, leading to weight loss of the hydrogel [177] . Our data concur with other studies on that both the DTT concentration and monomers' mass ratios

(which determine the amount of disulfide bonds) determine the degradation rate of G1 hydrogels.

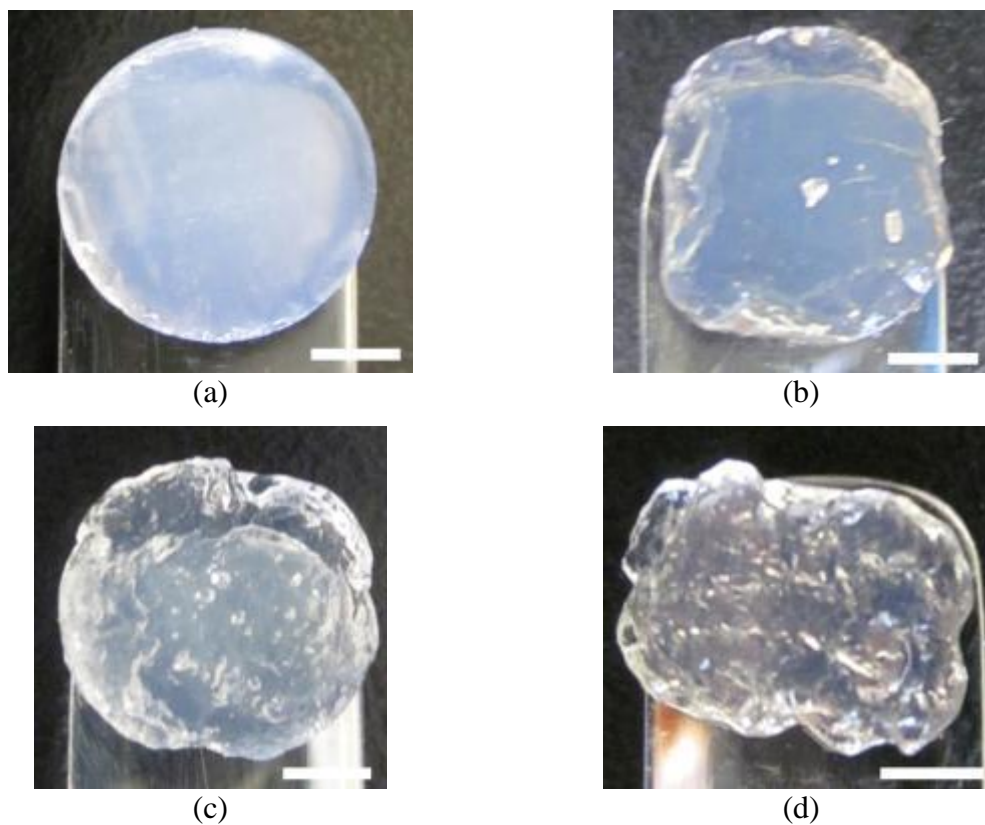
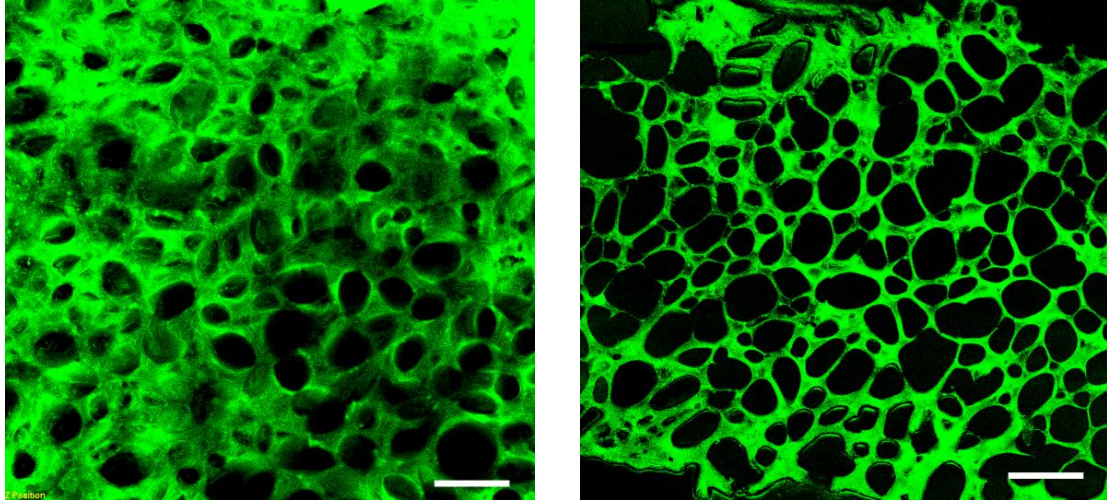


Figure 4.6 Photographs of hydrogel G1'-b underwent degradation with 10 mM DTT over (a) 1 hr, (b) 2 days, (c) 5 days, (d) 10 days. (Scale bar is 3mm)



(a)

(b)

Figure 4.7 Cryosection images of partially degraded hydrogels G1'-b underwent degradation over 10 days in (a) 0.1 mM DTT and (b) 10 mM DTT. Scale bars represent 200 μ m for both images

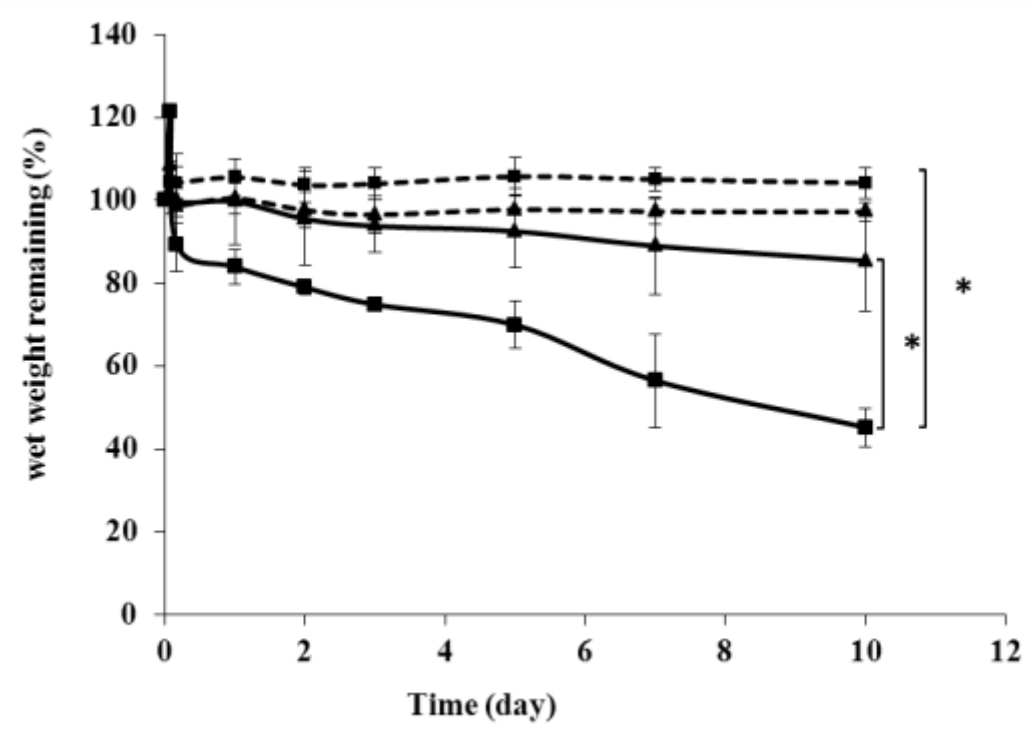


Figure 4.8 *In vitro* reductive degradation profile of G1-b (Dash line) and G1'-b (Solid lines) hydrogel incubated in 0.1 mM (triangles) and 10 mM (cubes) DTT (n=3)

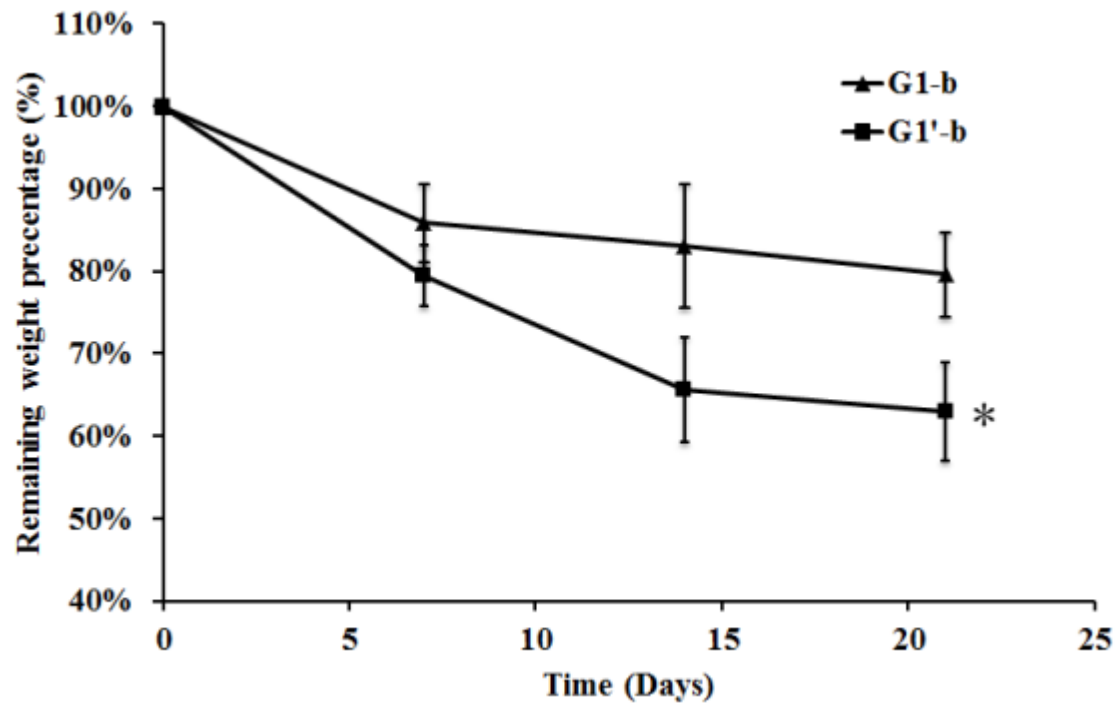


Figure 4.9 *In vivo* reductive degradation profile of G1-b and G1'-b hydrogel (n=6)

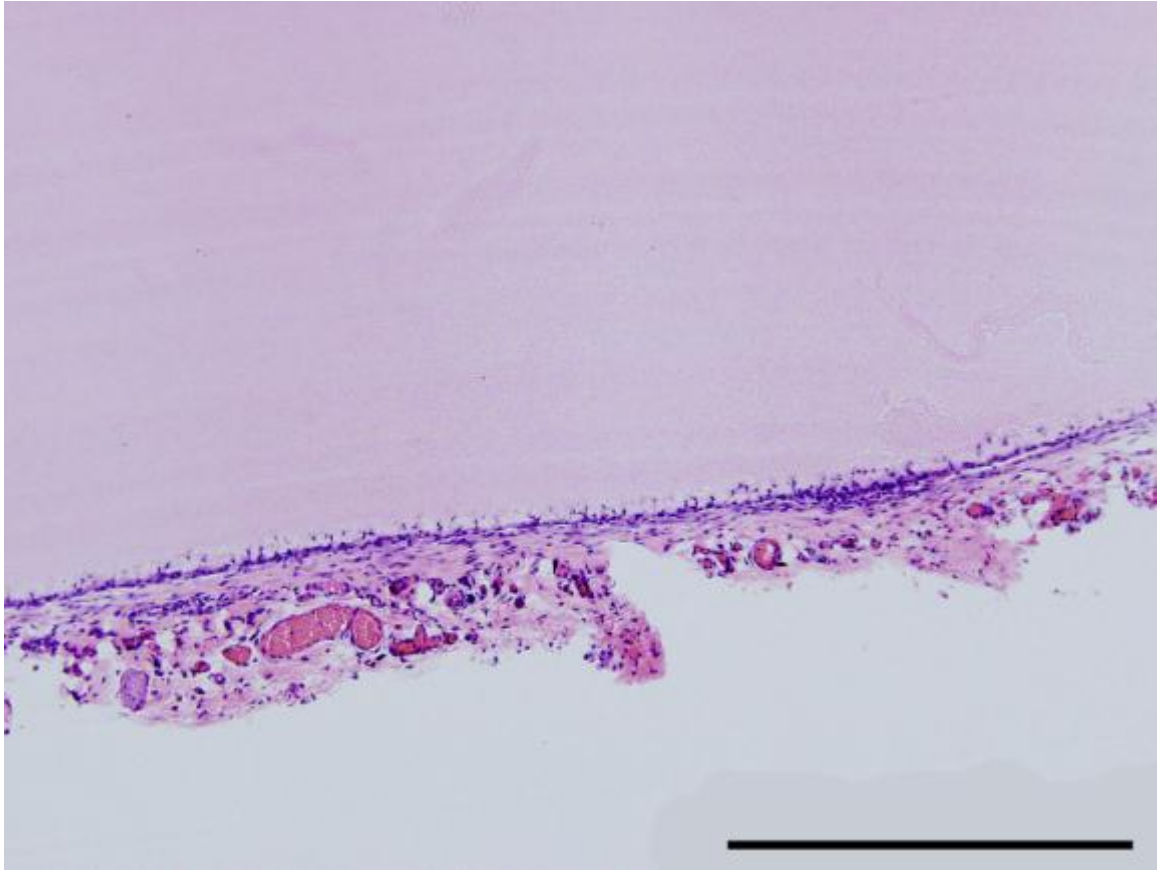


Figure 4.10 H&E staining of fibrous tissue surrounding hydrogel G1-b after 7 days; scale bars represent 200 μm

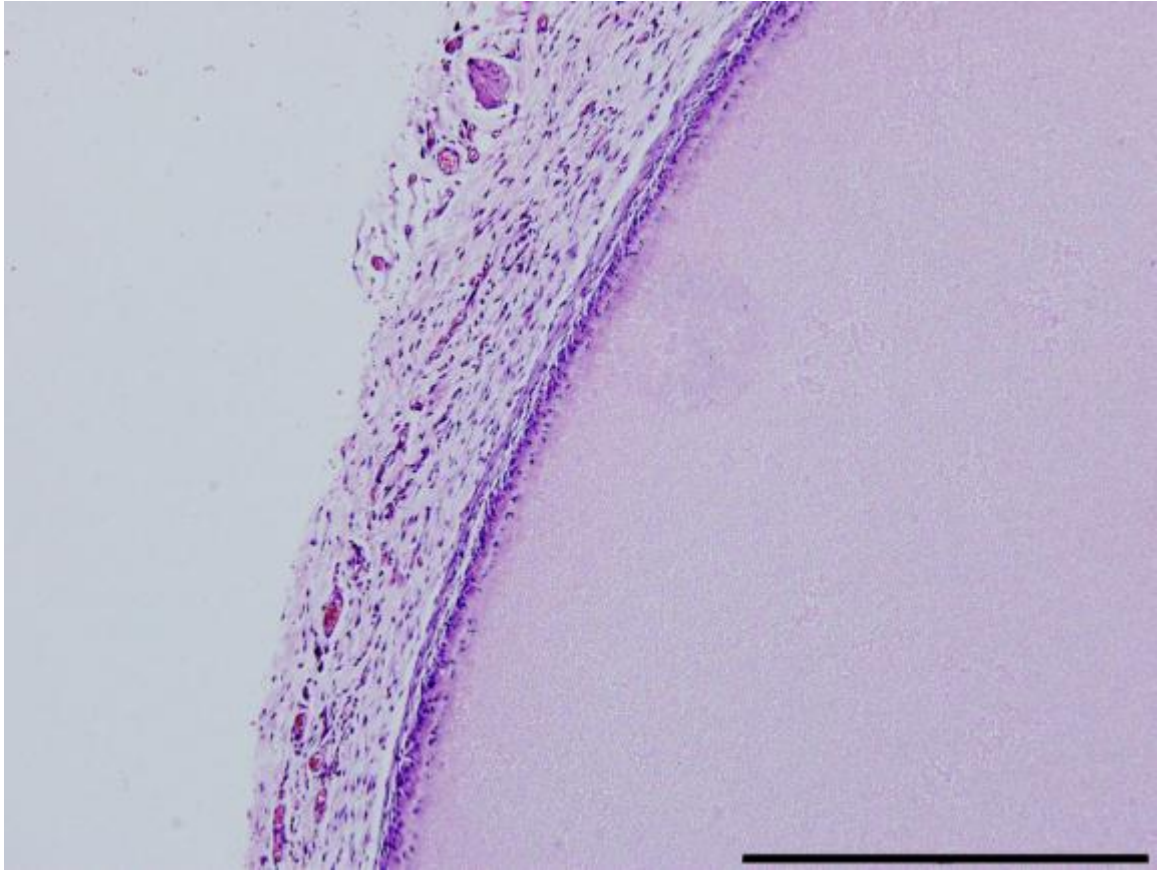


Figure 4.11 H&E staining of fibrous tissue surrounding hydrogel G1-b after 14 days;
scale bars represent 200 μm

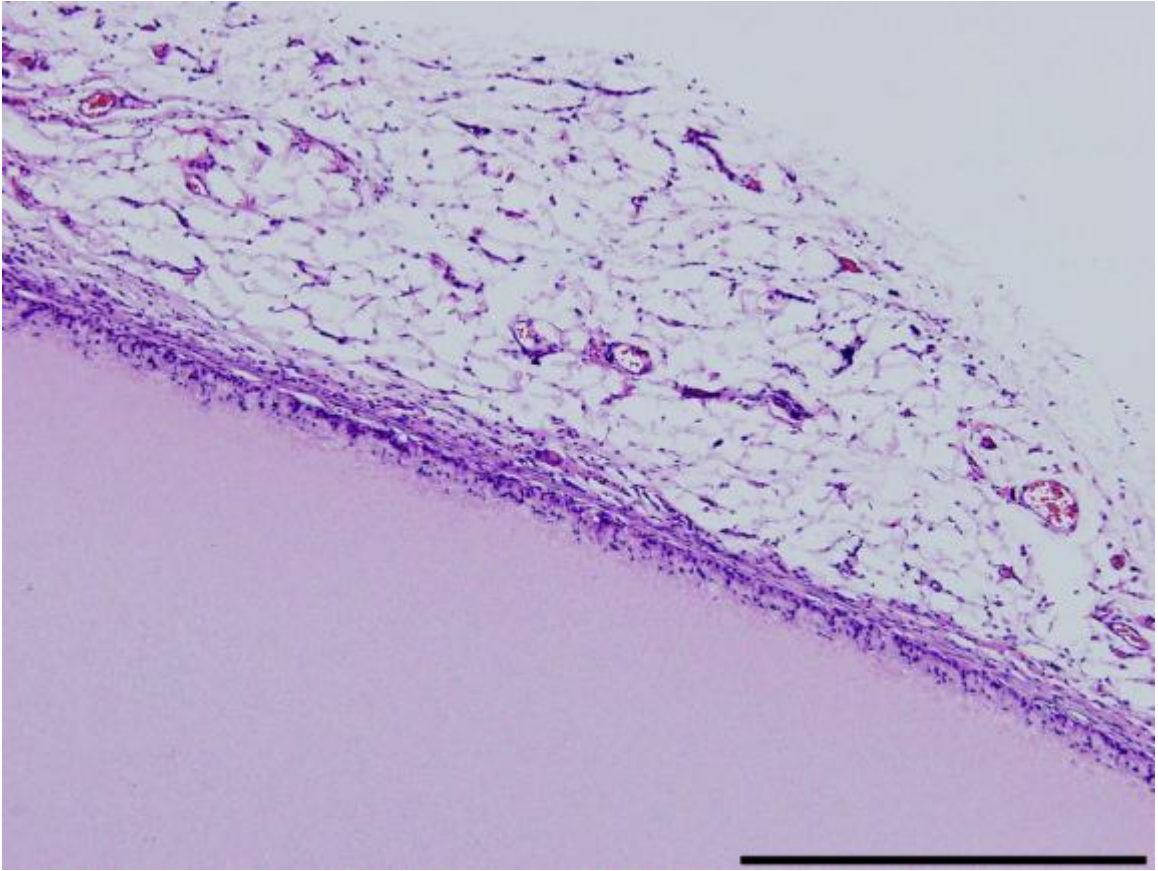


Figure 4.12 H&E staining of fibrous tissue surrounding G1-b after 21 days; scale bars represent 200 μm

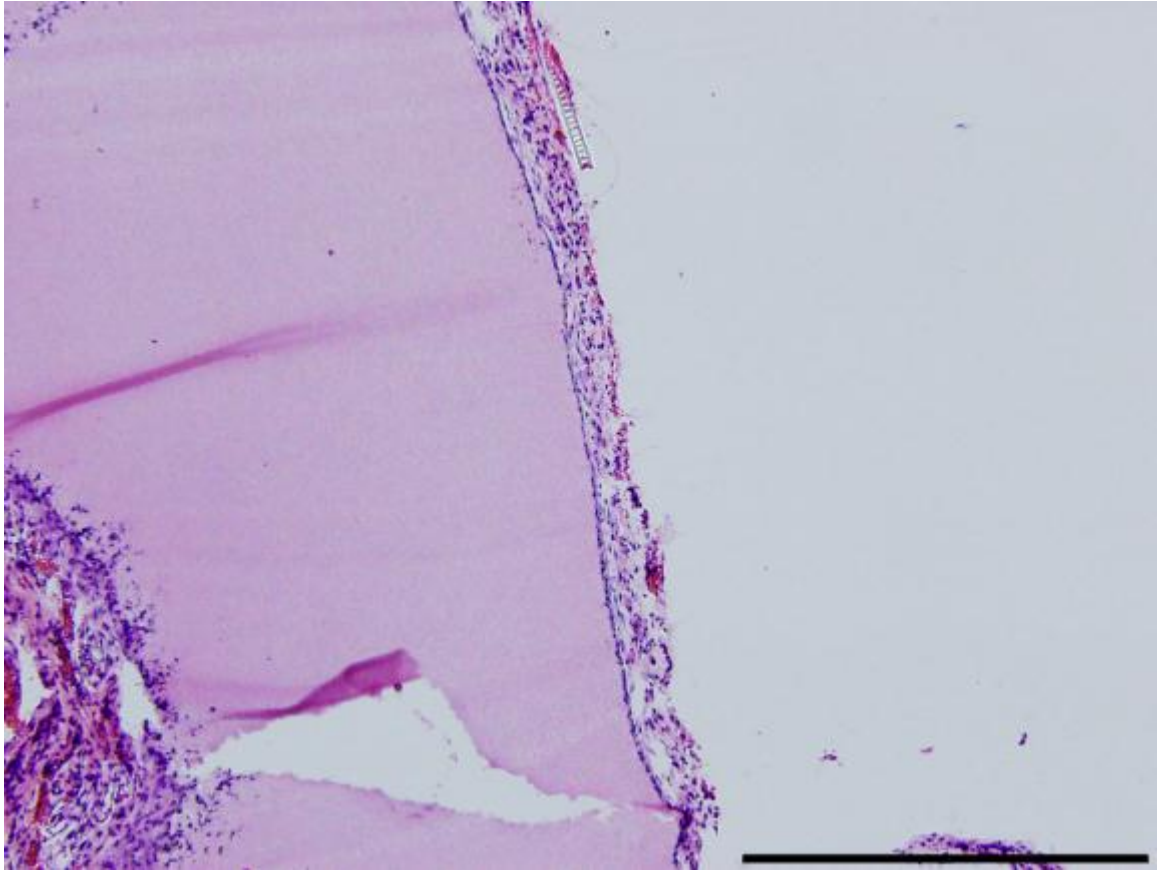


Figure 4.13 H&E staining of fibrous tissue surrounding hydrogel G'1-b after 7 days; scale bars represent 200 μm

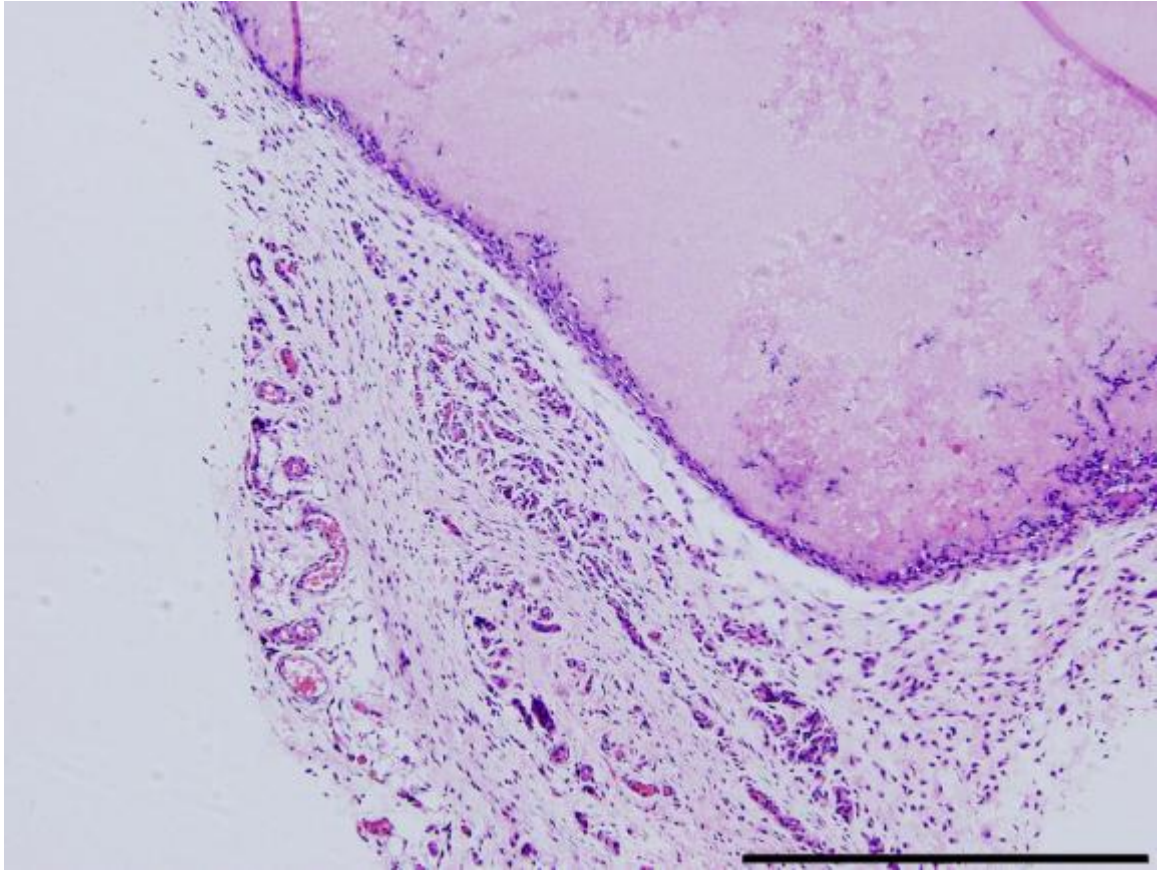


Figure 4.14 H&E staining of fibrous tissue surrounding hydrogel G1'-b after 14 days;
scale bars represent 200 μm

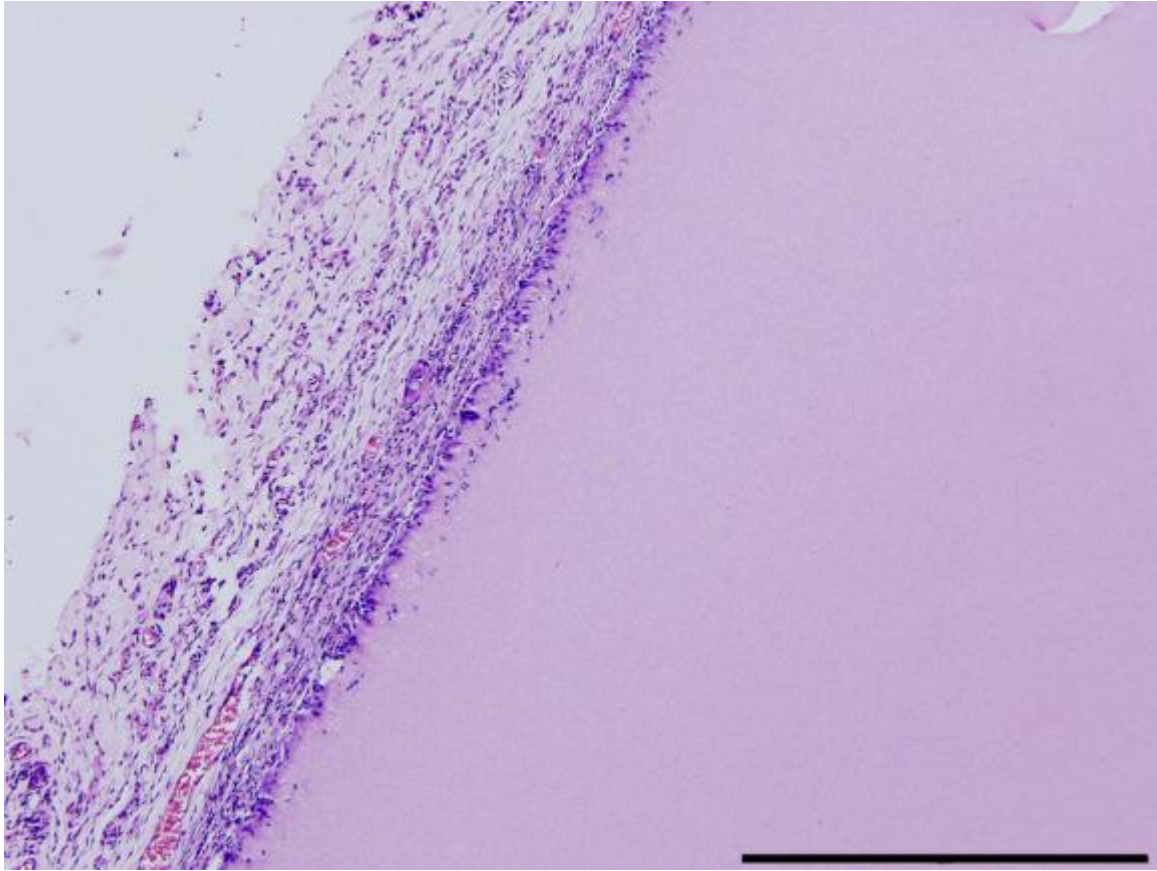


Figure 4.15 H&E staining of fibrous tissue surrounding G1'-b after 21 days; scale bars represent 200 μm

4.1.4 Analysis of mechanical properties of hydrogels

A main aspect of TE is to design biomimetic niche to regulate cell with differentiation into specific lineage [10]. Evidence reveals that, in addition to genetic and molecular mediators (e.g., growth factors, transcription factors), physical interactions between cells

and scaffolds also contribute to stem cell activity and fate [11]. It has been reported that the stiffness of local matrix has profound influence on the development, differentiation, disease, and regeneration of cells [12]. The stiffness of G1 hydrogels was designed to be tunable in this study. Their stiffness was evaluated by a texture analyzer via monitoring a force-distance curve in a compression model. (Figure 4.16). G2 hydrogels were selected as a control group. Stiffness (g/mm) was calculated from software. The concentration of precursor solution affects the crosslinking density [1] and consequently the gel stiffness. As shown in Figure 4.17, hydrogels prepared from different precursor concentrations exhibited significantly different stiffness. However, a G1 hydrogel showed no significant difference on stiffness from its G2 control sample at the two lower concentrations of 62 mg/ml and 124 mg/ml. It indicates that the amount of PAA does not affect gel stiffness at relatively low monomer mass concentration. However, when the concentration increased to 248 mg/ml, the stiffness of G1 hydrogel was about 500 g/mm, significantly lower than that of G2 hydrogel, which is about 900 g/mm.

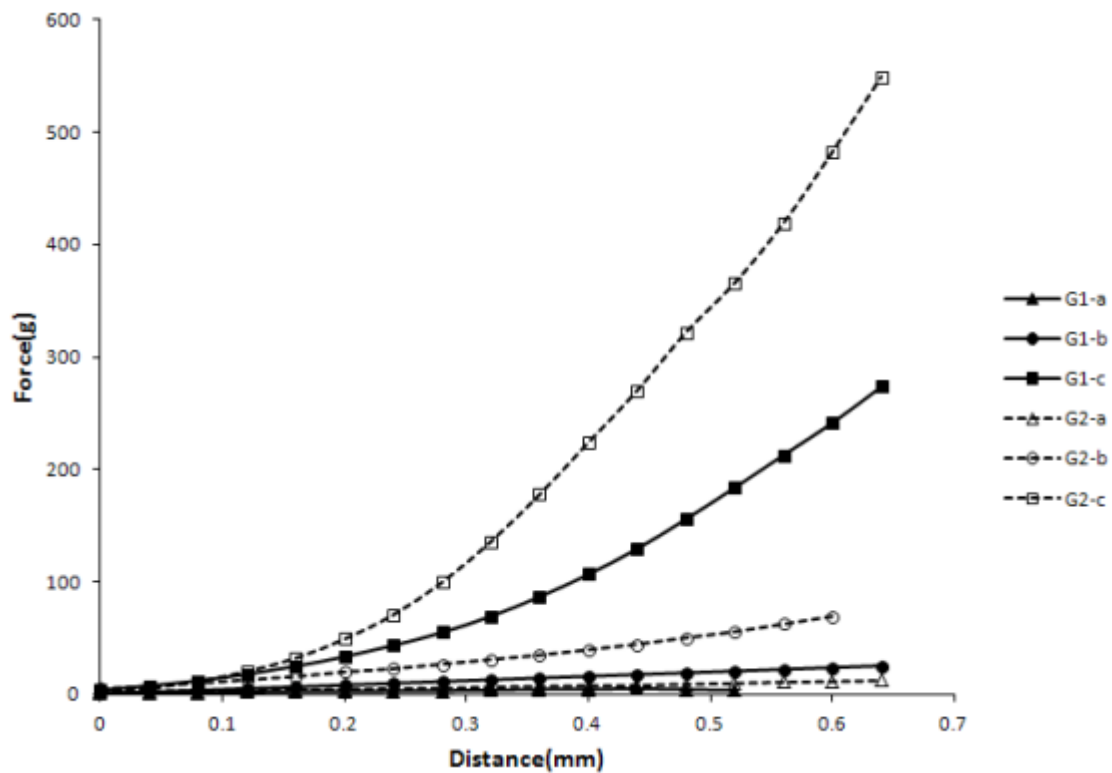


Figure 4.16 Typical Force–distance curves of hydrogels at different precursor solution concentrations.

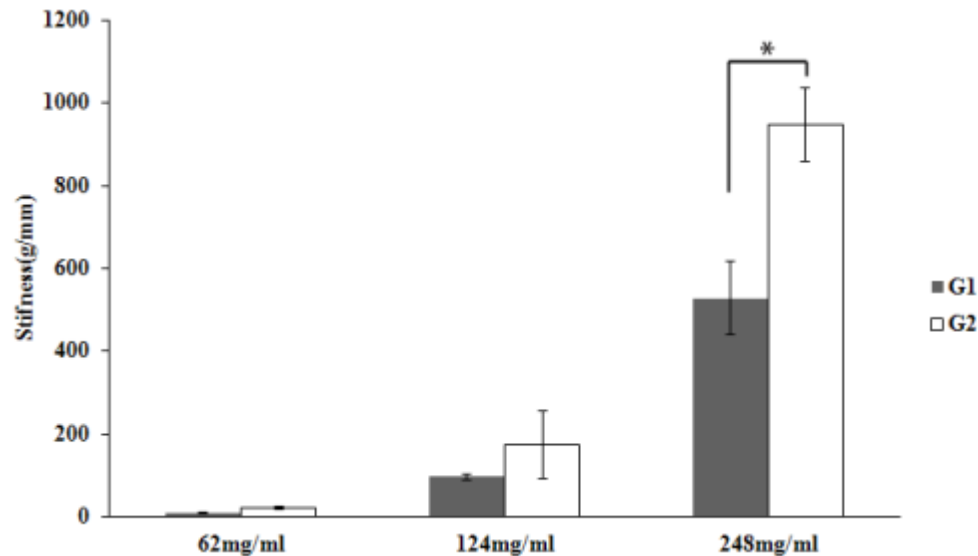


Figure 4.17 Stiffness of hydrogels at at different precursor solution concentrations; and hydrogels G2 were control group; (n=3)

4.1.5 Cell Viability

To evaluate cell viability on the developed hydrogels, pre-osteoblast cells were seeded on hydrogels and cultured for 2 and 7 days. The cell viability was evaluated by MTT assay. Viability of cells seeded on Tissue Culture Plates (TCPs) was normalized to 100 %. As shown in Figure 4.18 and Figure 4.19, higher cell viability was observed in G1 hydrogels than in G2 hydrogels after 2- and 7-day culture. The guanidine pendant combined with the adjacent carbonate group in acrylic acid mimics the structure of RGD and significantly promotes cell attachment. After one week, cell viability in the hydrogels containing PAA (G1) were comparable with cell growth on TCPS. (Figure 4.19) [94-96].

MTT assay is a preliminary method to evaluate cell viability on a material. Its result on hydrogels may not be valid if the cell population is low.[78], Cell viability of BMSCs cultured with hydrogel G1 was furthermore evaluated with Live/Dead staining since Live/Dead can differentiate live cells from dead ones under fluorescence microscopy. To show the long term cell viability and to evaluate cell proliferation, BMSCs were cultured on G1 hydrogels with different stiffness (G1-a and G1-b) for up to 28 days. After 7 days, almost 100 % of BMSCs on the soft hydrogel G1-a were alive (Figure 4.20). After 14 days, some dead BMSCs can be found in Figure 4.21 but most of them were still live cells. In addition, the number of BMSCs increased, and cells started to have contact with each other. This trend continued into day 28, with more than 90 % of the cells alive and appeared in a net-like morphology (Figure 4.22). After 7 days, most of the BMSCs on the stiffer hydrogel G1-b were alive. In addition, a much higher cell number and a more spreading out morphology were observed on G1-b as compared to the softer hydrogel G1-a, suggesting that there had been cell proliferation. (Figure 4.23) The live BMSCs on G1-b are still the major cell type on day 14, and as shown in Figure 4.24, it kept the spreading out morphology which was also observed in 7 days result (Figure 4.23). The cell numbers were not only increased on days 14 (Figure 4.24) but even higher on day 28 (Figure 4.25) at a very dense cell population with an overall spreading morphology.

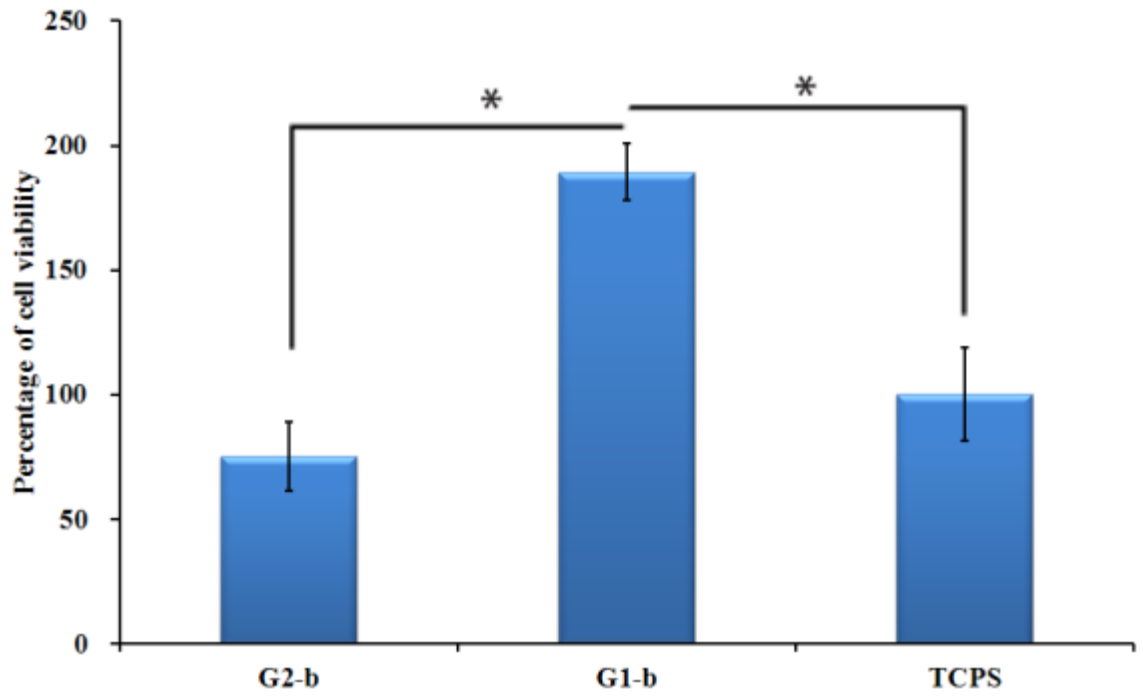


Figure 4.18 Cell viability of POB on hydrogel after 2days culture based on MTT assay
(absorbance is normalized to 1 for TCPS control sample); (n=6)

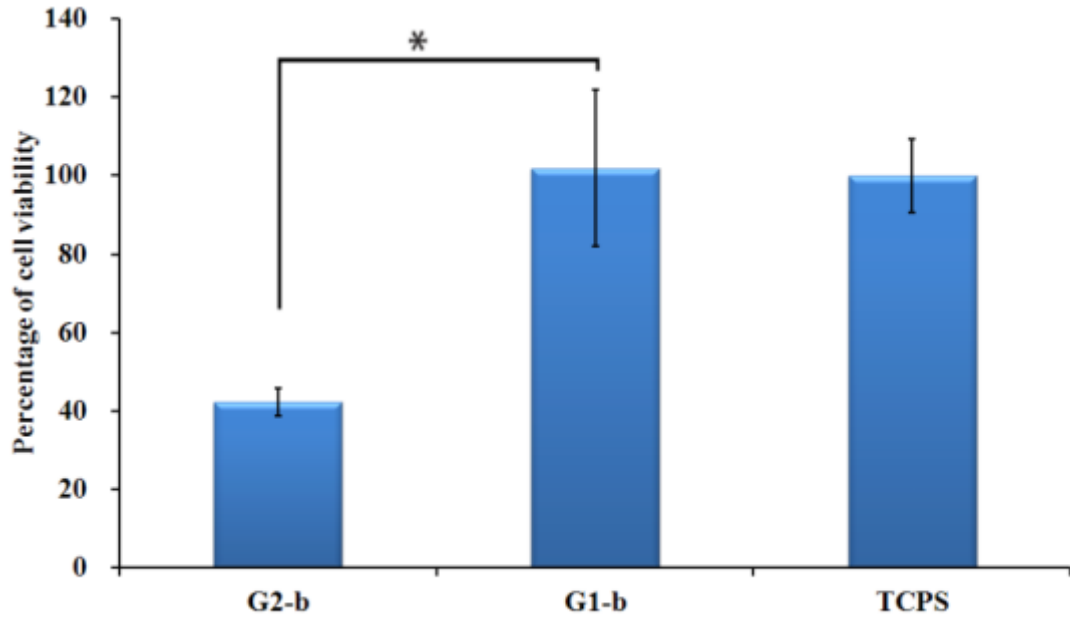


Figure 4.19 Cell viability of POB on hydrogel after 7days culture based on MTT assay
(absorbance is normalized to 1 for TCPS control sample); (n=6)

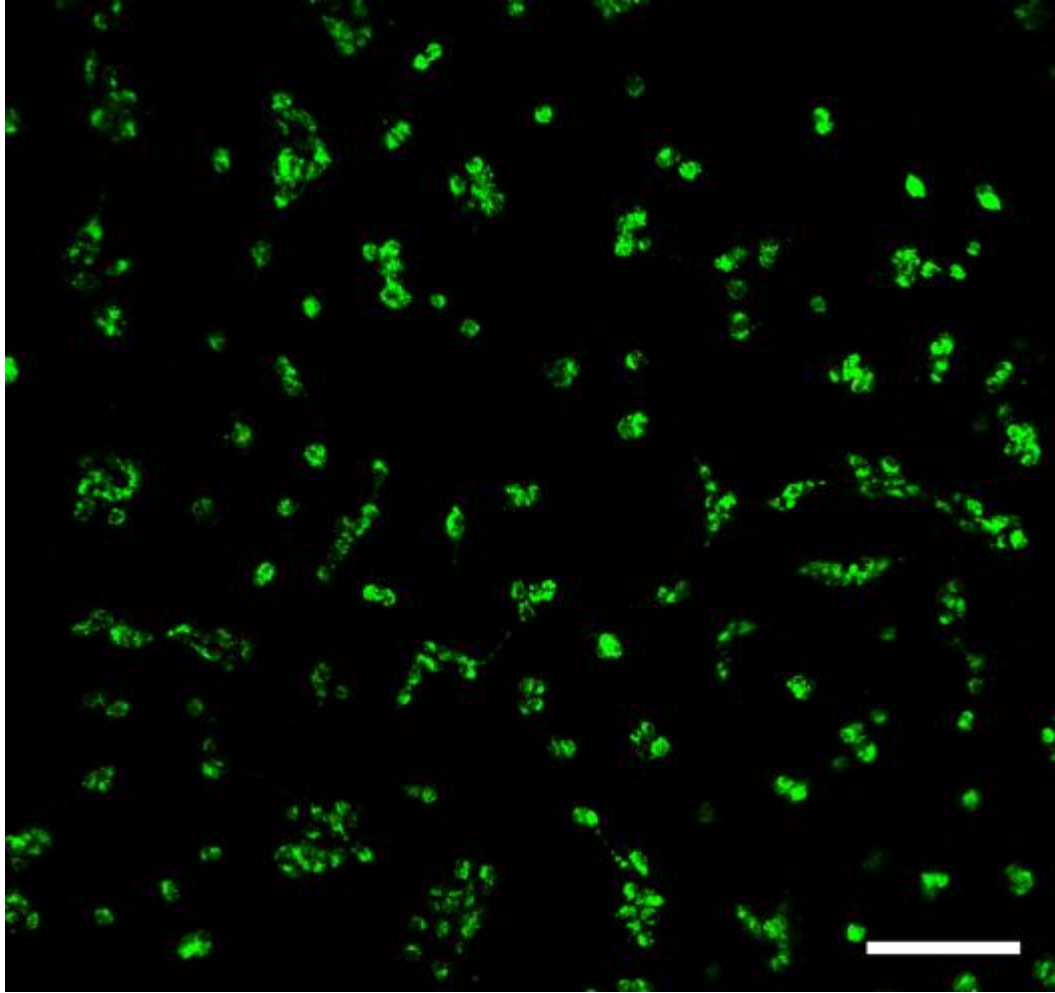


Figure 4.20 Live/Dead assay of BMSCs cultured on hydrogel G1-a for 7days Green for live cells, Red for dead cells (scale bar corresponding to 100um)

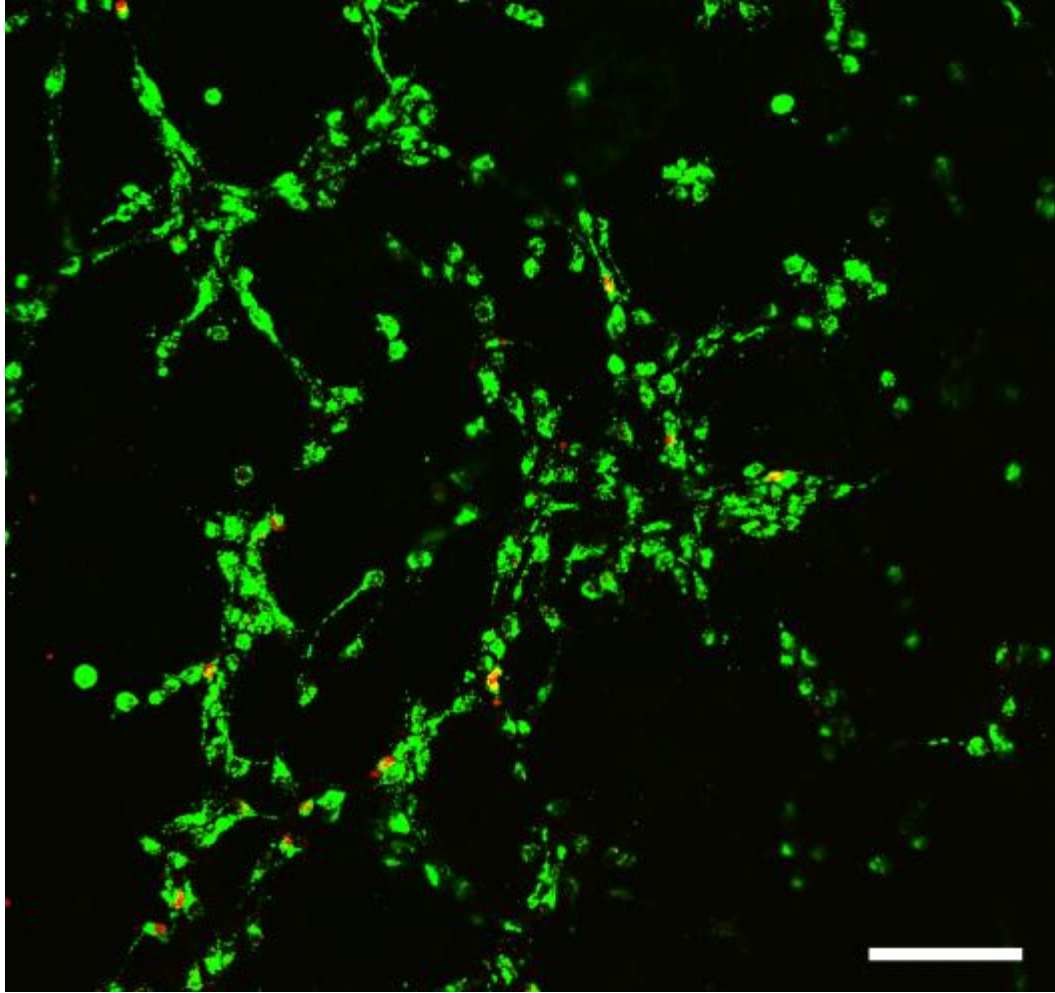


Figure 4.21 Live/Dead assay of BMSCs cultured on hydrogel G1-a for 14days Green for live cells, Red for dead cells (scale bar corresponding to 100um)

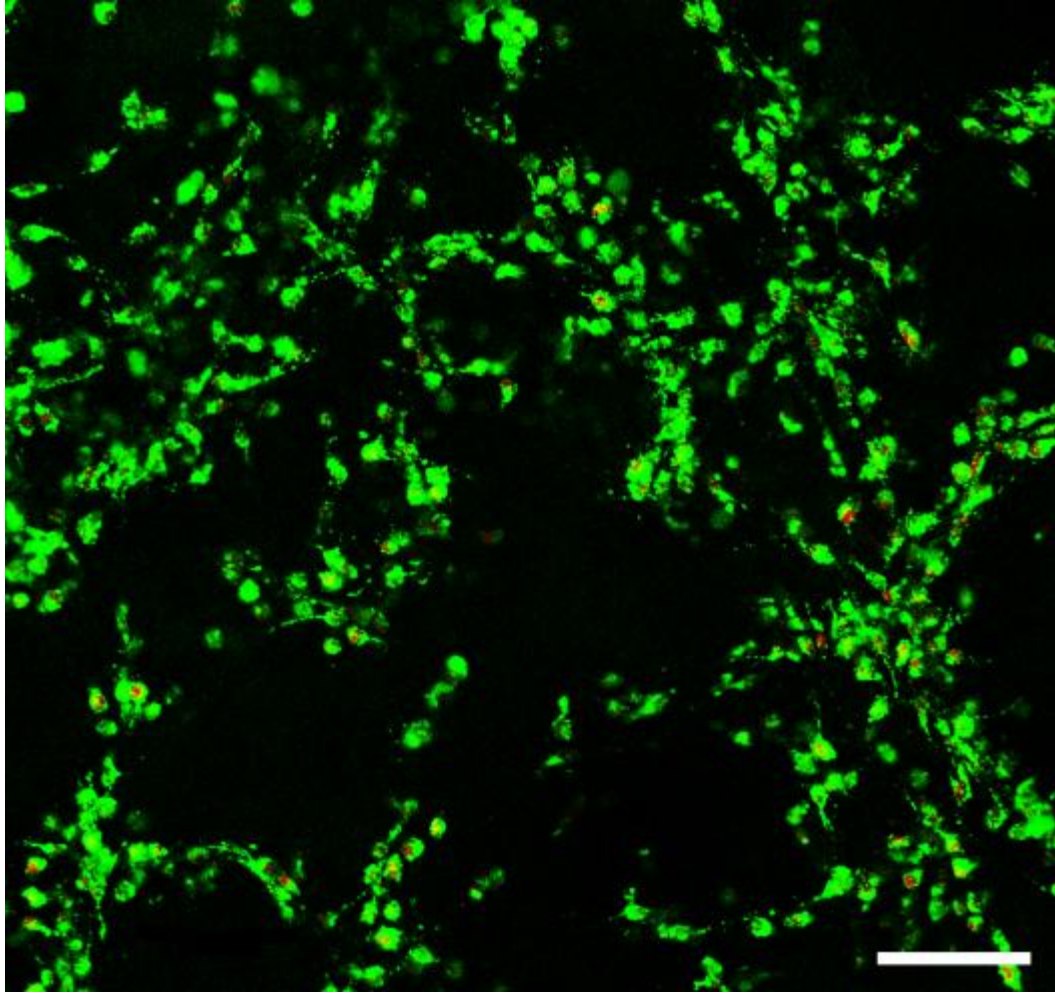


Figure 4.22 Live/Dead assay of BMSCs cultured on hydrogel G1-a for 28days Green for live cells, Red for dead cells (scale bar corresponding to 100um)

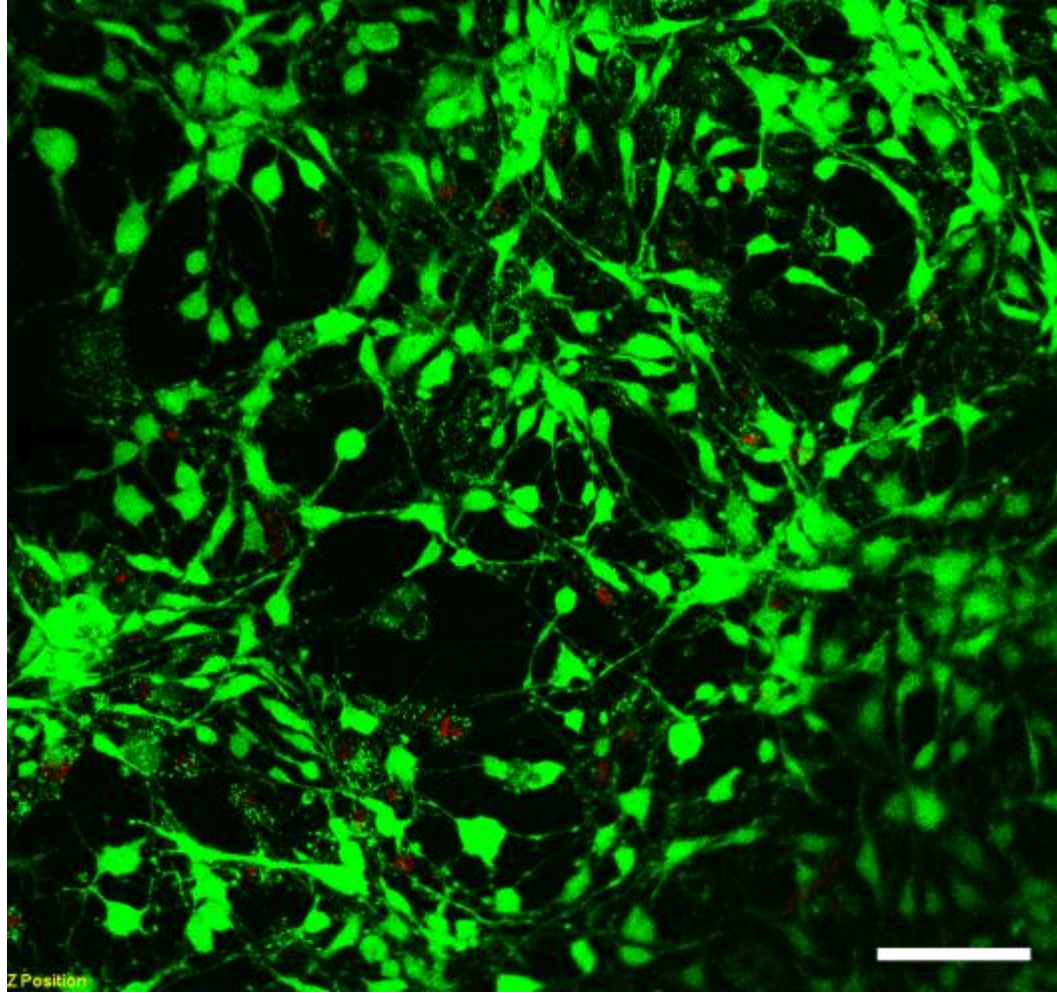


Figure 4.23 Live/Dead assay of BMSCs cultured on hydrogel G1-b for 7days Green for live cells, Red for dead cells (scale bar corresponding to 100um)

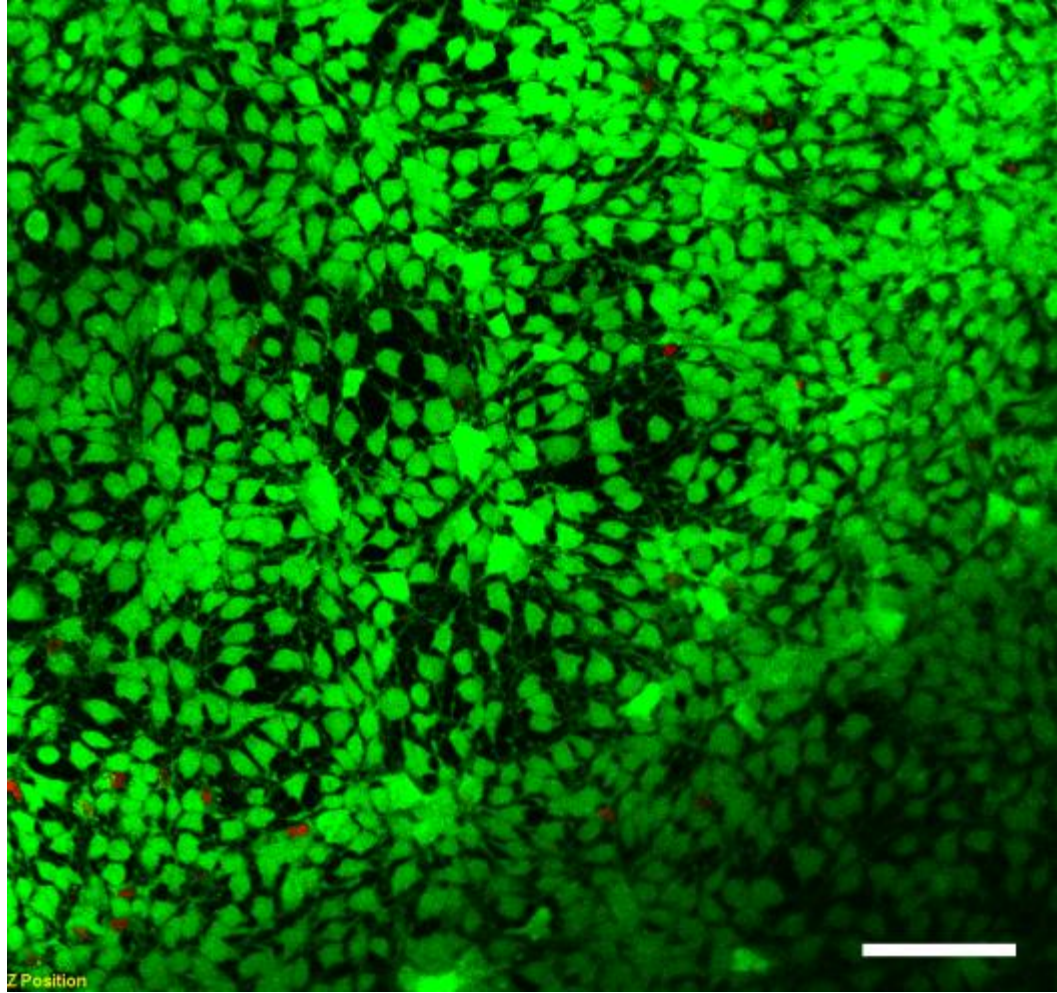


Figure 4.24 Live/Dead assay of BMSCs cultured on hydrogel G1-b for 14days Green for live cells, Red for dead cells (scale bar corresponding to 100um)

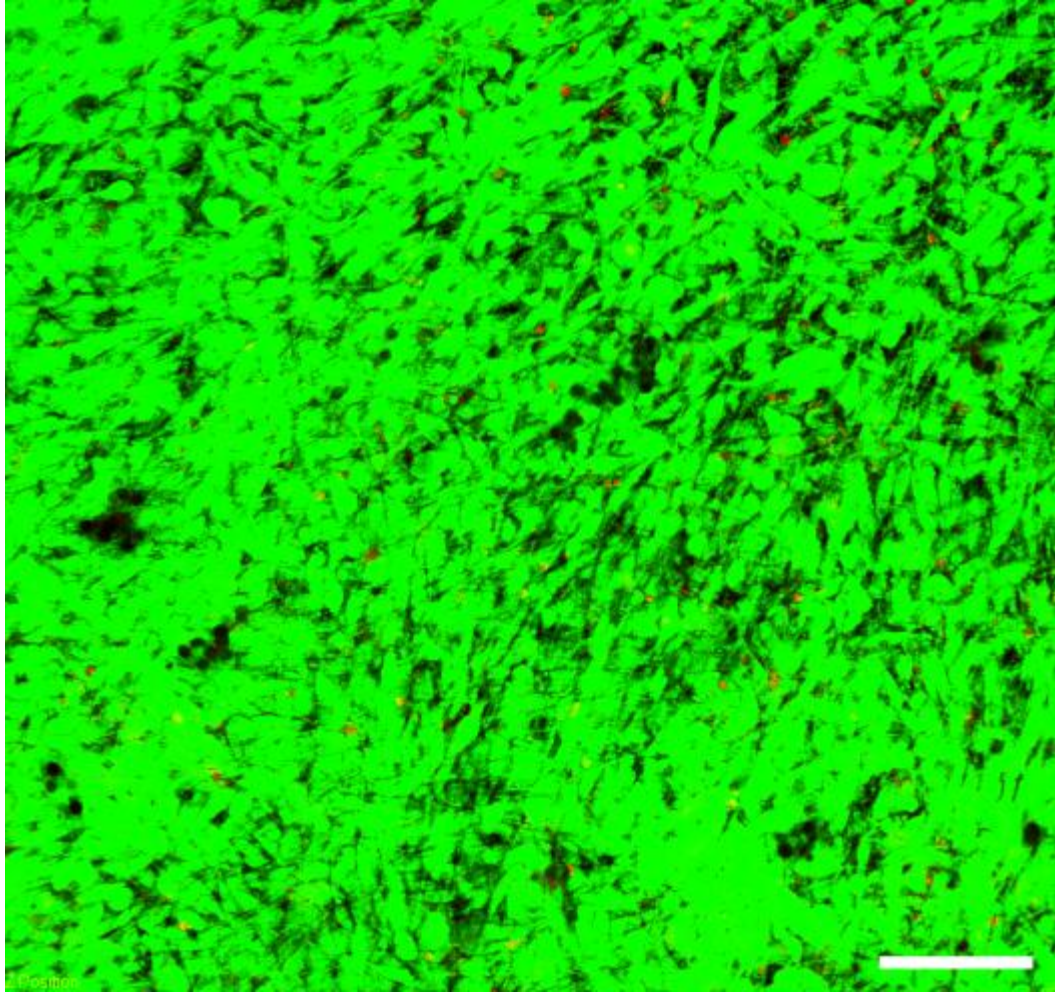


Figure 4.25 Live/Dead assay of BMSCs cultured on hydrogel G1-b for 28days Green for live cells, Red for dead cells (scale bar corresponding to 100um)

4.1.6 Cell Morphology on hydrogels.

In order to investigate cell morphology on hydrogels, nuclei and F-actin of C2C12, HDF and pre-osteoblast cells (POB) were immunostained and observed using confocal

laser scanning microscopy. As shown in Figure 4.26, C2C12 cells on G1 hydrogels were observed to be spreading and migration extensively, similar to those on TCPs (Figure 4.28). However, they were in a round shape on G2 hydrogels. (Figure 4.27). For HDF-2 and POB, similar results were observed. (Figure 4.29, Figure 4.30, Figure 4.31, Figure 4.32, Figure 4.33, and Figure 4.34). These results indicated that G1 hydrogels were more suitable for cell attachment and adhesion than G2 hydrogels.

We further culture BMSCs on G1 hydrogels with different stiffness to investigate whether stiffness have an effect on the morphology of BMSCs. As shown in Figure 4.35 and Figure 4.39, BMSCs attached on both hydrogels and showed spreading out morphology. However, the distribution of cytoskeleton BMSCs on G1-b had a more organized morphology than that on G1-a (the softer one). This phenomenon retained after one week (Figure 4.37 and Figure 4.41). The adhesion status of cells is dynamic on soft gels and static on stiff gels.[12] The results suggested that hydrogel stiffness has an effect on cell morphology.

G1 hydrogels with BMSCs cells were also examined using a 3D confocal microscope. On day 1, the depth scanning images for both G1 hydrogels (G1-a and G1-b) showed a mono-layer (approximately 15 μm) of cells. (Figure 4.36 and Figure 4.40) After 7 days, most of the cells on G1-a migrated from the surface into the gel block for a distance of about 100 μm as shown in Figure 4.38. Cells on G1-b also showed signs of migration but only a few of them demonstrated deep penetration. (Figure 4.42) Lo *et. al.* reported in 2000 that cells can migrate into polyacrylamide hydrogels and the migration distance depends on the rigidity of the hydrogels.[180] Wang *et al* reached the same conclusion on

gelatin hydrogels [181]. In this study, the PAA crosslinker-incorporated PEGDA hydrogel allowed deep migration of BMSCs, suggesting that hydrogel stiffness does have effects on cell migration behaviour. The effects of hydrogel stiffness on other cell functions require further investigations.

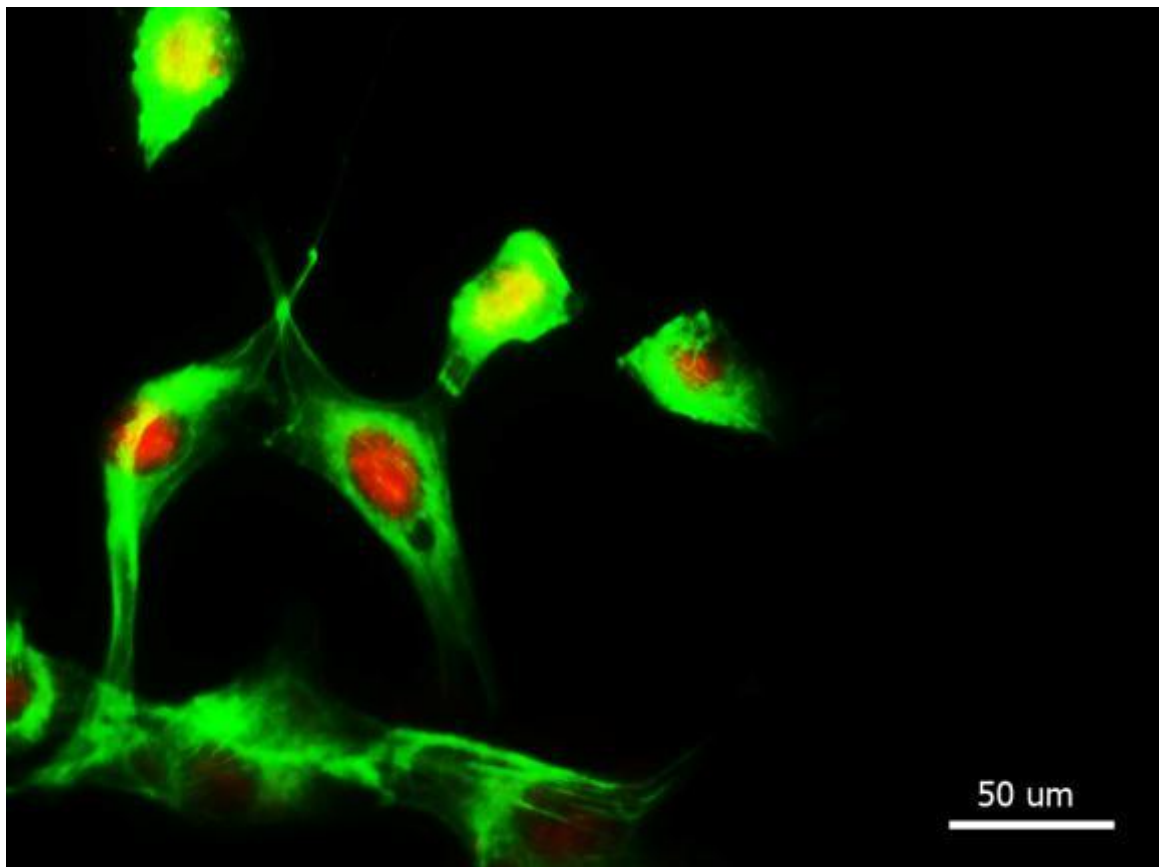


Figure 4.26 Morphology of C2C12 cells on hydrogel G1-b for 1 day. Green is cytoskeleton, and red is cell nucleus for all immunostaining images unless otherwise noted.

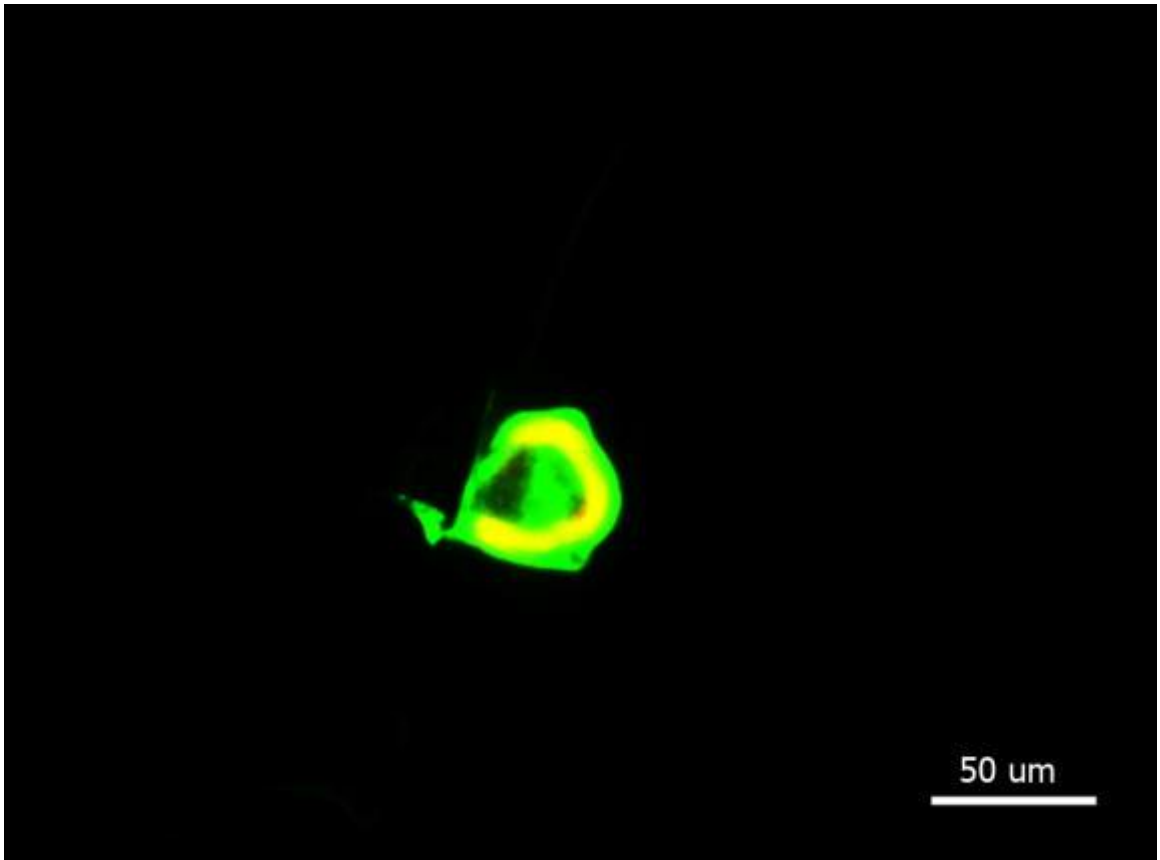


Figure 4.27 Morphology of C2C12 cells on hydrogel G2-b for 1 day

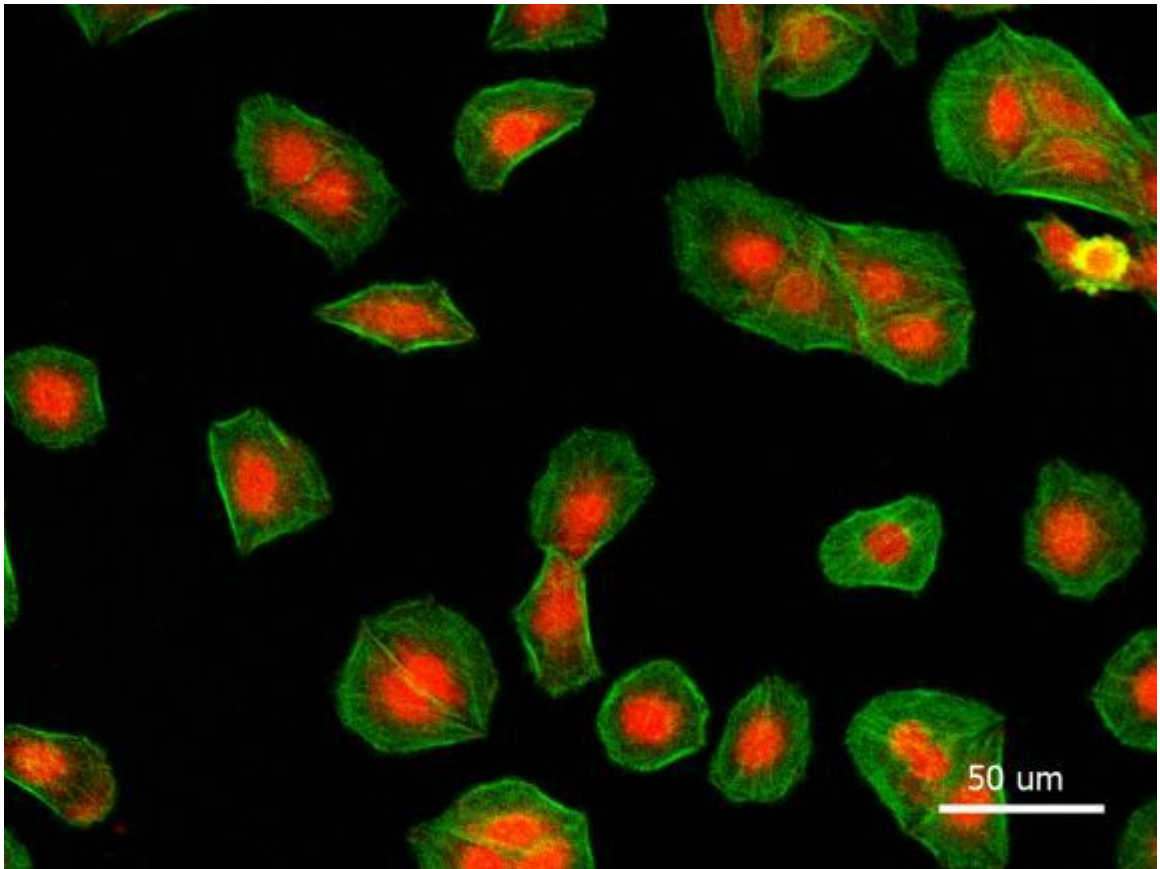


Figure 4.28 Morphology of C2C12 cells on TCPs for 1 day

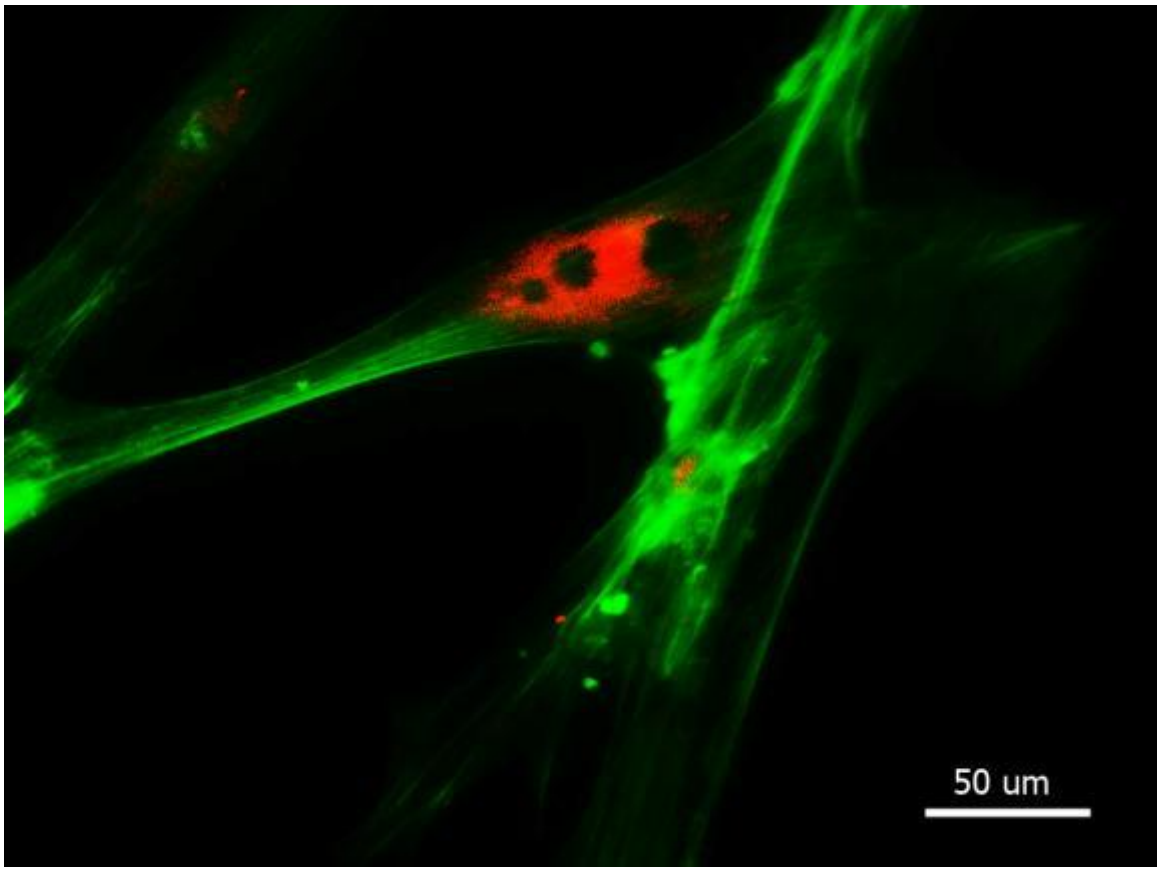


Figure 4.29 Morphology of HDF-2 cells on hydrogel G1-b for 1 day

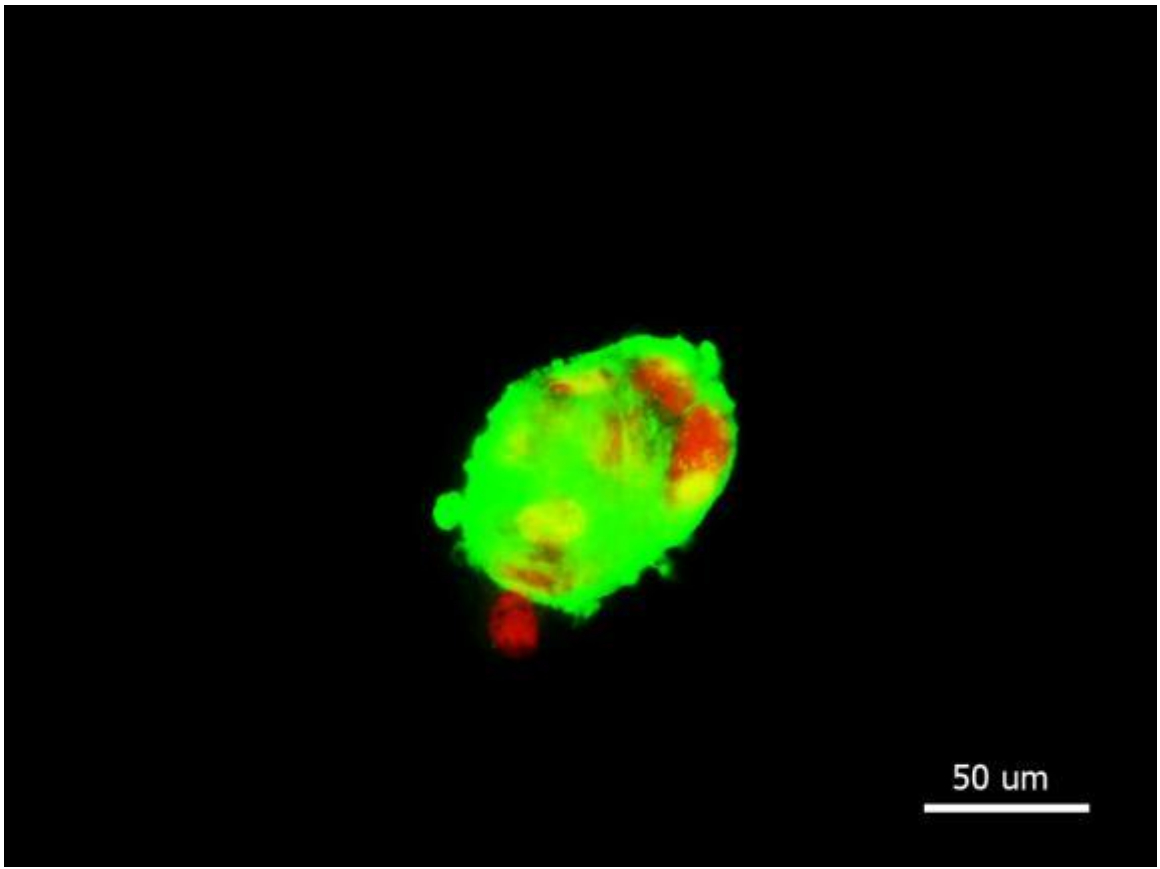


Figure 4.30 Morphology of HDF-2 cells on hydrogel G2-b for 1 day

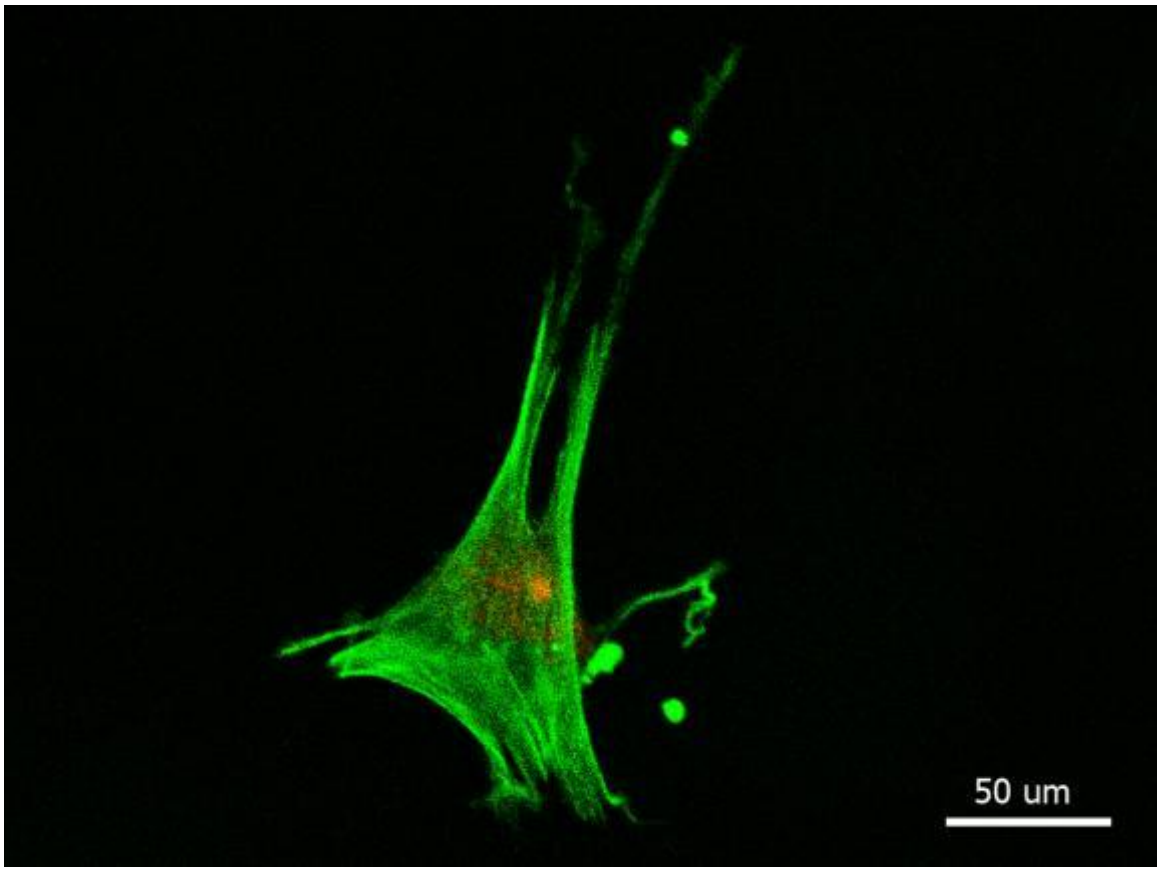


Figure 4.31 Morphology of HDF-2 cells on hydrogel TCPs for 1 day

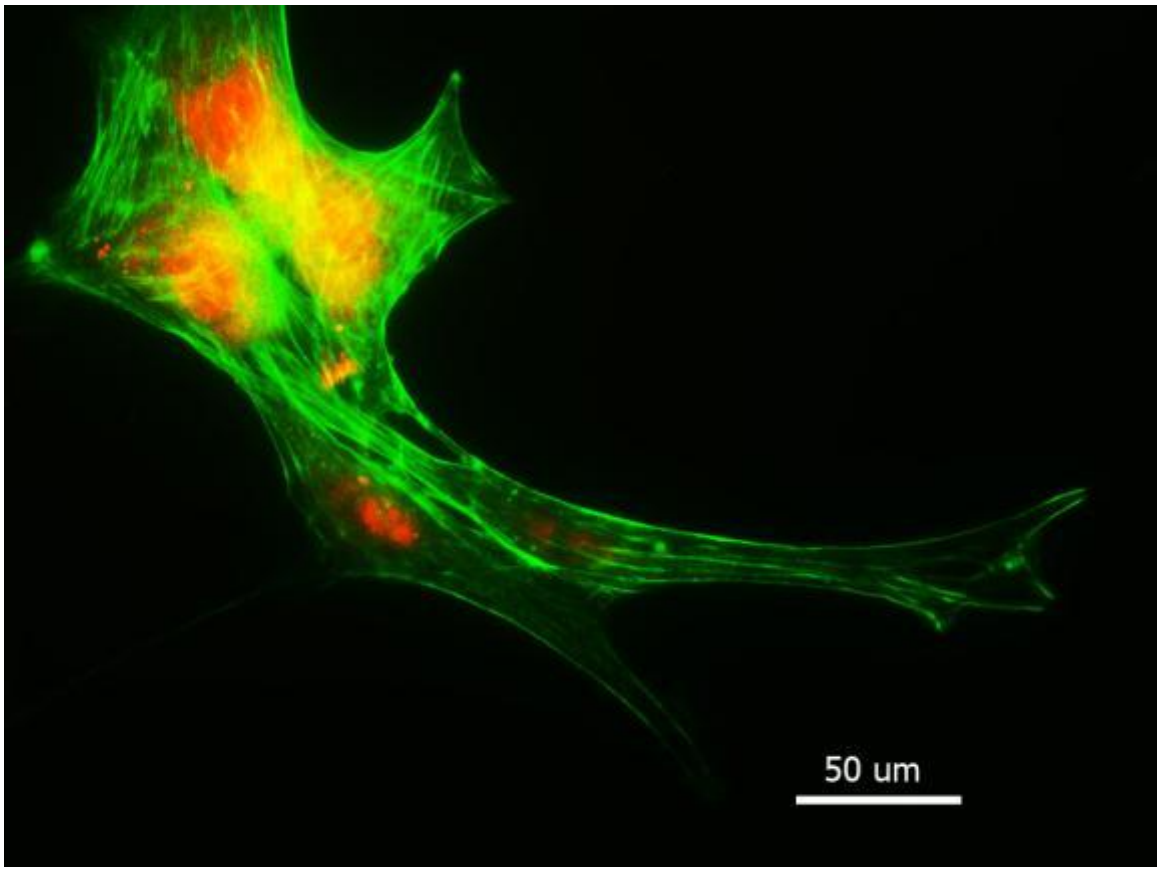


Figure 4.32 Morphology of POB cells on hydrogel G1-b for 1 day

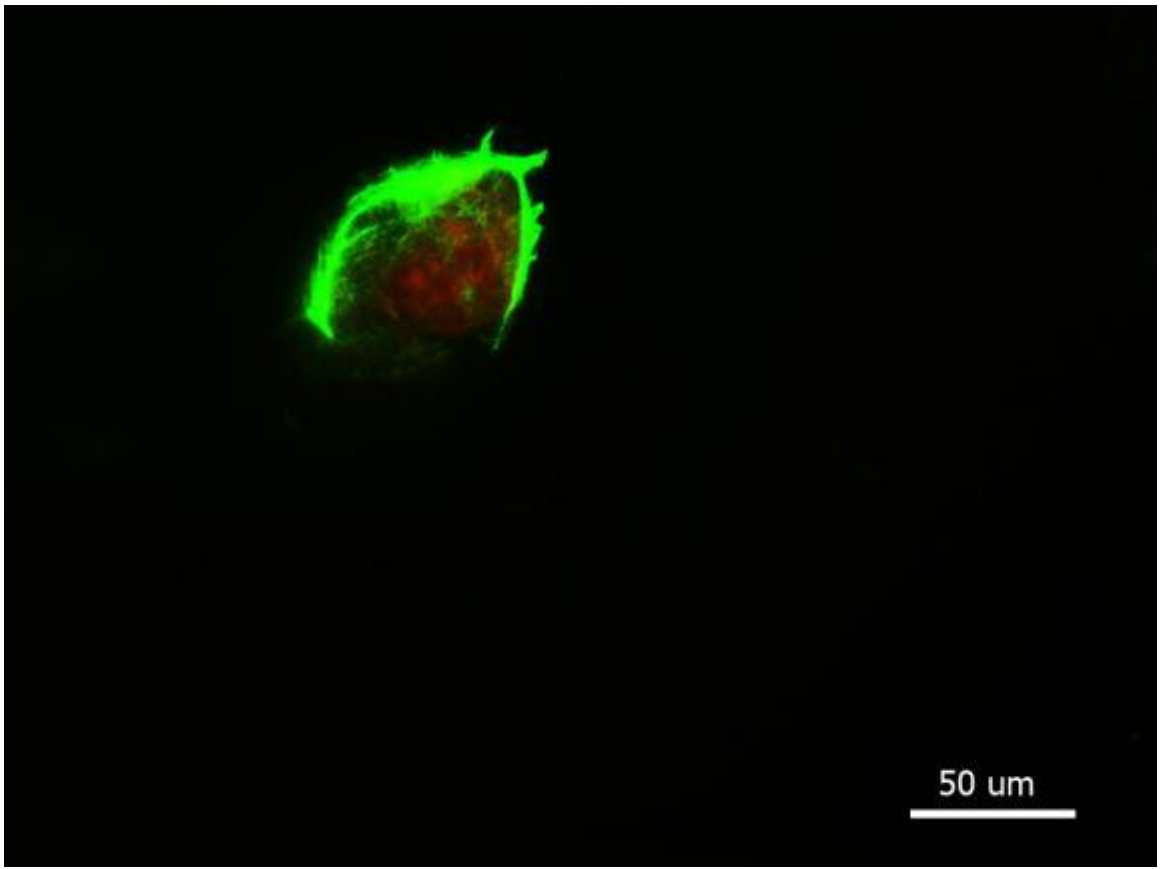


Figure 4.33 Morphology of POB cells on hydrogel G2-b for 1 day

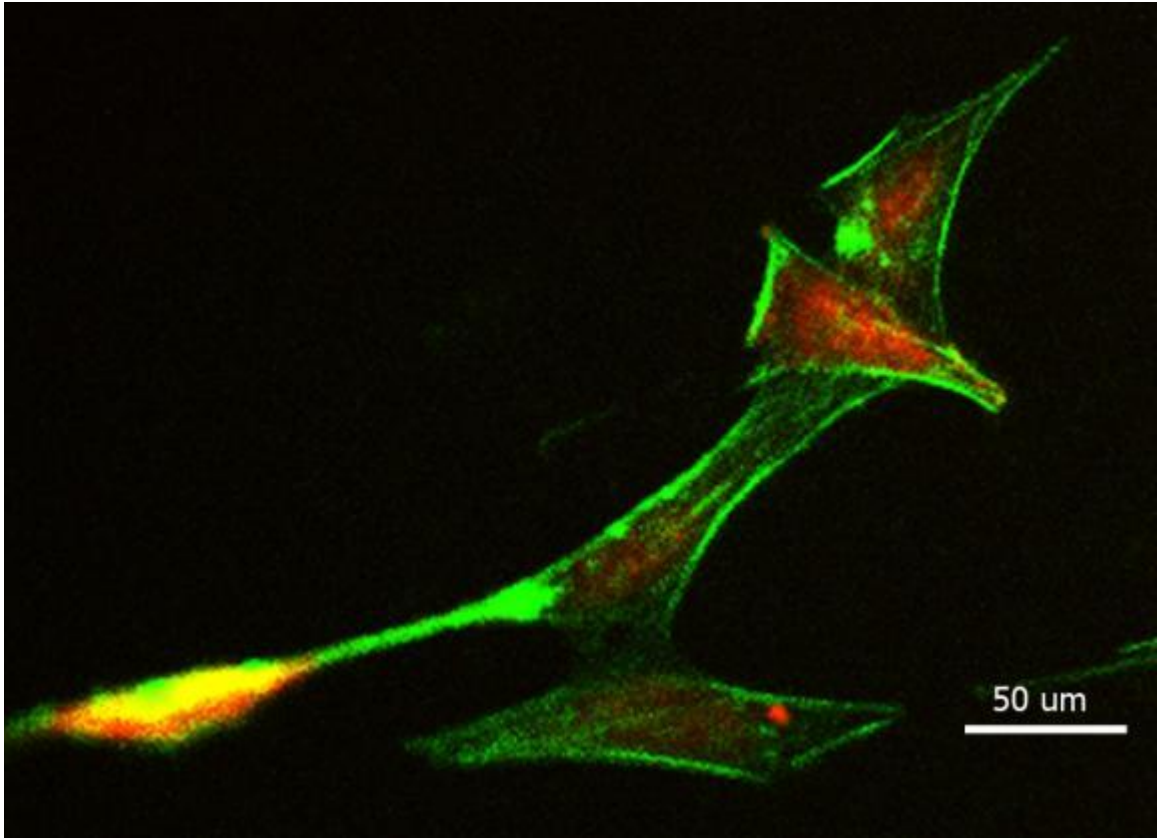


Figure 4.34 Morphology of POB cells on TCPs for 1 day

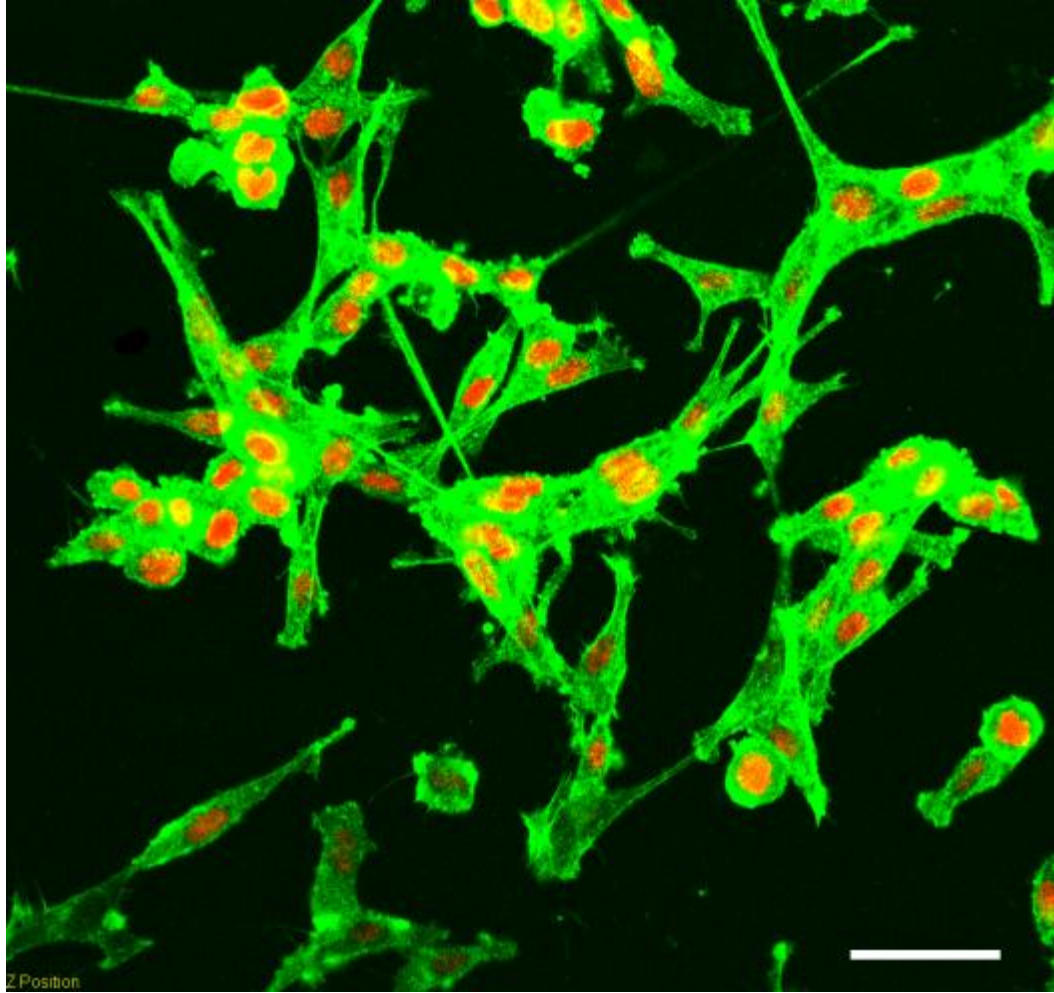


Figure 4.35 Morphology of BMSCs on G1-a for 1 day; scale bar is 50um.

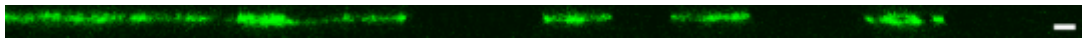


Figure 4.36 3D ingrowths of BMSCs in G1-a gel for 1 day; scale bar is 20um.

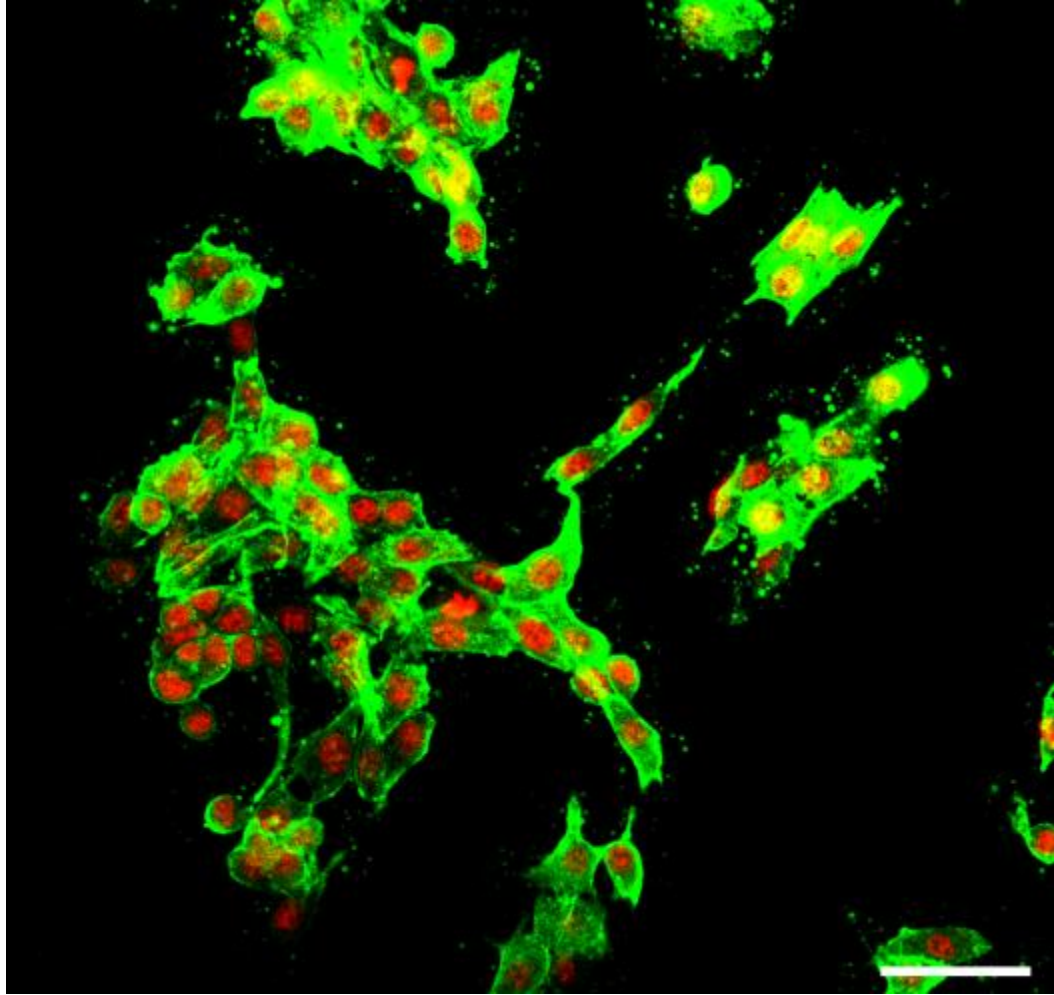


Figure 4.37 Morphology of BMSCs on G1-a for 7 days; scale bar is 50um.



Figure 4.38 3D ingrowths of BMSCs in G1-a gel for 7 days; scale bar is 50um

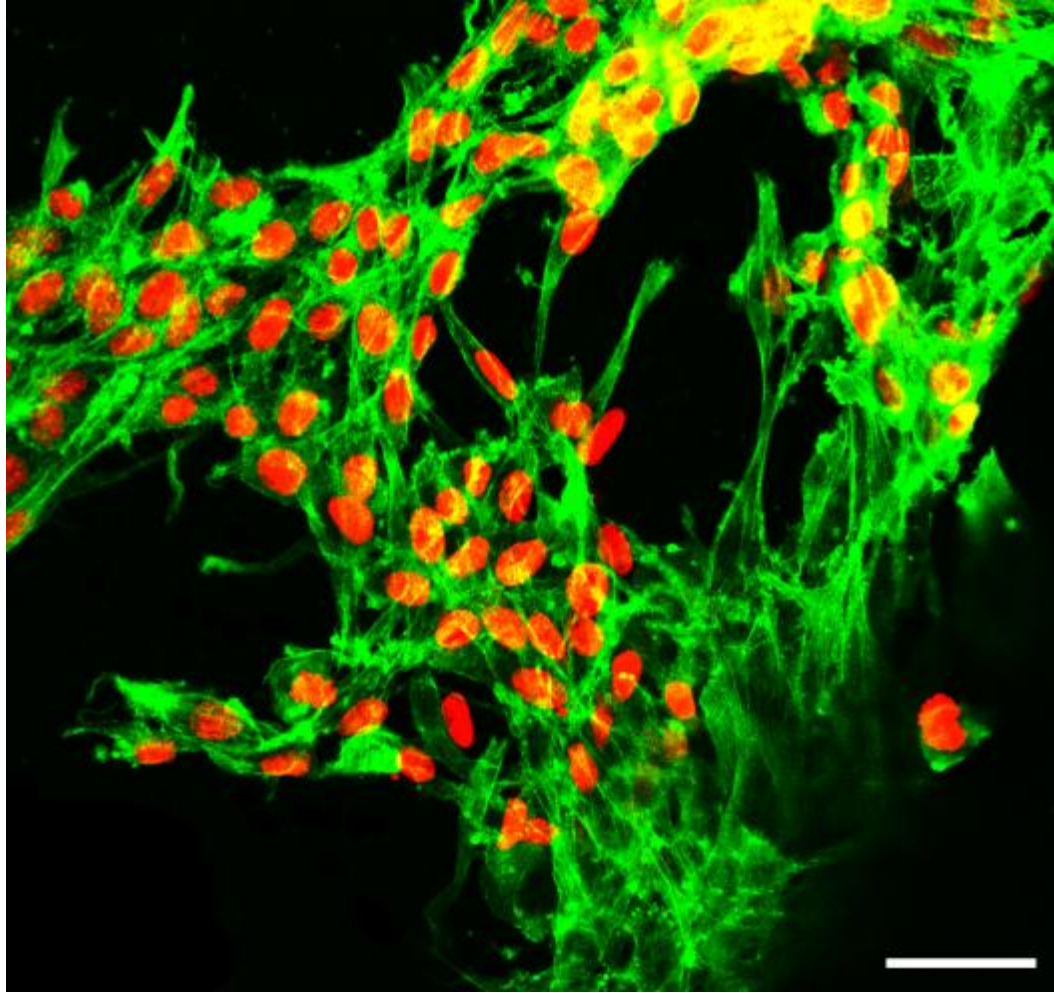


Figure 4.39 Morphology of BMSCs on G1-b for 1 day; scale bar is 50um.

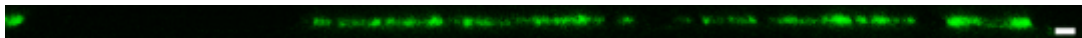


Figure 4.40 3D ingrowths of BMSCs in G1-b gel for 1 day; scale bar is 20um.

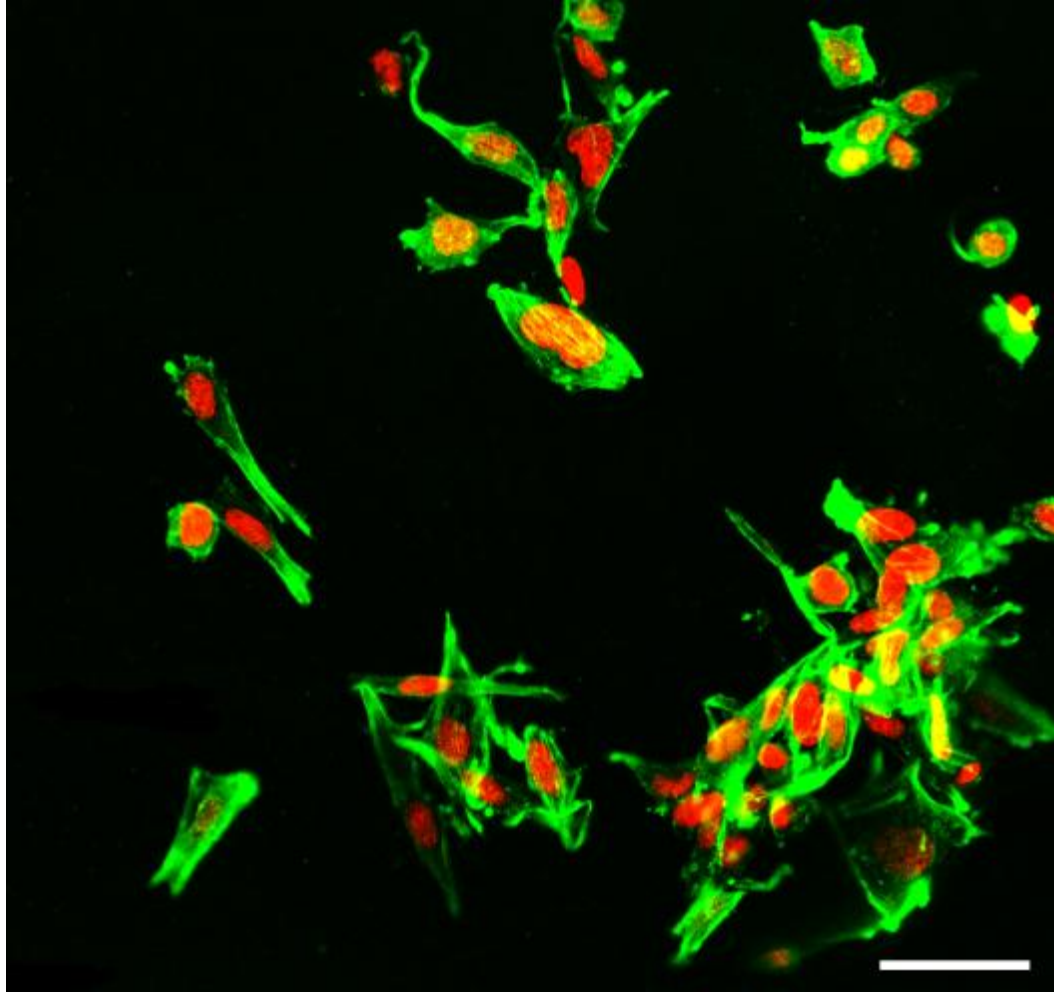


Figure 4.41 Morphology of BMSCs on G1-b for 7 days; scale bar is 50um.

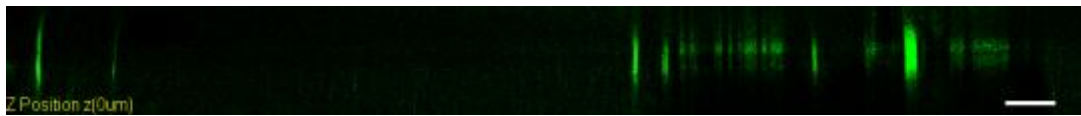


Figure 4.42 Depth scanning of BMSCs in G1-b gel for 7 days; scale bar is 50um

4.1.7 Osteogenic differentiation of BMSCs

To evaluate the osteogenic differentiation of encapsulated BMSCs, the changes in the osteogenic marker mRNAs for BSP, ALP, OC, OPN in response to the stimulation from different types of hydrogels were determined using real time-qPCR. As shown in Figure 4.43 to Figure 4.46, osteogenic genes expression in BMSCs increased significantly in G1b and G1c groups for day 1. On day 4 and day 7, the expression levels of BSP, ALP, OC and OPN in BMSCs co-encapsulated in G1c hydrogels were significantly higher than the other hydrogels and the TCPs groups.

For osteogenesis, bone sialoprotein gene(BSP) is an important gene and its protein can be expressed by osteoblasts or differentiated stem cells.[182] On day 1, the expression of BSP gene is increased with the increase of hydrogel stiffness, and same trend is observed on day 4 and day 7 (Figure 4.43). It has been reported that the local matrix stiffness has important implications for development, differentiation, disease, and regeneration of cells [12]. Our results also indicates that stem cells can response to the hydrogel stiffness which agrees to the discovery of Discher *et al.* [12] Osteocalcin (OC) is, a critical marker in late stage of bone differentiation.[183] As shown in Figure 4.44, the expression profiling of OC is almost the same to that of BSP while the expression level is much higher than that of BSP. Osteopontin (OPN) is another human gene product that related to osteogenetic differentiation [184]. Its proteins serves as an organic linking component of bone. The expression level of OPN is relatively lower than that of both BSP and OC. But still, the stiff gel (G1-c) was the best group for OPN expression, and the soft one was the lowest

among all three gels on osteogenesis (Figure 4.45) Alkaline phosphatase (ALP) is an enzyme that presents in all tissue in human body to remove the phosphate group from nucleotides or proteins et al. High levels of ALP may indicate an event of active bone formation, making ALP a marker for bone metabolism.[185] The ALP expression is evaluated when BMSCs were cultured on G1 hydrogels with different stiffness. The stiffest G1 gel has the highest ALP expression level throughout one week even though the level of ALP is highest on day 1 and it decreased with time goes by. (Figure 4.46)

Four osteogenetic genes expression results suggest that the fate of cells on a hydrogel can be affected by the hydrogel stiffness. Combined with the stiffness testing results shown in Figure 4.17, it was found that when the stiffness of a hydrogel is higher than about 100 g/mm, the BMSCs will differentiate into bone cells.

In bone regeneration, mineral depositions can be observed. Von Kossa staining was further used to confirm the osteogenetic differentiation of BMSCs by examining the calcium deposits of BMSCs on G1 hydrogels. The black part represents the calcium deposits and pink for cell staining. The mineralization of hydrogel G1-a after 4 weeks was shown in Figure 4.47. Black area can barely be found. However, the black mineralization spots can be easy found around cells on hydrogel G1-b which has a higher stiffness than G1-a (Figure 4.48). When cells were cultured on hydrogels G1-c, the gel with highest stiffness, there were a large amount of calcium deposition. (Figure 4.49) The von Kossa result not only confirmed the osteogenesis of BMSCs on hydrogel G1, but also suggested that the stiffness of hydrogels can control the BMSCs differentiation.

Based on these results, it can be concluded that hydrogel G1 with a high stiffness show the ability to effectively induce osteogenesis followed by secreting extracellular matrix molecules for bone tissue.

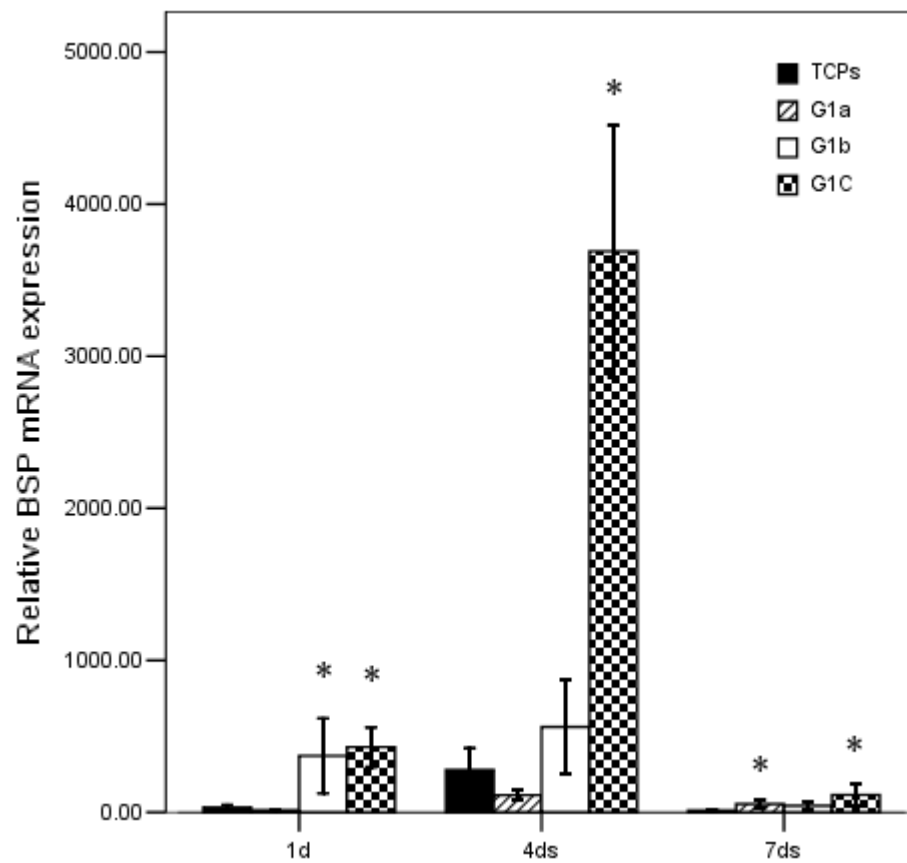


Figure 4.43 BSP expression profiling of mouse BMSCs cultured on hydrogels G1 with different stiffness for different times (a, b,c corresponding to different stiffness respectively from soft, medium, to stiff). Data values are expressed as mean±SE (n=3).

“*” means $p < 0.05$ vs the TCPs group

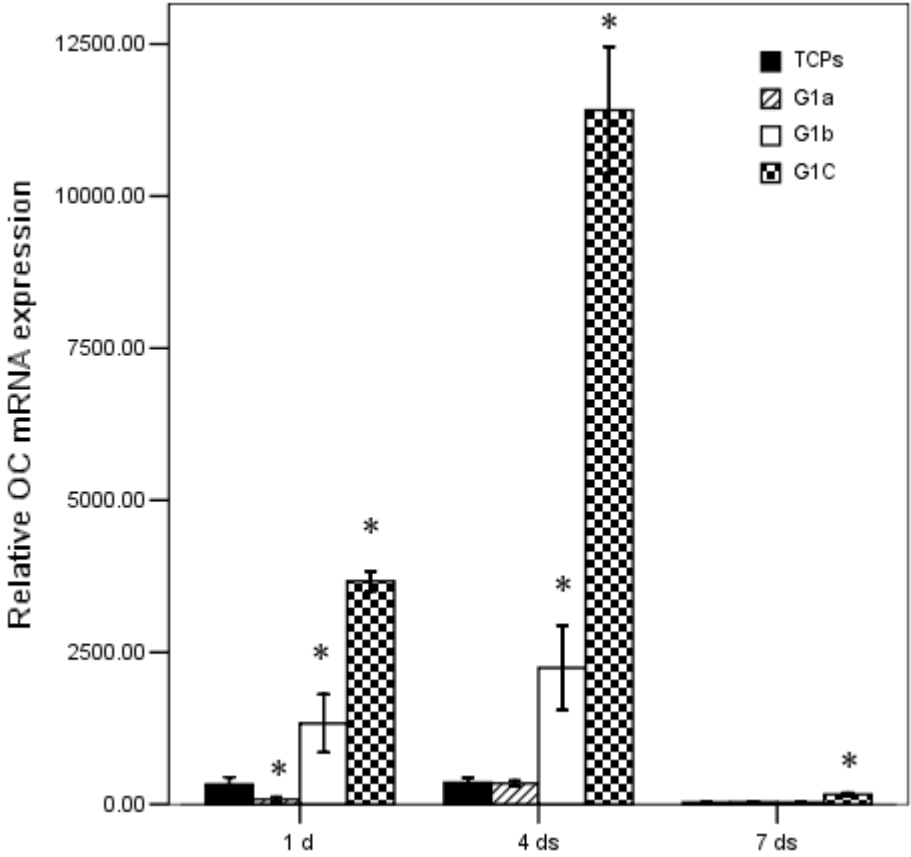


Figure 4.44 OC expression profiling of mouse BMSCs cultured on hydrogels G1 with different stiffness for different times. Data values are expressed as mean±SE (n=3). “*”

means $p < 0.05$ vs the TCPs group

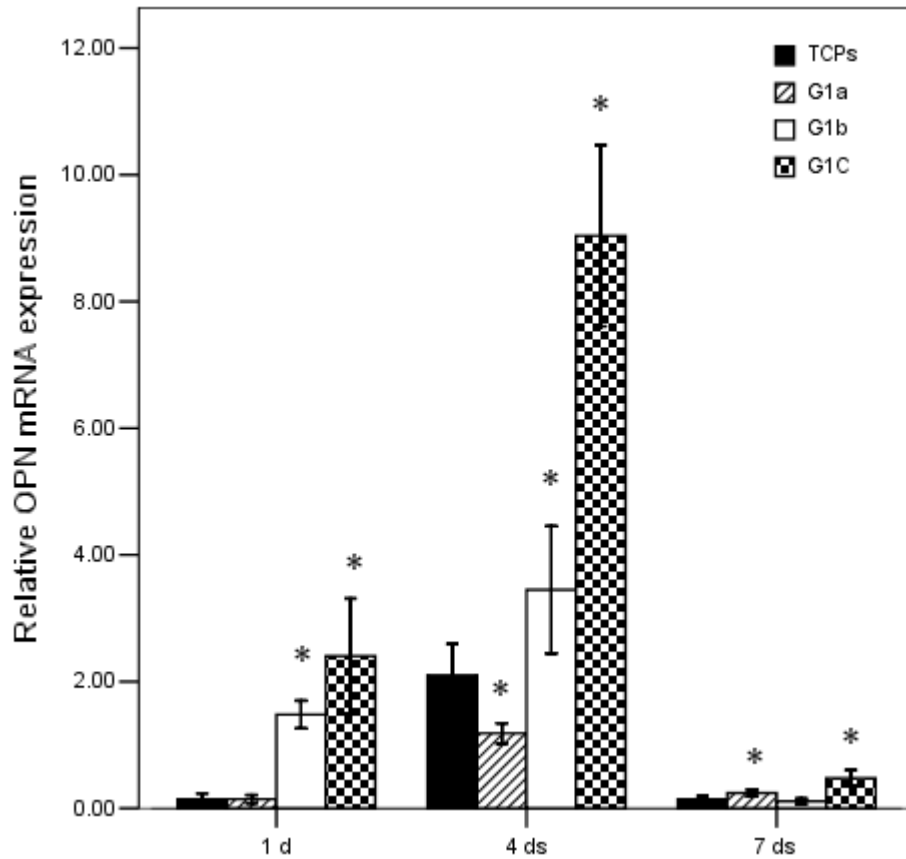


Figure 4.45 OPN expression profiling of mouse BMSCs cultured on hydrogels G1 with different stiffness for different times. Data values are expressed as mean±SE (n=3). “*”

means $p < 0.05$ vs the TCPs group

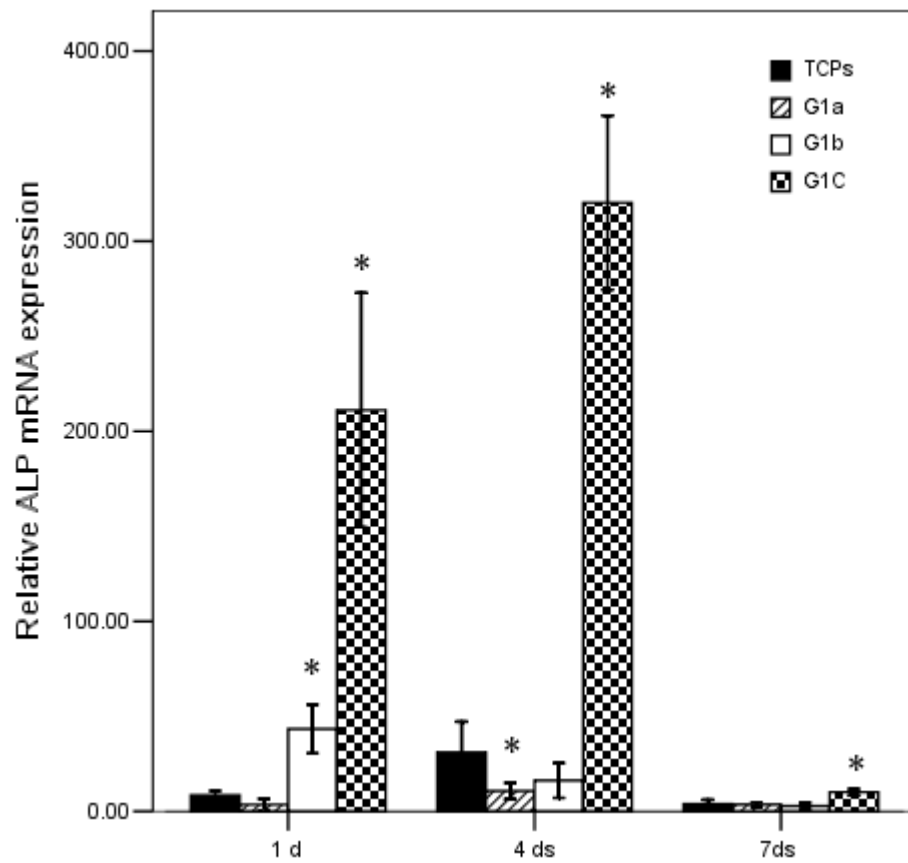


Figure 4.46 ALP expression profiling of mouse BMSCs cultured on hydrogels G1 with different stiffness for different times. Data values are expressed as mean \pm SE (n=3). “*”

means $p < 0.05$ vs the TCPs group

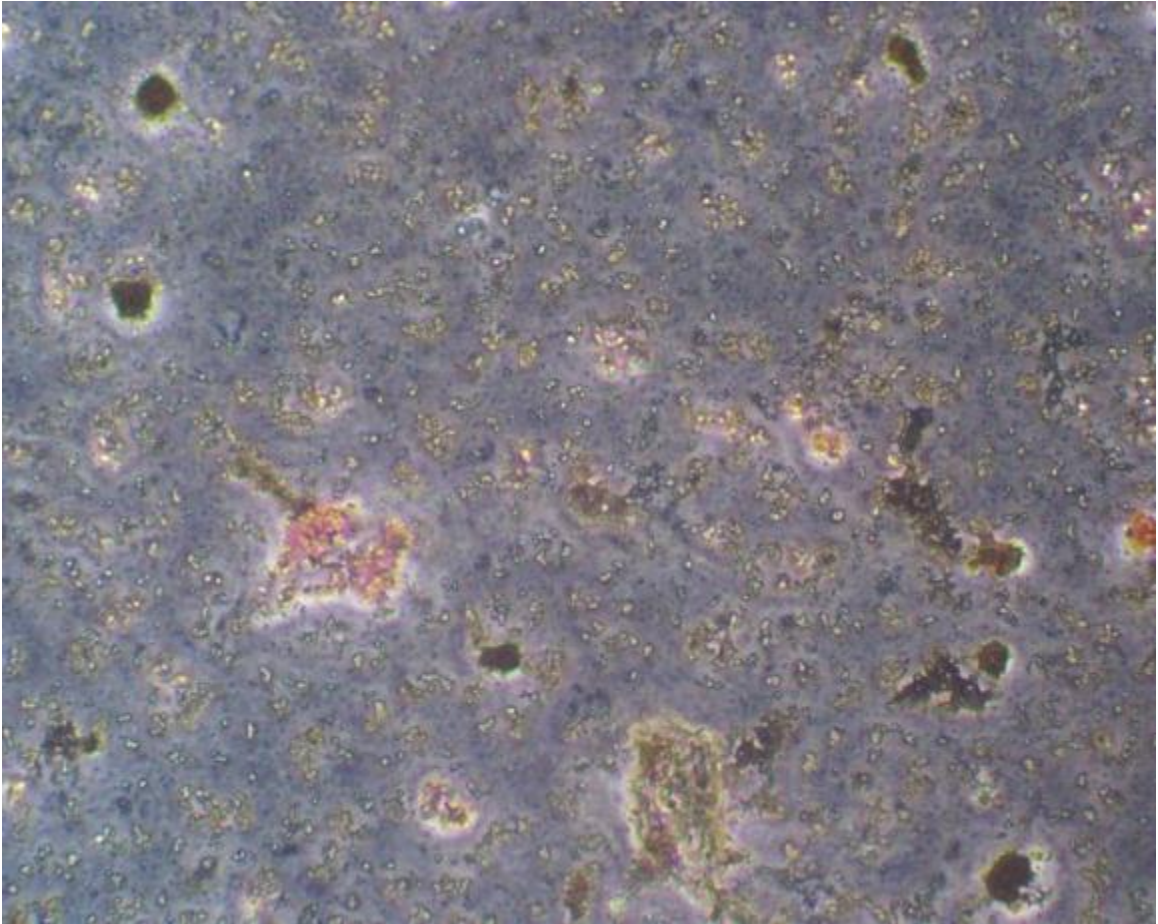


Figure 4.47 von Kossa staining of Pre-Osteoblast cultured on hydrogel G1-a for 4 weeks.

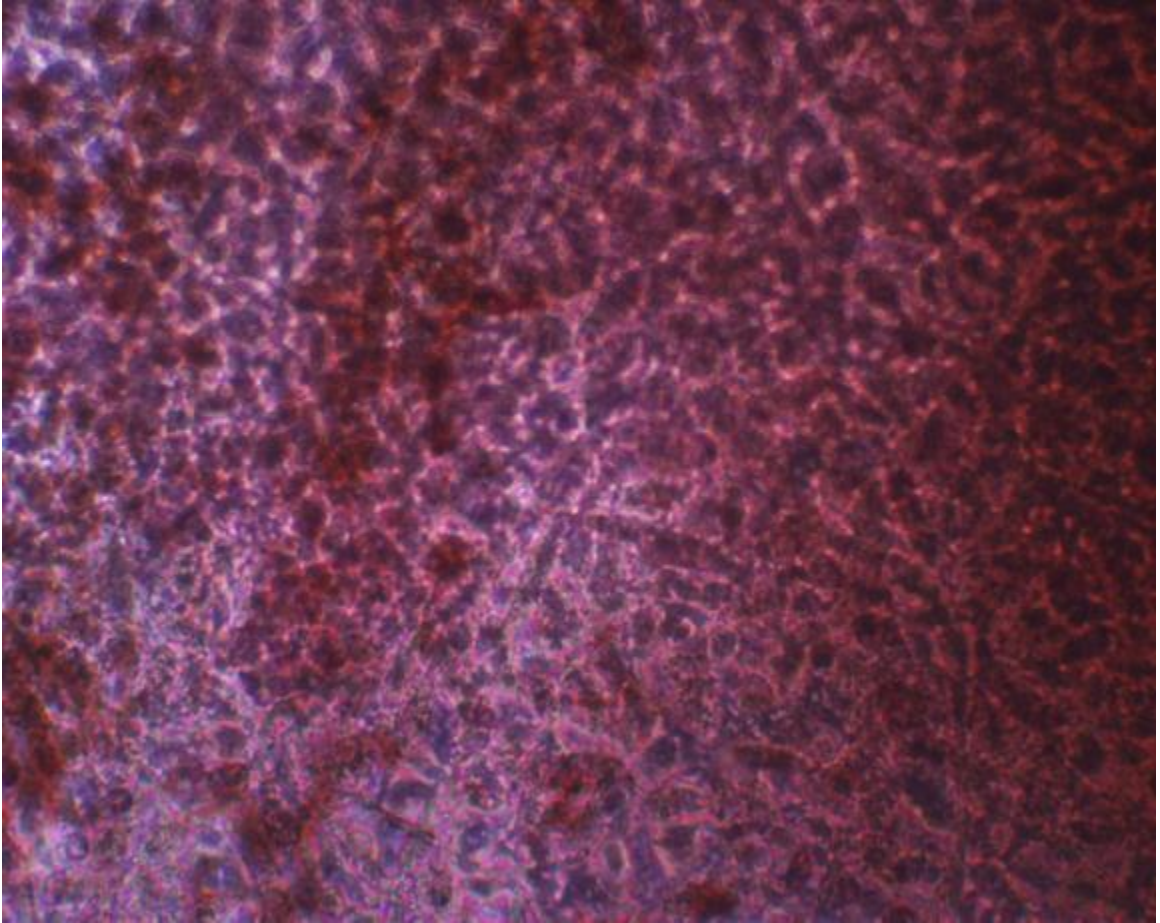


Figure 4.48 von Kossa staining of Pre-Osteoblast cultured on hydrogel G1-b for 4 weeks.

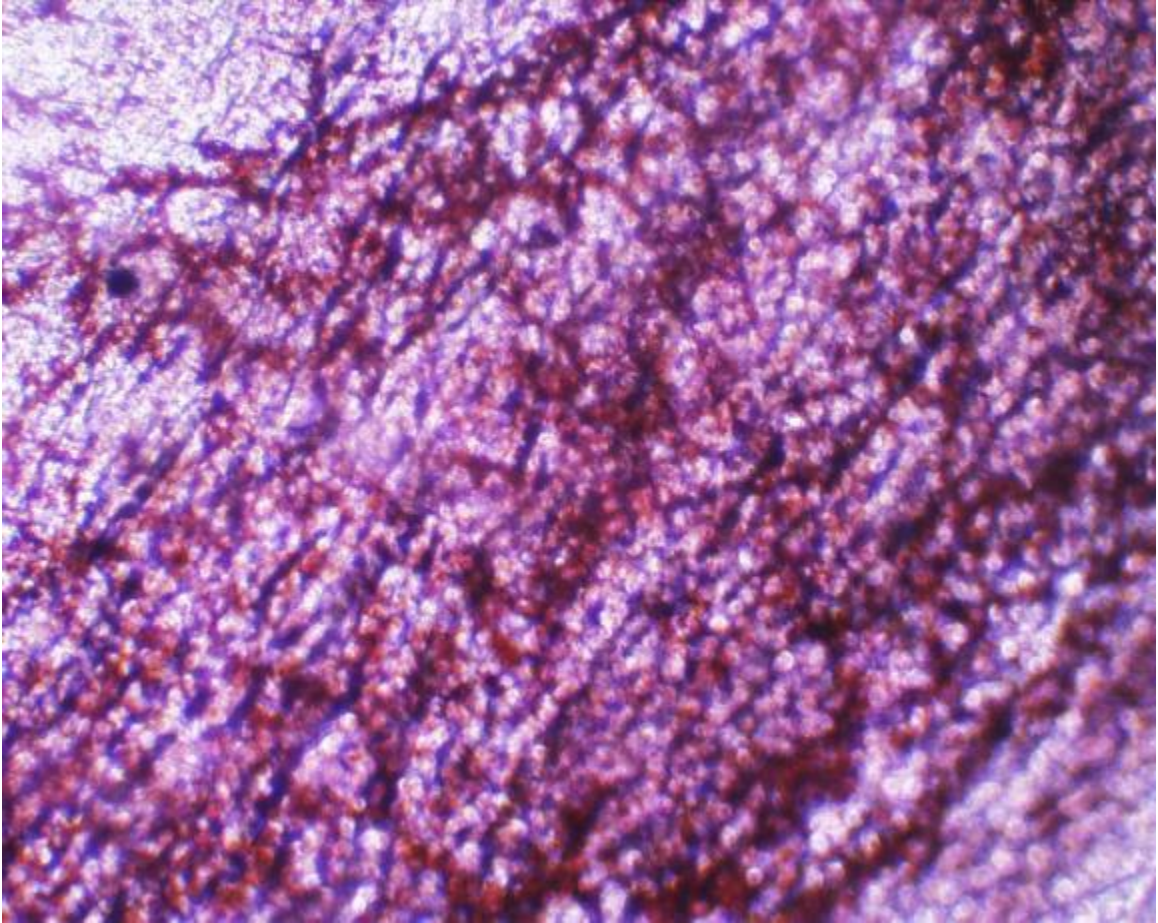


Figure 4.49 von Kossa staining of Pre-Osteoblast cultured on hydrogel G1-c for 4 weeks.

TE and regenerative medicine have obtained an intense commitment from research to business with the promise of rebuilding tissues and organs to replace the diseased. As a strategy, cell therapy has a pronounced advantage to apply and advance native biology into clinical needs. However, cell is highly dependent on and regulated by the physical-chemical environment. There is an urgent need to develop biomimetic ECM with the potentiality to guide cell behaviors. As a synthetic ECM, the designed hydrogel should be able to combine the simplicity with manageable mimetic chemistry. Specifically, the gel

can be synthesized with a simple routine and main an instructive potentiality- cell adhesion, stiffness tuning, bio-compatibility and biodegradability. The design and develops of hydrogel for bone regeneration has met the aforementioned requirement.

4.2 Hydrogel for cancer therapy

4.2.1 Chemical structure of polysaccharide derivatives and hydrogels

Chemical structure of OS hydrogel, D-OS hydrogel, O-alg, S-chi, alginate, and chitosan were characterized by FTIR (Figure 4.50). Compared with chitosan spectrum, the S-chi spectrum shows a new absorption peak at around 1733 cm^{-1} which is contributed from the carboxylate group. [186] Both alginate and O-alg spectrum were very similar, and there is no any signal for aldehyde functionalities which is due to the formation of hemiacetals. In both hydrogel spectrums, the characteristic peak of the hemiacetal structure at 831 cm^{-1} suggests that the coupling reaction was followed between $-\text{CHO}$ groups of O-alg and $-\text{NH}_2$ of S-chi. [187]

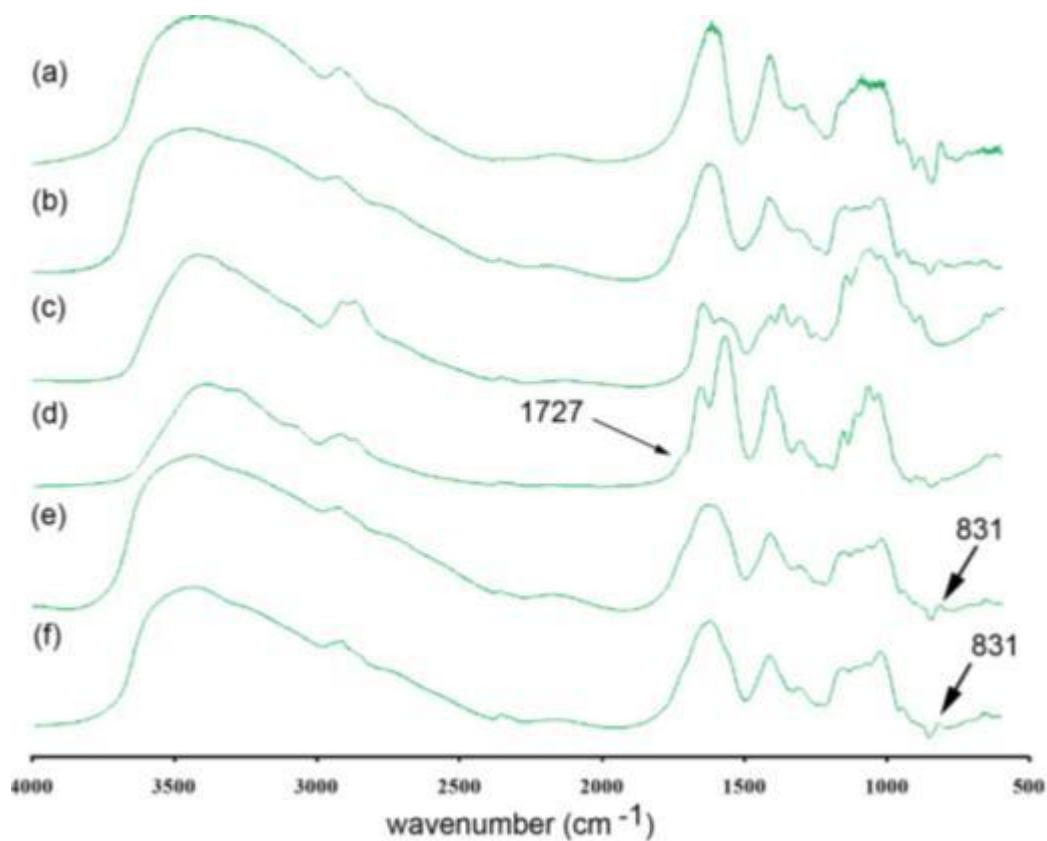


Figure 4.50 FTIR spectrum of (a) Alginate (b) O-alg (c) Chitosan (d) S-Chi (e) OS hydrogel (f) D-OS hydrogel

4.2.2 Morphology and structure of hydrogel

The OS hydrogel freeze-dried morphology was observed under scanning electron microscopy (SEM) (Figure 4.51 b). Isotropic OS hydrogel exhibited a regular, uniform morphology in SEM micrographs. We use cryosection technology to view D-OS cross-section morphology with CLSM by showing DOX in D-OS because freeze-dry process will leads to artifact in gel morphology. [106] DOX fluorescence can be excited by using

an argon laser at 488 nm and the emission was collected through a 530-nm long-pass filter.[188] (Figure 4.51 c) Both SEM and cryosection CLSM results show micro-porous structure of inner-morphology of hydrogel OS and D-OS. This micro-porous structure allows for promote cell migration[189] proliferation and tissue development[91]. In this study, these porous in hydrogel D-OS might render itself a faster drug release with fewer blockages after the drug is disassociated from the hydrogel main body.

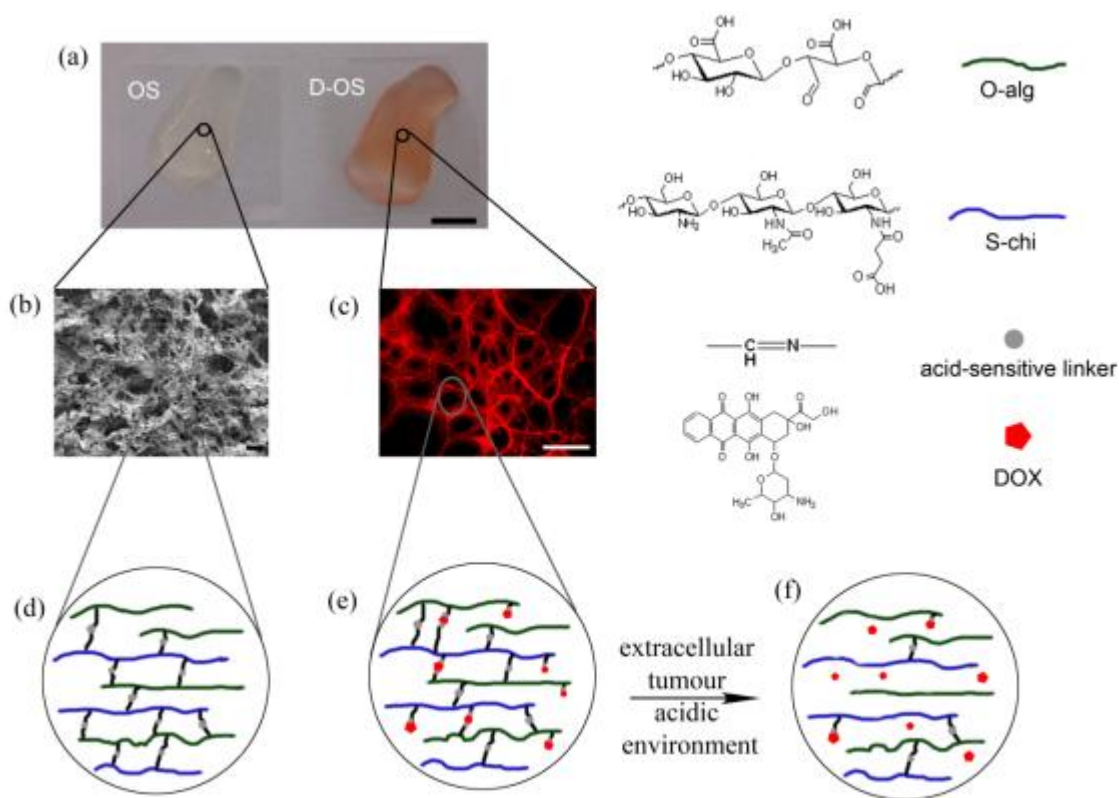


Figure 4.51 Morphology of OS and D-OS hydrogel. (a) Photographs of OS and D-OS hydrogels the scale bar in is 0.5 cm. (b) A SEM image shows the freeze-dried morphology of OS hydrogels and the scale bar is 50 μ m. (c) A CLSM image shows the DOX (Red) in

D-OS hydrogels and the scale bar is 100 μm . (d-f) Scheme illustration of chemical structure of (d) OS and (e) D-OS hydrogel and (f) drug release from the hydrogel main body; O-alg in blue line, S-chi in green line, acid-sensitive linker in gray dot, and DOX in red pentagon.

4.2.3 Rheological Properties of hydrogels

The change of viscosity of the solution is a key indicator of gelation under preceding [190]. The viscosity change by time of gel precursor solution was tested under zero-shear at room temperature and the gelation time was evaluated from the viscosity change (Figure 4.52). The gelation time for D-OS hydrogel (with DOX) is around 5 mins and for OS hydrogel (without DOX) is about 7 mins. The gelation time for DOX conjugated hydrogel is a little bit shorter than the one without DOX which might be due to the role of DOX as crosslinking points. However, both gels have similar viscosity after the gel formed at around 1600 Pa·s.

Storage and loss moduli measure the ability of viscoelastic materials to store and dissipate deformation energy during loading. Compared to viscous liquids, hydrogels show ratios of storage modulus to loss modulus (G'/G'') higher than 1. [191] Dynamic shear oscillation measurements at small strain were used to characterize the storage (G') and loss (G'') moduli of hydrogels OS and D-OS. As shown in Figure 4.53, both OS and D-OS hydrogel shows similar result on the ratio of G' to G'' at around 10. It means both materials show similar elasticity, and both of them form very stable hydrogels.

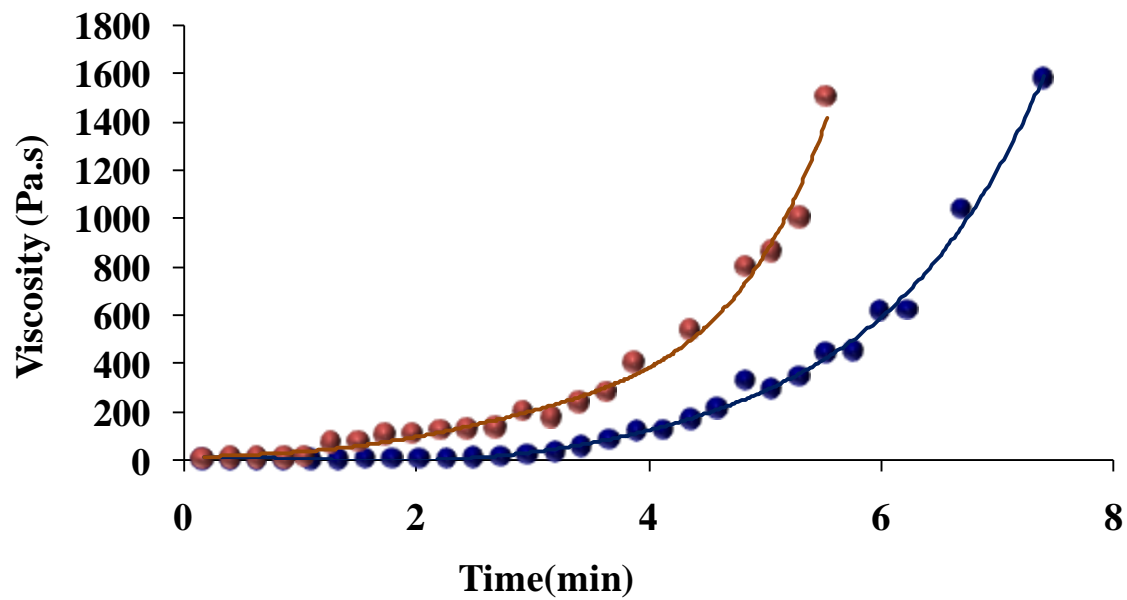


Figure 4.52 Zero-shear viscosities of hydrogels OS and D-OS; orange line is D-OS and blue line is OS

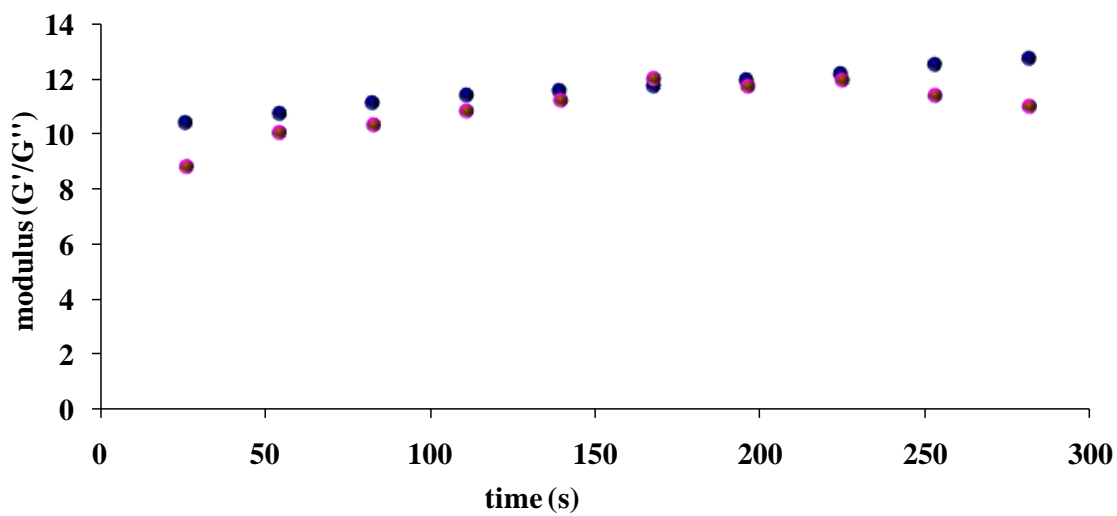


Figure 4.53 Storage/loss modulus of hydrogels OS and D-OS; orange dots are D-OS, and blue dots are OS

4.2.4 In Vitro DOX release from the D-OS hydrogel

The pH-dependent DOX releasing from D-OS hydrogel was characterized by directly incubation of gels in buffer solution. At predetermined time intervals, 3 ml of incubation solution was taken out and 3 ml of fresh PBS was added to refill the incubation solution to 15 ml. UV absorbance of DOX released in PBS buffers was recorded with a UV-vis spectrophotometer at wavelength of 480 nm, which is the characteristic maximum absorbance of DOX in solution. As shown in Figure 4.54, there was a release of about only 5% of the incorporated DOX within 48 h in PBS at pH 7.4. However, as designed, the rate of DOX release from D-OS hydrogel at pH 6.8 was much higher after 24hrs than at pH 7.4. There was an even higher of DOX release at pH 5 at around 65% within 48 hrs. These results indicate a high acid-sensitive release of DOX from hydrogels main body. After around 33 hrs, the drug release at all three pHs did not have significant change. The rest drug in D-OS hydrogel cannot be released might due to the interaction of Schiff base, hydrogen bond, or other non-covalent bonds [164].

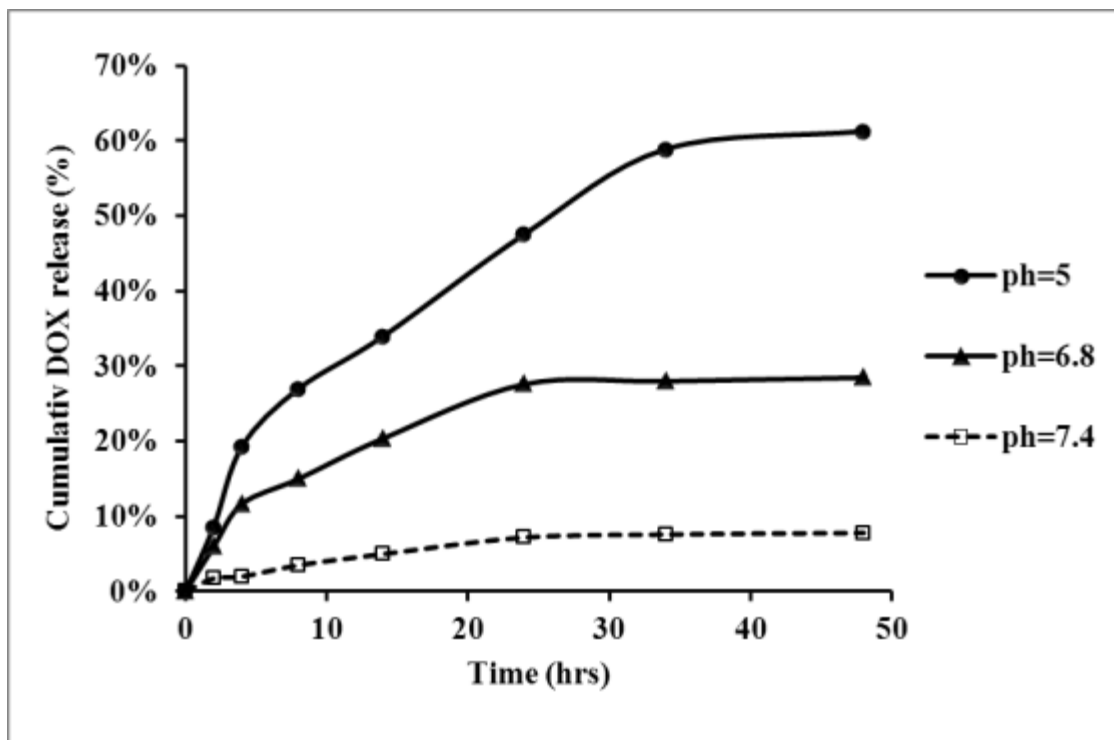


Figure 4.54 DOX release from D-OS hydrogel in PBS buffers at different pH values.

4.2.5 Cell morphology and intercellular distribution of DOX

Cell morphology observation can be used to show the cell apoptosis or necrosis [192]. We first investigate whether there is any difference on cell morphologies between the cell cultured without D-OS and with D-OS after 24 hr culture in pH 7.4 Medium. As showed in Figure 4.55 and Figure 4.56, the cell morphologies were similar to each other between the cell cultured without D-OS and with D-OS. Both of them showed very normal morphology. DOX concentration lower than $0.1 \mu\text{M}$ will not significantly inhibit the cell division.[193] Since in pH 7.4 only around 5% conjugated DOX released from the

hydrogel to the culture medium when DOX concentration is around only 4.6 nM, these drugs did not obviously change the cell morphology.

We further examined the morphology of the cells cultured on TCPs without D-OS in pH 6.8 medium to determine whether medium at pH 6.8 is suitable for MCF-7 culture. After 24 hrs culture, the morphology of MCF-7 did not show any sign of apoptosis or necrosis. (Figure 4.57)

Then, we incubated cells with D-OS in pH 6.8 medium. After same period culture, the cells lose its original skeleton morphology (Figure 4.58) compared to cells cultured with D-OS in pH 7.4 medium (Figure 4.56). The cytoskeletons of cells in pH 6.8 Medium have shrink in some degree, and the nucleus occupied most of the space in cell which indicated the cell necrosis or apoptosis.(Figure 4.61) [194] For DOX distribution, as shown in Figure 4.62, DOX were accumulated in cell nucleus area by showing intensive red color in nucleus space. Combined with Figure 4.63, most of DOX have been absorbed by nucleus and others have stayed in cytoplasm area. These results showed the distribution of DOX in cell which is the most direct proof of DOX releasing from the hydrogel, and showed the inhibition effect of DOX on MCF-7 cancer cells.

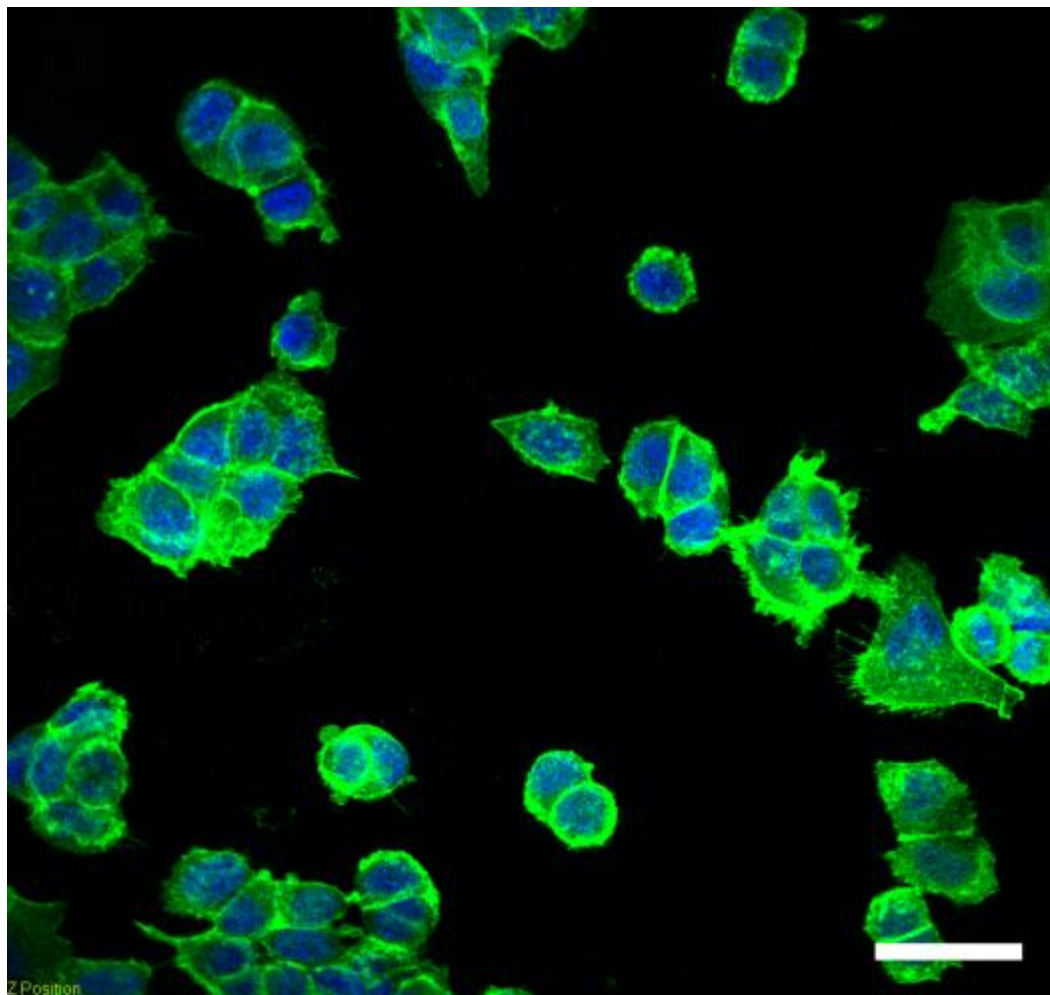


Figure 4.55 Confocal microscopy images of MCF-7 cultured on TCPs without D-OS hydrogels at pH 7.4 medium for 24 hrs. F-actin showing green color corresponding to cytoskeleton and blue color to Topro-3 stained nucleus; scale bar is 100 μm .

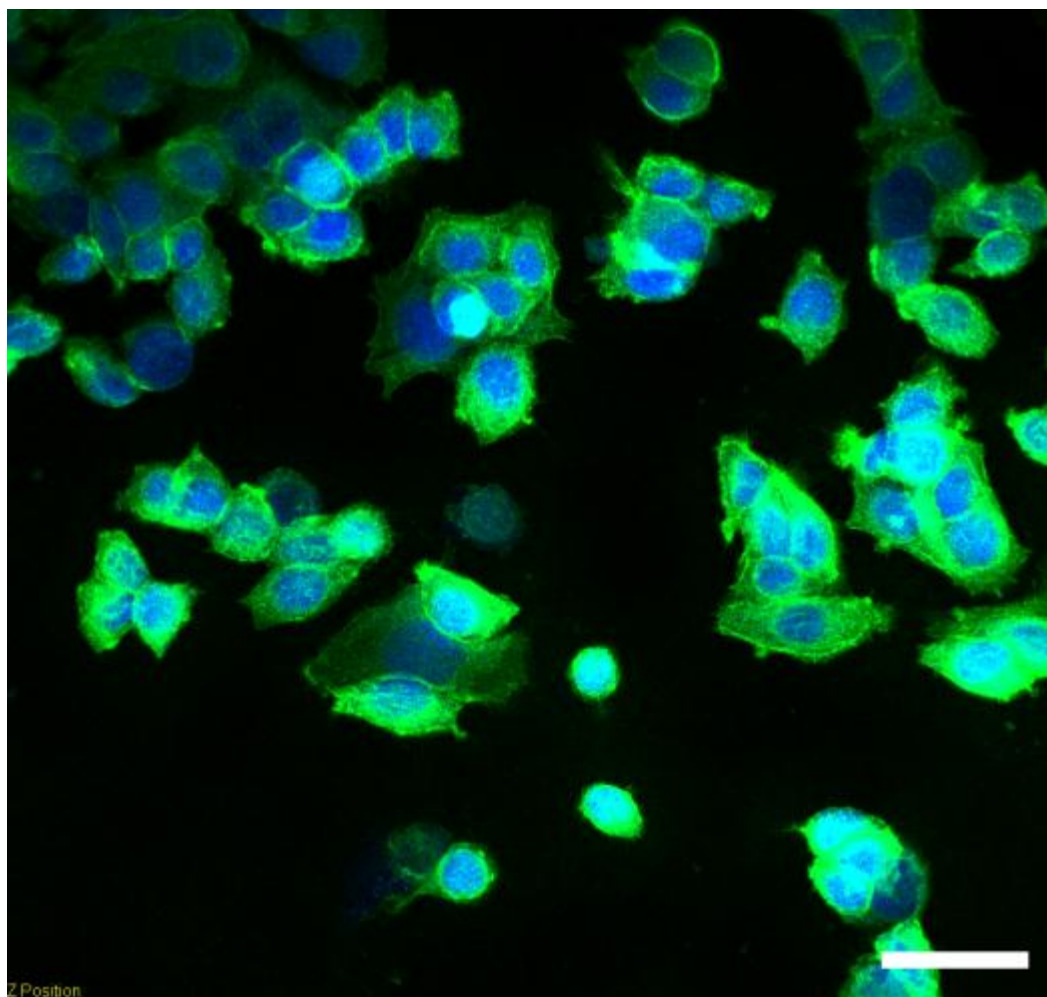


Figure 4.56 Confocal microscopy images of MCF-7 cultured on TCPs with D-OS hydrogels at pH 7.4 medium for 24 hrs. F-actin showing green color corresponding to cytoskeleton and blue color to Topro-3 stained nucleus; scale bar is 100 μ m

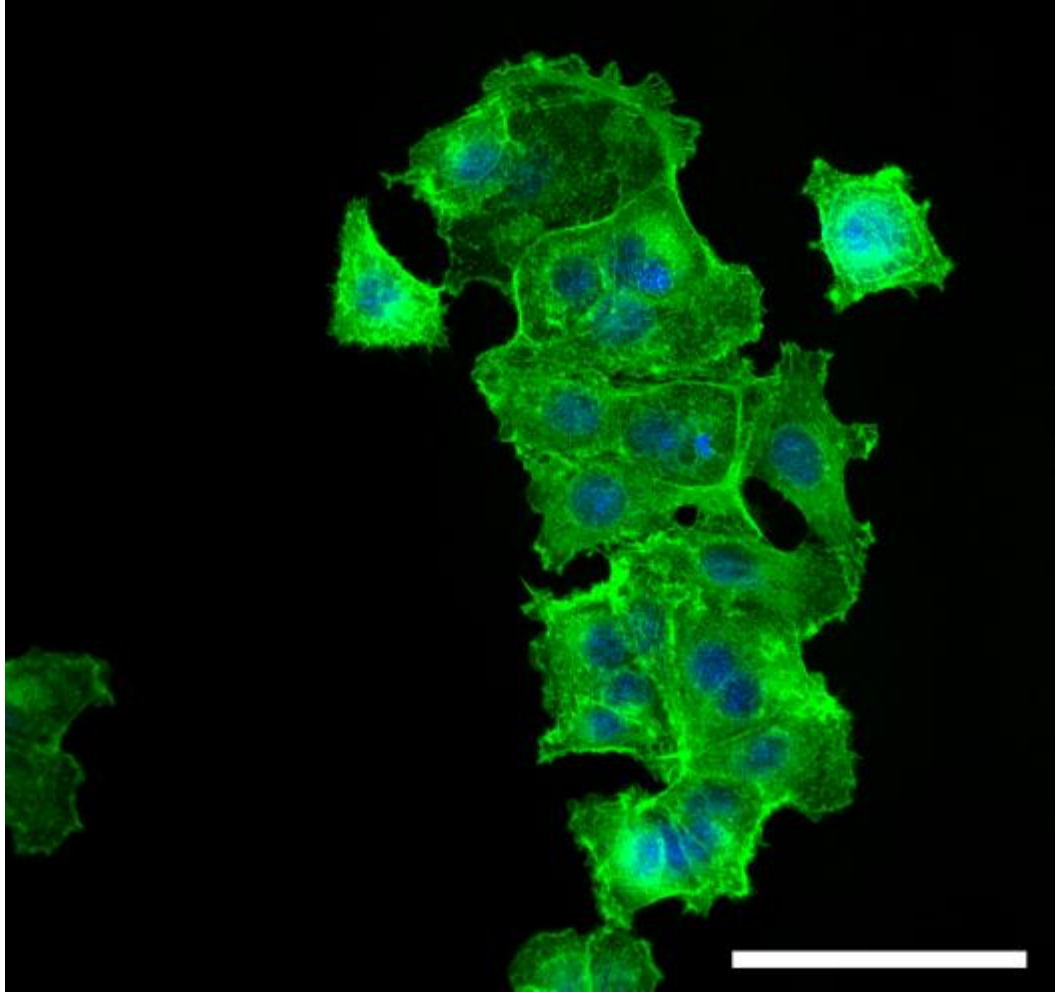


Figure 4.57 Confocal microscopy images of MCF-7 cultured on TCPs without D-OS hydrogels at pH 6.8 medium for 24 hrs. F-actin showing green color corresponding to cytoskeleton and blue color to Topro-3 stained nucleus; scale bar is 100 μm

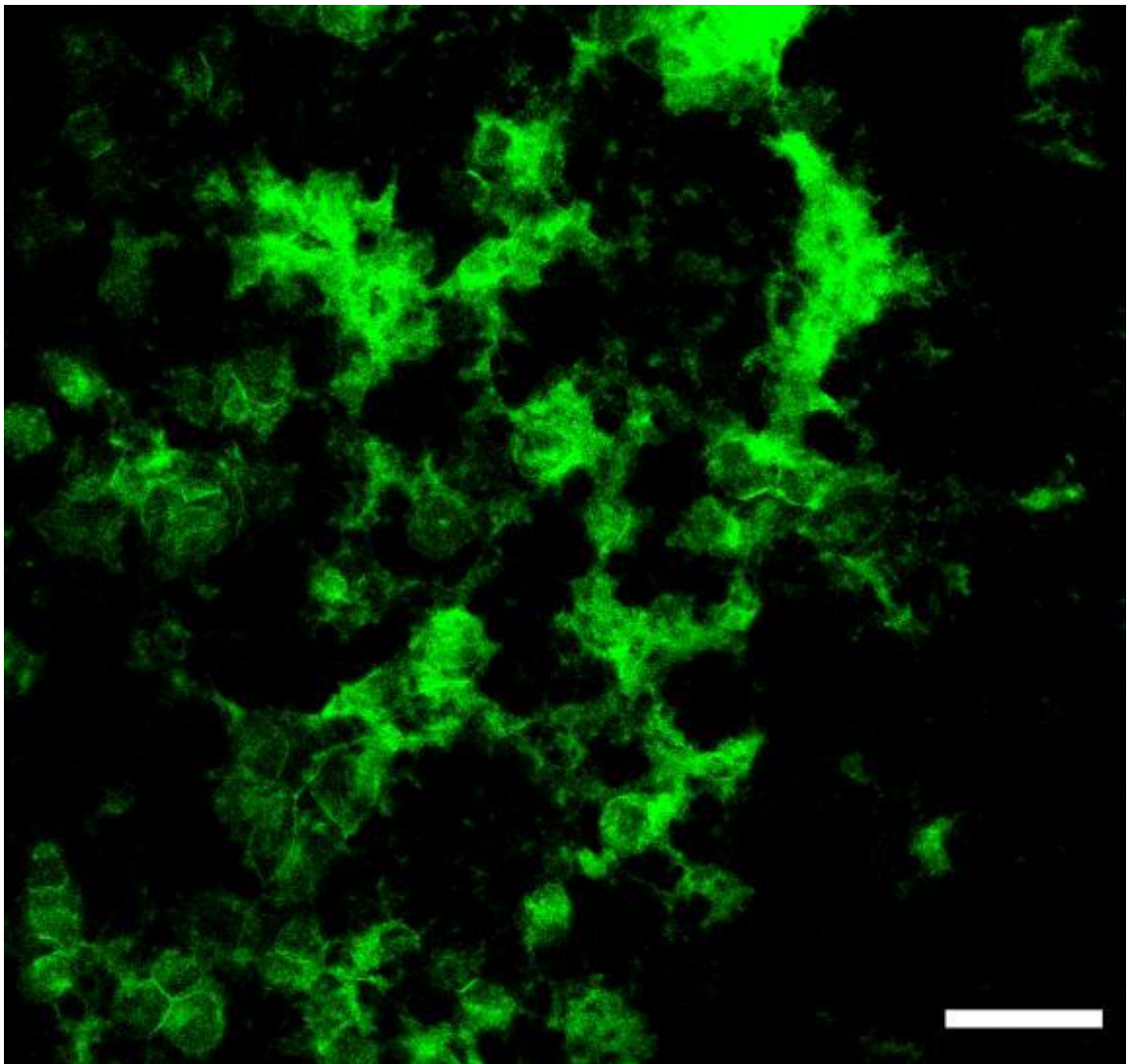


Figure 4.58 Confocal microscopy images of cytoskeleton of MCF-7 cultured on TCPs with D-OS hydrogels at pH 6.8 medium for 24 hrs; scale bar is 100 μm .

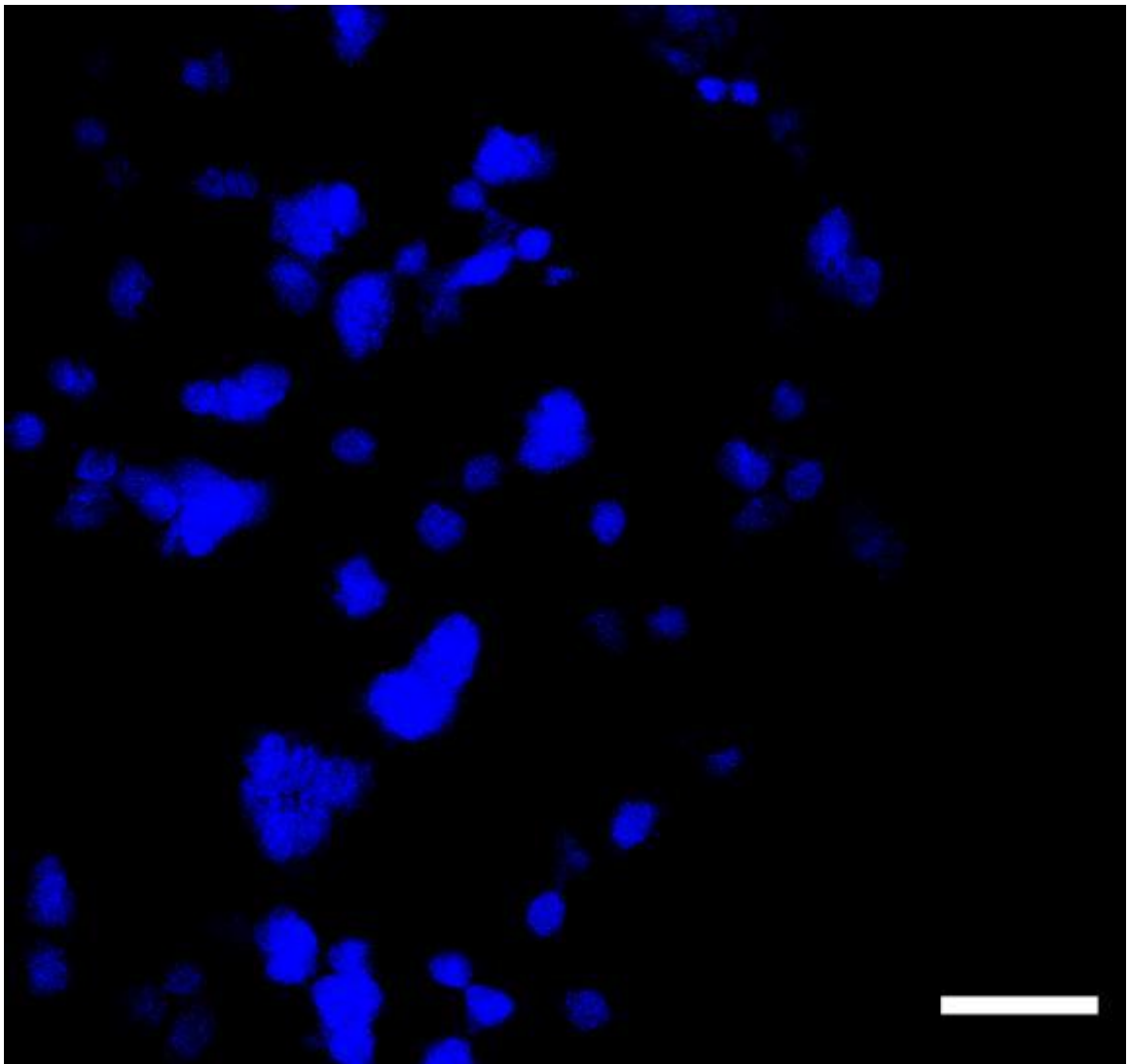


Figure 4.59 Confocal microscopy images of nucleus of MCF-7 cultured on TCPs with D-OS hydrogels at pH 6.8 medium for 24 hrs; scale bar is 100 μ m. The color is changed by the software from red to blue to differentiate from the DOX red fluorescence.

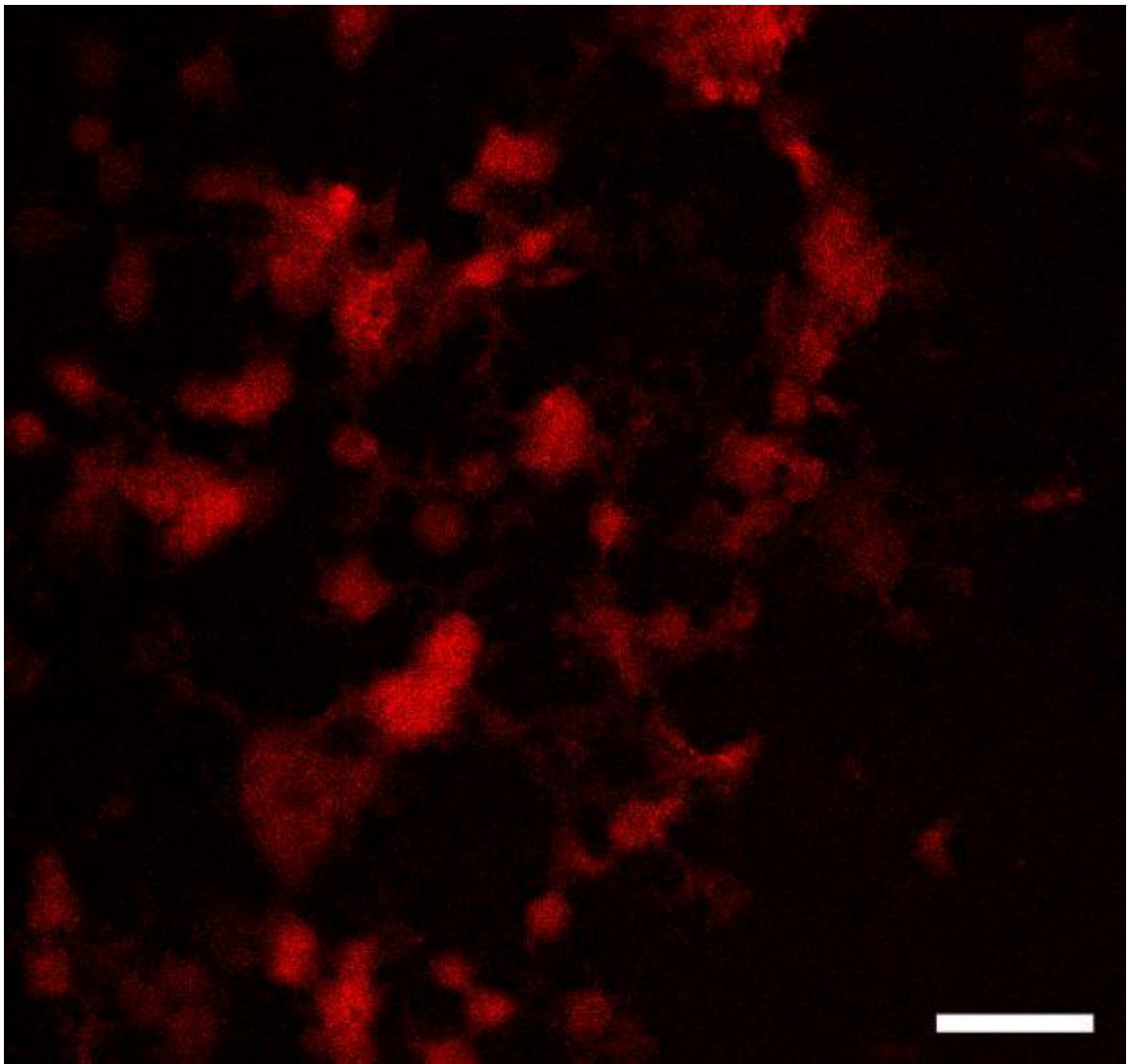


Figure 4.60 Confocal microscopy images of DOX distribution when MCF-7 cultured on TCPs with D-OS hydrogels at pH 6.8 medium for 24 hrs; scale bar is 100 um.

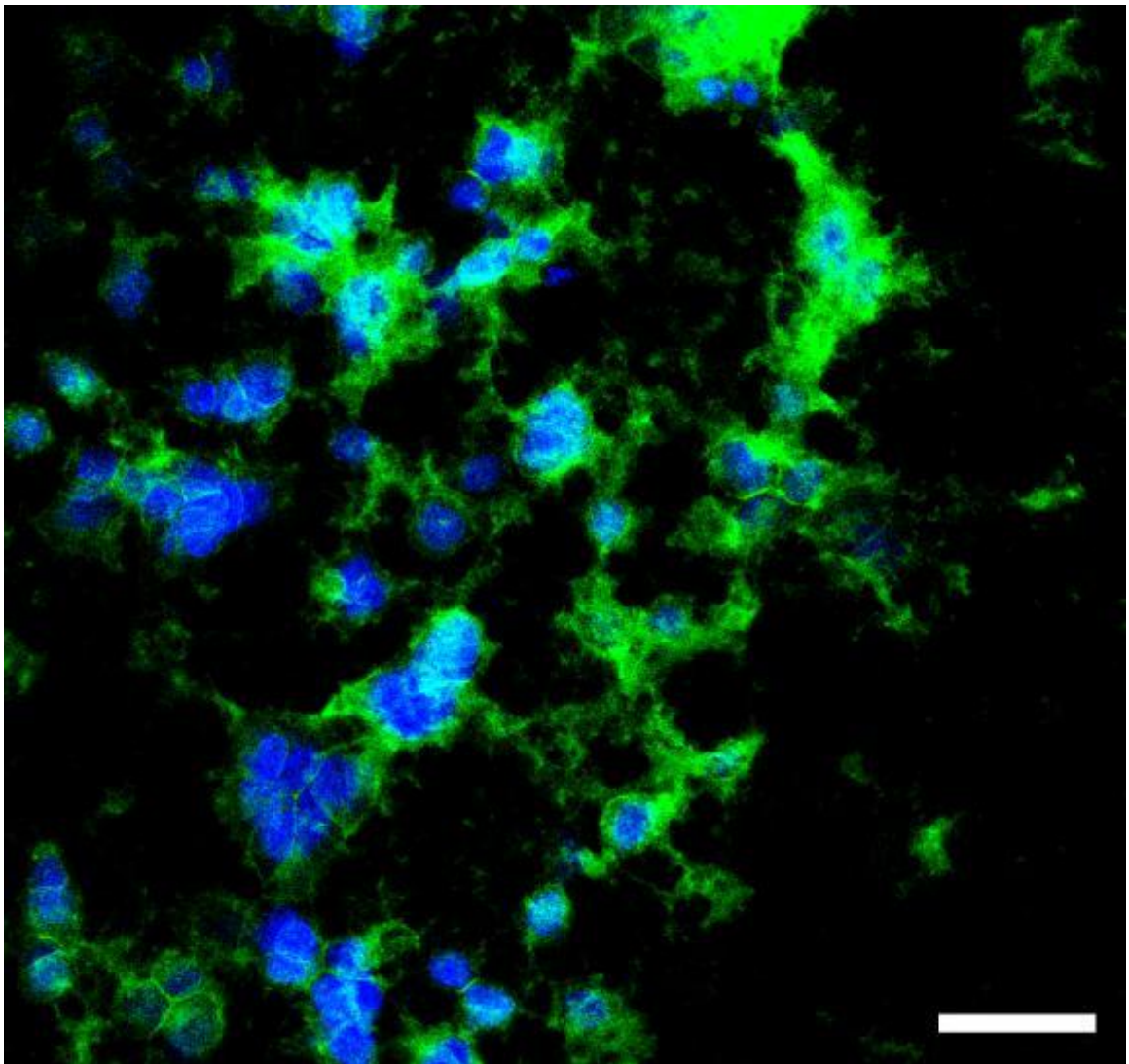


Figure 4.61 The overlays images of nuclear and cytoskeleton of MCF-7 cultured on TCPs with D-OS hydrogels at pH 6.8 medium for 24 hrs; scale bar is 100 μ m. Green color corresponds to cytoskeleton and blue color to nucleus.

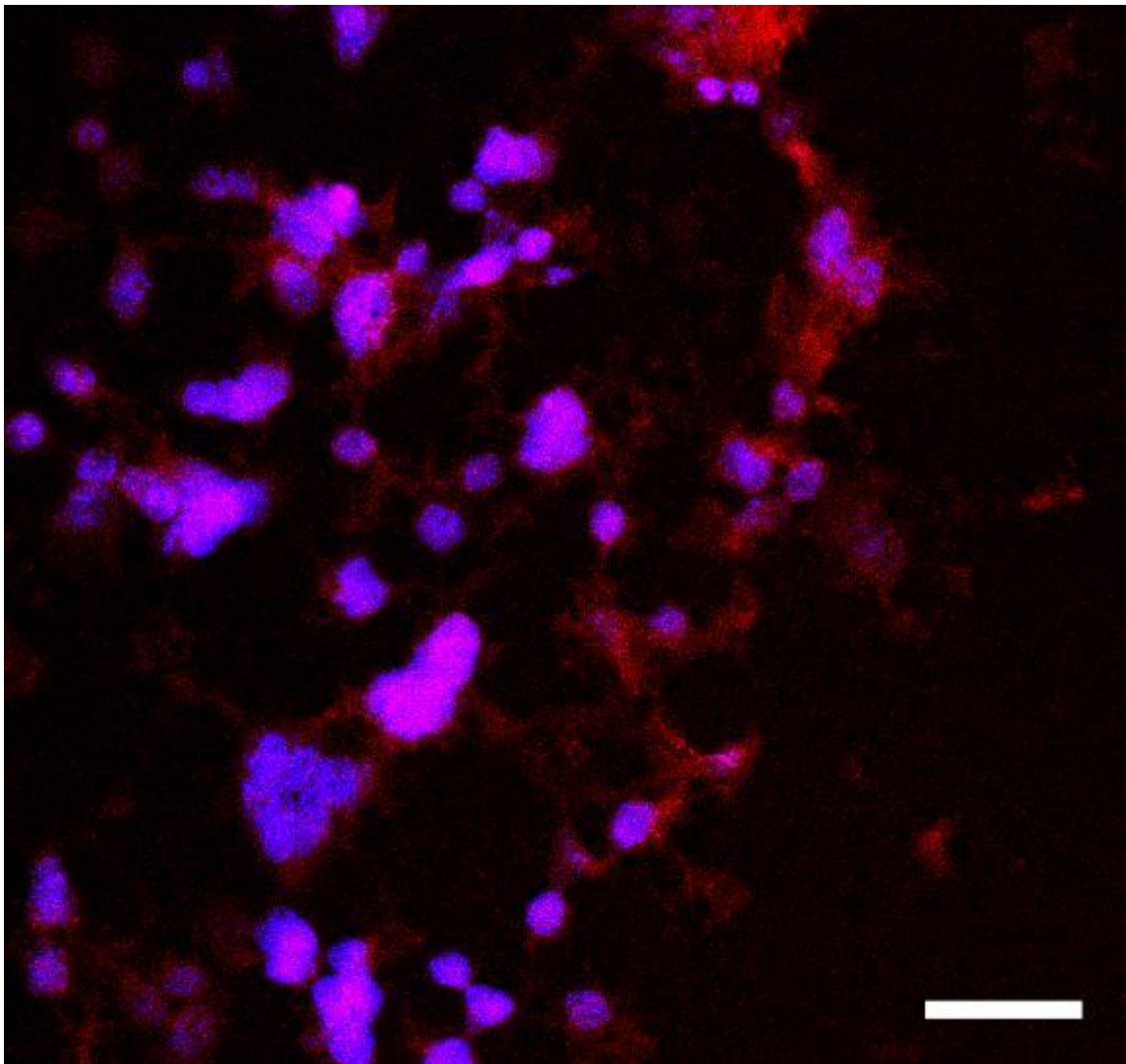


Figure 4.62 The overlays images of nuclear of MCF-7 cultured on TCPs with D-OS hydrogels at pH 6.8 medium for 24 hrs and DOX distribution in them; scale bar is 100 μ m. Blue color corresponds to nucleus, red color to DOX, and purple to DOX distribution area in nucleus

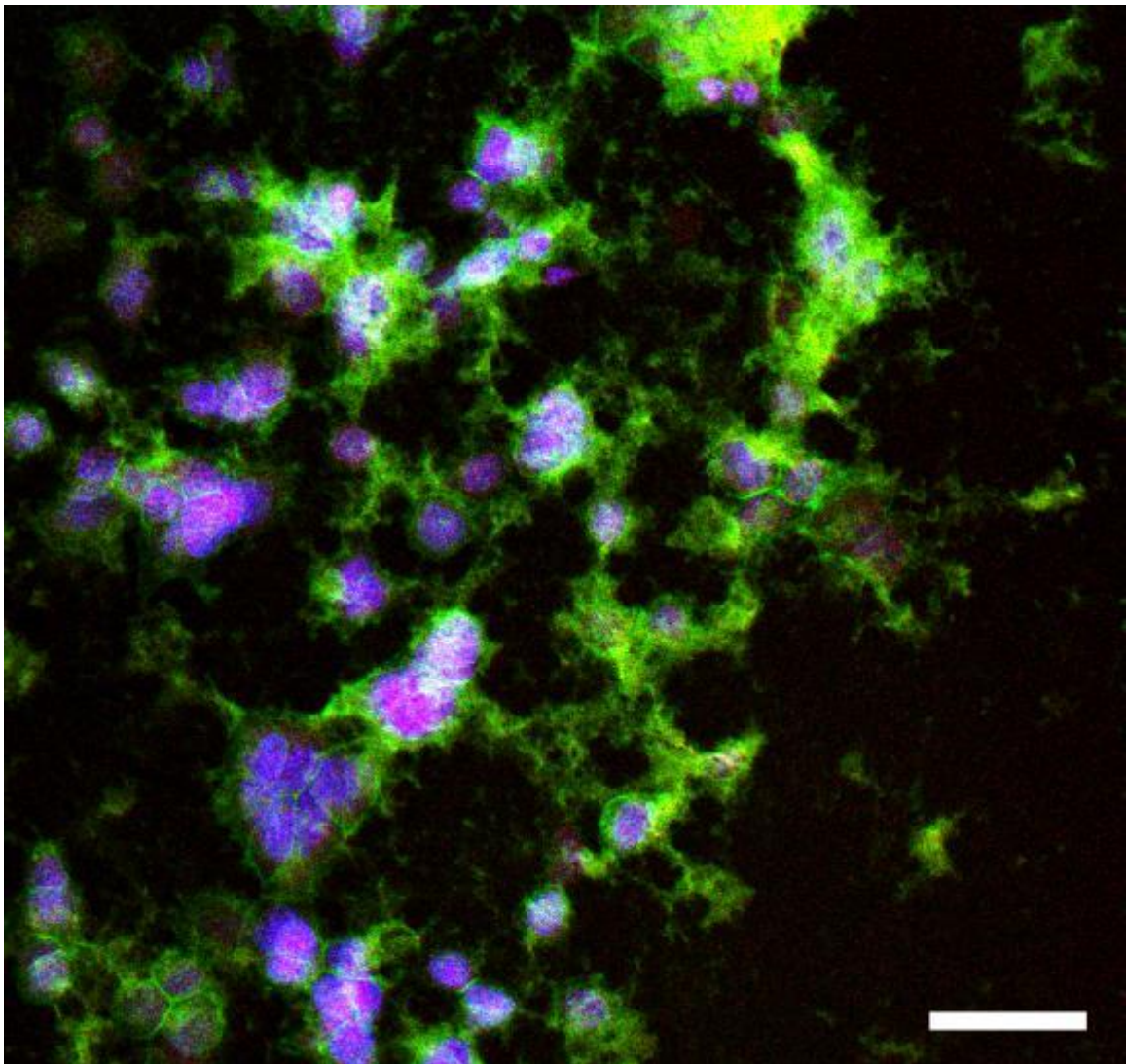


Figure 4.63 The overlays images of cytoskeleton, nuclear of MCF-7 cultured on TCPs with D-OS hydrogels at pH 6.8 medium for 24 hrs and intercellular distribution of DOX; scale bar is 100 μm . Green color corresponds to cytoskeleton, blue to nucleus, red color to DOX, and purple to DOX distribution area in nucleus,

4.2.6 Cytotoxicity of OS and D-OS hydrogel

The MTT result can present the cell inhibition rate after treated with materials. The lower absorbance means higher cell inhibition rate.[154] In Figure 4.64, MCF-7 cells cultured in pH 7.4 medium for 24 hrs have similar viability for TCPs, OS hydrogel, and even D-OS hydrogel. Since DOX released from D-OS hydrogel after 24 hrs at pH 7.4 environment is only around 5% (Figure 4.54), D-OS hydrogel would not induce significant apoptosis on cells at pH 7.4 environment. We further changed the pH of cell culture medium from 7.4 to 6.8 to create a weak acidic tumour tissue mimicking environment, and investigated the cytotoxicity for various culture times (Figure 4.65). After 2hr, cells cultured with D-OS hydrogel still have no significant apoptosis due to low amount of DOX released (Figure 4.54). For 24 hrs culture, around 30% of DOX is released from D-OS hydrogel (Figure 4.54), and around 50 % of cells cultured with D-OS hydrogel are significantly inhibited compared to TCPs group. After 48 hrs, the cell viability did not have significant change compared to 24 hrs group. One of the reason might be the release amount of DOX after 48 hr is close to that of 24 hrs. (Figure 4.54)

Viability cells in normal culture medium and that of in weak acidic medium were also qualitatively evaluated with Live/Dead staining. As shown in Figure 4.66, viability of MCF-7 treated with D-OS in normal culture medium was appeared to be > 99% after one day culture. However, in Figure 4.67, a large portion of image shows red color since a lot of dead cells showing red color combined with DOX red fluorescence. A large number of

MCF-7 cells cultured with D-OS hydrogel were dead in pH 6.8 culture medium and it's consistent with MTT result. Combined with the data in Figure 4.54 and Figure 4.65, these results indicate that D-OS hydrogel is high sensitive to pH thus holding excellent cell inhibition rate in environment close to tumour site while having minimal toxicity towards cells in neutral physiological environment.

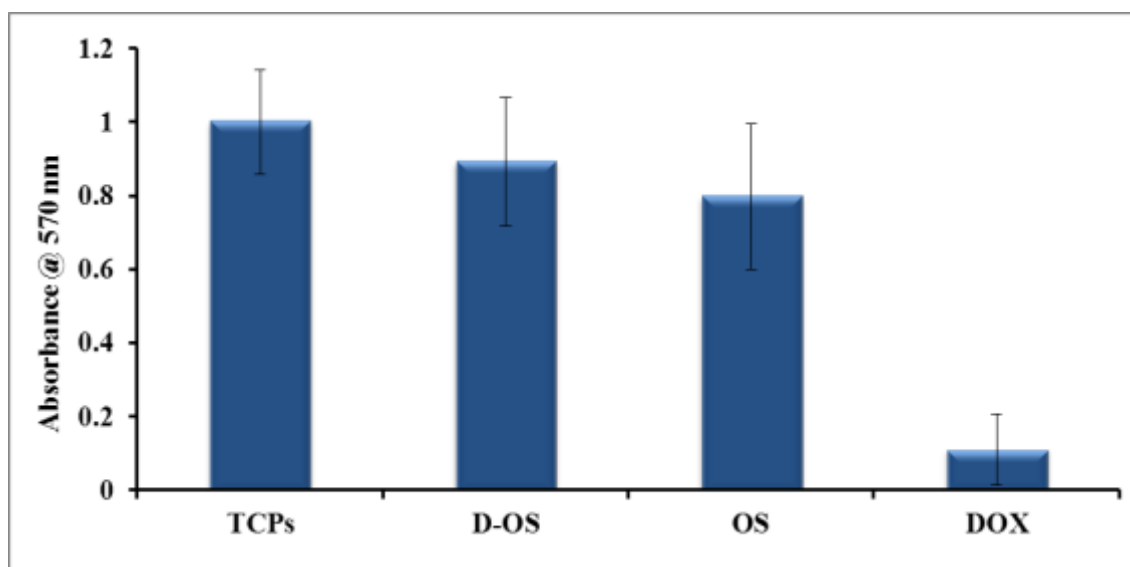


Figure 4.64 Cell viability at pH 7.4 culture environment for 24 hrs based on MTT assay (absorbance is normalized to 1 for TCPS control sample) (n=6)

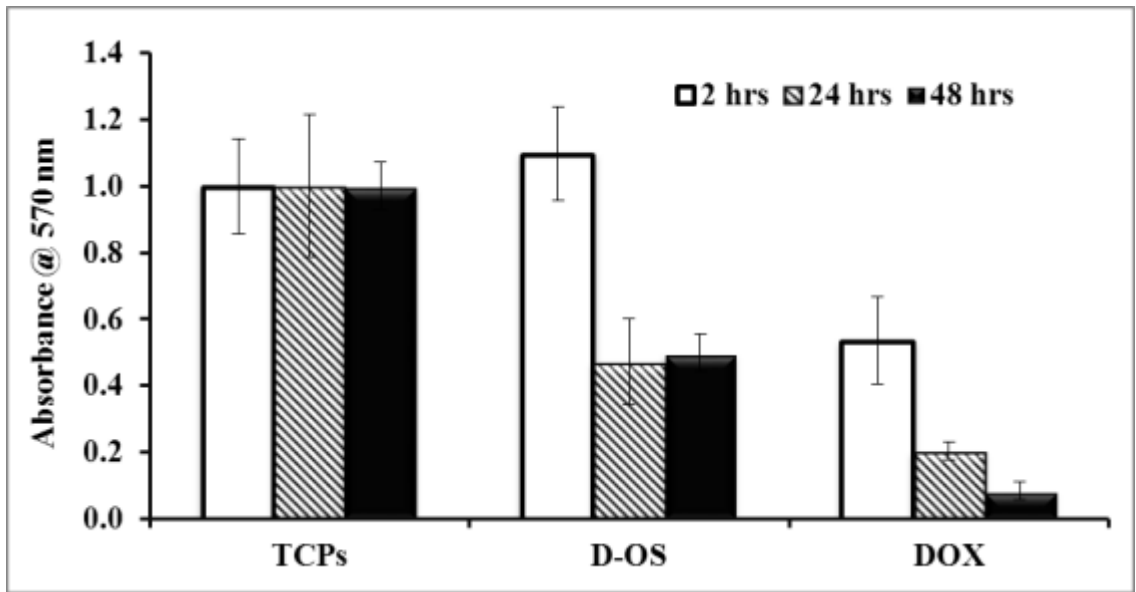


Figure 4.65 Cell viability at pH 6.8 culture environment for 2 hrs, 24 hrs and 48 hrs based on MTT assay (absorbance is normalized to 1 for TCPS control sample) (n=6)

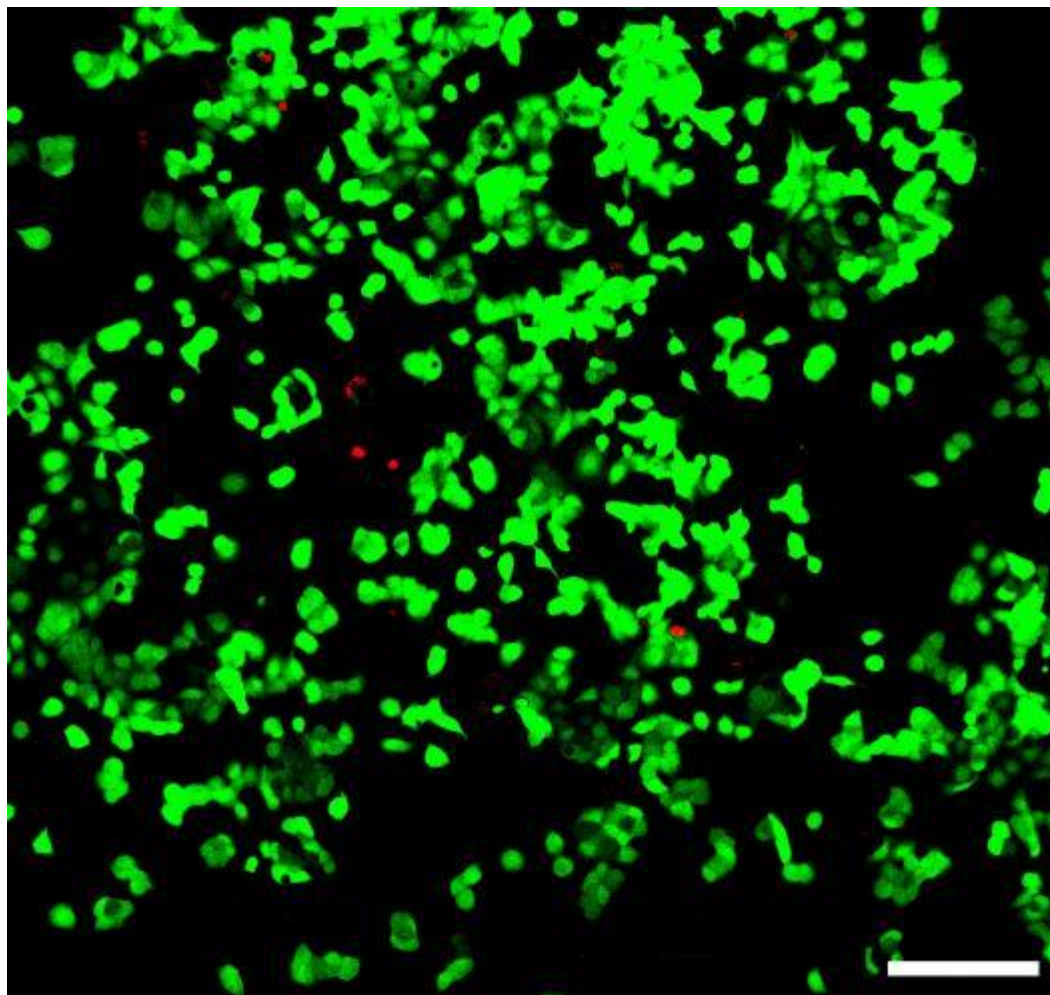


Figure 4.66 Live/Dead assay of MCF-7 cells cultured with hydrogel D-OS for 24 hrs at pH 7.4 culture environment; Green for live cells, Red for both dead cells and DOX; scale bars are 200 μm .

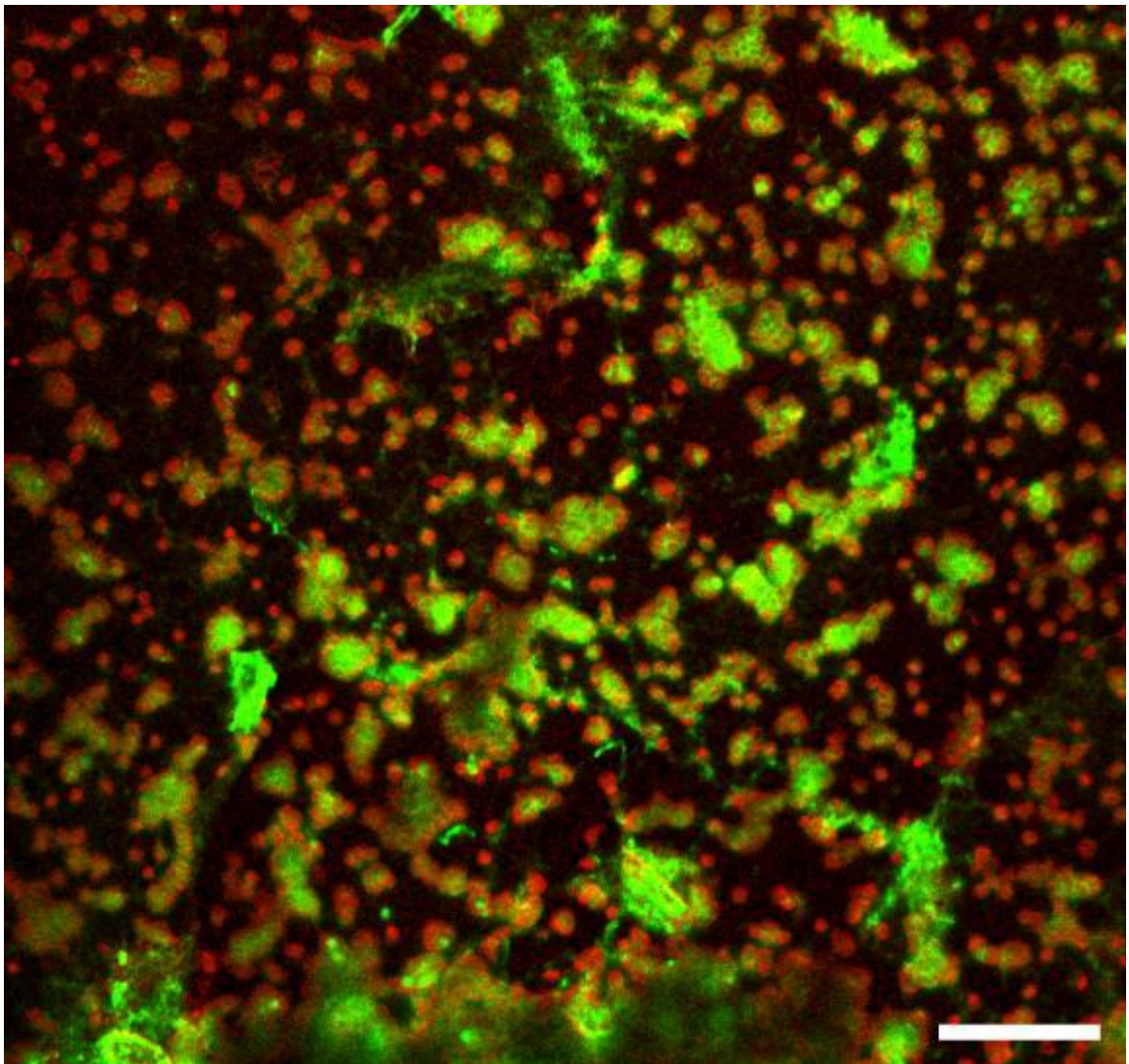


Figure 4.67 Live/Dead assay of MCF-7 cells cultured with hydrogel D-OS for 24 hrs at pH 6.8 culture environment; Green for live cells, Red for both dead cells and DOX; scale bars are 200 μm .

5 Conclusion

In the thesis, the versatility of hydrogels was presented by successfully control of cell behaviors using two novel hydrogel formulations. The main context of the work is investigation of chemical and physical properties of hydrogels, and cell behaviors, including cell adhesion, migration, viability, differentiation and apoptosis. All the results strongly suggested hydrogels can be an easy-controllable and useful platform to solve biomedical problems of controlling stem cell differentiation and selectively releasing cancer drug and improve disease therapy performance, especially on TE and cancer therapy.

5.1 TE

In the first part for TE, I synthesized and developed a novel multifunctional cationic poly amido amine with vinyl groups end-capped to form a biodegradable, biocompatible and cell attachable hydrogels. Disulfide bonds in hydrogel make hydrogel reductively degradable, and hydrogel reductive degradation can be controlled by reductive agent concentration. Hydrogels prepared by the multifunctional crosslinker, agmatine-containing PAA crosslinker can successfully support cell adhesion 2D spreading and 3D ingrowths. The carboxyl groups were introduced simultaneously with PAA crosslinker further improved the cell adhesion. The hydrogel stiffness can be simply changed by the precursor solution concentration. The design and develops of hydrogel for bone

regeneration have met the aforementioned requirement. The hydrogels prepared from this novel multifunctional crosslinker can be a promising candidate of TE scaffold.

5.2 Cancer therapy

In second part for the cancer therapy, I successfully use two nature polymer derivatives to develop a novel pH sensitive drug release system by using injectable in-situ formed hydrogel. This self-crosslinking hydrogel is formed based on Schiff base interaction, and anticancer drug DOX is incorporated into hydrogel main body by the same reaction. The acid-sensitive property of Schiff base offers this hydrogel a high sensitive drug release profile under different pH value which is verified by UV-vis spectrometry, MTT assay and Live/Dead assay. CLSM images confirmed the distribution of DOX in cell nucleus, and further indicated the successfully release of DOX from hydrogel main body at weakly acidic environment.

6 Reference

1. Peppas, N.A. and Chemical Rubber Company., *Hydrogels in medicine and pharmacy*. 1986, Boca Raton, Fla.: CRC Press.
2. Smeds, K.A., et al., *Synthesis of a novel polysaccharide hydrogel*. *Journal of Macromolecular Science-Pure and Applied Chemistry*, 1999. **A36**(7-8): p. 981-989.
3. Wichterle, O. and D. Lim, *Hydrophilic Gels for Biological Use*. *Nature*, 1960. **185**(4706): p. 117-118.
4. Peppas, N.A., et al., *Hydrogels in Biology and Medicine: From Molecular Principles to Bionanotechnology*. *Advanced Materials*, 2006. **18**(11): p. 1345-1360.

5. Hoffman, A.S., *Hydrogels for biomedical applications*. Advanced Drug Delivery Reviews, 2002. **54**(1): p. 3-12.
6. Lanza, R., R. Langer, and J. Vacanti, *Principles of Tissue Engineering* 1997: ACADEMIC PRESS
7. Geckil, H., et al., *Engineering hydrogels as extracellular matrix mimics*. Nanomedicine, 2010. **5**(3): p. 469-484.
8. Patel, M. and J.P. Fisher, *Biomaterial scaffolds in pediatric tissue engineering*. Pediatric Research, 2008. **63**(5): p. 497-501.
9. Lutolf, M.P., P.M. Gilbert, and H.M. Blau, *Designing materials to direct stem-cell fate*. Nature, 2009. **462**(7272): p. 433-441.
10. Peppas, N.A., *A practical approach to bodybuilding*. Nature, 1997. **389**(6650): p. 453-453.
11. Guilak, F., et al., *Control of Stem Cell Fate by Physical Interactions with the Extracellular Matrix*. Cell stem cell, 2009. **5**(1): p. 17-26.
12. Discher, D.E., P. Janmey, and Y.L. Wang, *Tissue cells feel and respond to the stiffness of their substrate*. Science, 2005. **310**(5751): p. 1139-1143.
13. Huebsch, N., et al., *Harnessing traction-mediated manipulation of the cell/matrix interface to control stem-cell fate*. Nature Materials, 2010. **9**(6): p. 518-526.
14. Rowley, J.A., G. Madhambayan, and D.J. Mooney, *Alginate hydrogels as synthetic extracellular matrix materials*. Biomaterials, 1999. **20**(1): p. 45-53.
15. Wang, L.S., et al., *Injectable biodegradable hydrogels with tunable mechanical properties for the stimulation of neurogenic differentiation of human mesenchymal stem cells in 3D culture*. Biomaterials, 2010. **31**(6): p. 1148-57.
16. Ta, H.T., C.R. Dass, and D.E. Dunstan, *Injectable chitosan hydrogels for localised cancer therapy*. Journal of Controlled Release, 2008. **126**(3): p. 205-216.
17. Papac, R.J., *Origins of cancer therapy*. Yale Journal of Biology and Medicine, 2001. **74**(6): p. 391-398.
18. Lim, E.-K., et al., *pH-Triggered Drug-Releasing Magnetic Nanoparticles for Cancer Therapy Guided by Molecular Imaging by MRI*. Advanced Materials, 2011. **23**(21): p. 2436-2442.
19. Langer, R., *New methods of drug delivery*. Science, 1990. **249**(4976): p. 1527-1533.
20. Stuart, M.A.C., et al., *Emerging applications of stimuli-responsive polymer materials*. Nat Mater, 2010. **9**(2): p. 101-113.
21. Merkel, T.J., et al., *Using mechanobiological mimicry of red blood cells to extend circulation times of hydrogel microparticles*. Proceedings of the National Academy of Sciences, 2011. **108**(2): p. 586-591.
22. Scott, R.C., et al., *Aiming for the heart: targeted delivery of drugs to diseased cardiac tissue*. Expert Opinion on Drug Delivery, 2008. **5**(4): p. 459-470.
23. Seidman, A., et al., *Cardiac Dysfunction in the Trastuzumab Clinical Trials Experience*. Journal of Clinical Oncology, 2002. **20**(5): p. 1215-1221.
24. Brufsky, A., *Trastuzumab-Based Therapy for Patients With HER2-Positive Breast Cancer: From Early Scientific Development to Foundation of Care*. American

- Journal of Clinical Oncology, 2010. **33**(2): p. 186-195
10.1097/COC.0b013e318191bfb0.
25. Ferrari, M., *Cancer nanotechnology: Opportunities and challenges*. Nature Reviews Cancer, 2005. **5**(3): p. 161-171.
 26. Scheufele, D.A., et al., *Scientists worry about some risks more than the public*. Nat Nano, 2007. **2**(12): p. 732-734.
 27. Bae, Y., et al., *Design of Environment-Sensitive Supramolecular Assemblies for Intracellular Drug Delivery: Polymeric Micelles that are Responsive to Intracellular pH Change*. Angewandte Chemie International Edition, 2003. **42**(38): p. 4640-4643.
 28. Smith, J.P., et al., *Drug retention and distribution after intratumoral chemotherapy with fluorouracil/epinephrine injectable gel in human pancreatic cancer xenografts*. Cancer Chemotherapy and Pharmacology, 1999. **44**(4): p. 267-274.
 29. Cho, J.-K., et al., *Injectable delivery system of 2-methoxyestradiol for breast cancer therapy using biodegradable thermosensitive poly(organophosphazene) hydrogel*. Journal of Drug Targeting, 2010. **19**(4): p. 270-280.
 30. Vemula, P.K., et al., *On-demand drug delivery from self-assembled nanofibrous gels: A new approach for treatment of proteolytic disease*. Journal of Biomedical Materials Research Part A, 2011. **97A**(2): p. 103-110.
 31. Lee, S.J., et al., *In vitro Release and in vivo Anti-tumor Efficacy of Doxorubicin from Biodegradable Temperature-sensitive Star-shaped PLGA-PEG Block Copolymer Hydrogel*. Polym. J, 2007. **40**(2): p. 171-176.
 32. Jeong, B., et al., *Biodegradable block copolymers as injectable drug-delivery systems*. Nature, 1997. **388**(6645): p. 860-862.
 33. Langer, R. and J.P. Vacanti, *Tissue Engineering*. Science, 1993. **260**(5110): p. 920-926.
 34. Vacanti, J.P., et al., *Selective Cell Transplantation Using Bioabsorbable Artificial Polymers as Matrices*. Journal of Pediatric Surgery, 1988. **23**(1): p. 3-9.
 35. Marler, J.J., et al., *Transplantation of cells in matrices for tissue regeneration*. Advanced Drug Delivery Reviews, 1998. **33**(1-2): p. 165-182.
 36. Kloxin, A.M., et al., *Mechanical Properties of Cellularly Responsive Hydrogels and Their Experimental Determination*. Advanced Materials, 2010. **22**(31): p. 3484-3494.
 37. Novak, K., *Epigenetics changes in cancer cells*. MedGenMed : Medscape general medicine, 2004. **6**(4): p. 17.
 38. Ravi Kumar, M.N.V., *A review of chitin and chitosan applications*. Reactive and Functional Polymers, 2000. **46**(1): p. 1-27.
 39. Wong, H.L., et al., *Chemotherapy with anticancer drugs encapsulated in solid lipid nanoparticles*. Advanced Drug Delivery Reviews, 2007. **59**(6): p. 491-504.
 40. Lin, C.-C. and A.T. Metters, *Hydrogels in controlled release formulations: Network design and mathematical modeling*. Advanced Drug Delivery Reviews, 2006. **58**(12-13): p. 1379-1408.

41. Qiu, Y. and K. Park, *Environment-sensitive hydrogels for drug delivery*. *Advanced Drug Delivery Reviews*, 2001. **53**(3): p. 321-339.
42. Denmeade, S.R., et al., *Prostate-Specific Antigen-Activated Thapsigargin Prodrug as Targeted Therapy for Prostate Cancer*. *Journal of the National Cancer Institute*, 2003. **95**(13): p. 990-1000.
43. Atkinson, J.M., et al., *Development of a Novel Tumor-Targeted Vascular Disrupting Agent Activated by Membrane-Type Matrix Metalloproteinases*. *Cancer Research*, 2010. **70**(17): p. 6902-6912.
44. Hubbell, J.A., *Biomaterials in Tissue Engineering*. *Nat Biotech*, 1995. **13**(6): p. 565-576.
45. Kochlamazashvili, G., et al., *The Extracellular Matrix Molecule Hyaluronic Acid Regulates Hippocampal Synaptic Plasticity by Modulating Postsynaptic L-Type Ca²⁺ Channels*. *Neuron*, 2010. **67**(1): p. 116-128.
46. Olczyk, P., et al., *Hyaluronan: Structure, metabolism, functions, and role in wound healing*. *Postepy Higieny I Medycyny Doswiadczalnej*, 2008. **62**: p. 651-659.
47. Zou, L., et al., *Effect of hyaluronan on osteogenic differentiation of porcine bone marrow stromal cells in vitro*. *Journal of Orthopaedic Research*, 2008. **26**(5): p. 713-720.
48. Gerecht, S., et al., *Hyaluronic acid hydrogen for controlled self-renewal and differentiation of human embryonic stem cells*. *Proceedings of the National Academy of Sciences of the United States of America*, 2007. **104**(27): p. 11298-11303.
49. Vercruyse, K.P., et al., *Synthesis and in Vitro Degradation of New Polyvalent Hydrazide Cross-Linked Hydrogels of Hyaluronic Acid*. *Bioconjugate Chemistry*, 1997. **8**(5): p. 686-694.
50. Takigami, S., M. Takigami, and G.O. Phillips, *Hydration characteristics of the cross-linked hyaluronan derivative hylan*. *Carbohydrate Polymers*, 1993. **22**(3): p. 153-160.
51. Kreil, G., *Hyaluronidases — a group of neglected enzymes*. *Protein Science*, 1995. **4**(9): p. 1666-1669.
52. Shu, X.Z., et al., *Disulfide-crosslinked hyaluronan-gelatin hydrogel films: a covalent mimic of the extracellular matrix for in vitro cell growth*. *Biomaterials*, 2003. **24**(21): p. 3825-3834.
53. Burdick, J.A., et al., *Controlled degradation and mechanical behavior of photopolymerized hyaluronic acid networks*. *Biomacromolecules*, 2005. **6**(1): p. 386-391.
54. Lee, F., J.E. Chung, and M. Kurisawa, *An injectable enzymatically crosslinked hyaluronic acid-tyramine hydrogel system with independent tuning of mechanical strength and gelation rate*. *Soft Matter*, 2008. **4**(4): p. 880-887.
55. Shu, X.Z., et al., *Disulfide Cross-Linked Hyaluronan Hydrogels*. *Biomacromolecules*, 2002. **3**(6): p. 1304-1311.

56. Mironov, V., et al., *Fabrication of tubular tissue constructs by centrifugal casting of cells suspended in an in situ crosslinkable hyaluronan-gelatin hydrogel*. *Biomaterials*, 2005. **26**(36): p. 7628-7635.
57. Jha, A.K., et al., *Controlling the adhesion and differentiation of mesenchymal stem cells using hyaluronic acid-based, doubly crosslinked networks*. *Biomaterials*, 2011. **32**(10): p. 2466-2478.
58. Müller, W.E.G., *The Origin of Metazoan Complexity: Porifera as Integrated Animals*. *Integrative and Comparative Biology*, 2003. **43**(1): p. 3-10.
59. Parkinson, J., et al., *The mechanical properties of simulated collagen fibrils*. *Journal of biomechanics*, 1997. **30**(6): p. 549-554.
60. Di Lullo, G.A., et al., *Mapping the Ligand-binding Sites and Disease-associated Mutations on the Most Abundant Protein in the Human, Type I Collagen*. *Journal of Biological Chemistry*, 2002. **277**(6): p. 4223-4231.
61. ZHANG, Z., G. LI, and B. SHI, *Physicochemical properties of collagen, gelatin and collagen hydrolysate derived from bovine limed split wastes*. Vol. 90. 2006, Dewsbury, ROYAUME-UNI: Society of Leather Technologists and Chemists. 6.
62. Lee, S.H., et al., *Poly(ethylene glycol) hydrogels conjugated with a collagenase-sensitive fluorogenic substrate to visualize collagenase activity during three-dimensional cell migration*. *Biomaterials*, 2007. **28**(20): p. 3163-3170.
63. Layman, H., et al., *The effect of the controlled release of basic fibroblast growth factor from ionic gelatin-based hydrogels on angiogenesis in a murine critical limb ischemic model*. *Biomaterials*, 2007. **28**(16): p. 2646-2654.
64. Lyons, F.G., et al., *The healing of bony defects by cell-free collagen-based scaffolds compared to stem cell-seeded tissue engineered constructs*. *Biomaterials*, 2010. **31**(35): p. 9232-9243.
65. Finotelli, P.V., et al., *Ca ALGINATE AS SCAFFOLD FOR IRON OXIDE NANOPARTICLES SYNTHESIS*. *Brazilian Journal of Chemical Engineering*, 2008. **25**(4): p. 759-764.
66. Cha, C., et al., *Integrative design of a poly(ethylene glycol)-poly(propylene glycol)-alginate hydrogel to control three dimensional biomineralization*. *Biomaterials*, 2011. **32**(11): p. 2695-2703.
67. Balakrishnan, B., et al., *Periodate oxidation of sodium alginate in water and in ethanol-water mixture: a comparative study*. *Carbohydrate Research*, 2005. **340**(7): p. 1425-1429.
68. Huang, Y., et al., *In vitro characterization of chitosan-gelatin scaffolds for tissue engineering*. *Biomaterials*, 2005. **26**(36): p. 7616-7627.
69. Leipzig, N.D., et al., *Differentiation of neural stem cells in three-dimensional growth factor-immobilized chitosan hydrogel scaffolds*. *Biomaterials*, 2011. **32**(1): p. 57-64.
70. Prabakaran, M. and J.F. Mano, *Chitosan-Based Particles as Controlled Drug Delivery Systems*. *Drug Delivery*, 2004. **12**(1): p. 41-57.
71. Gerrit, B., *Chitosans for gene delivery*. *Advanced Drug Delivery Reviews*, 2001. **52**(2): p. 145-150.

72. Vieira, E.F.S., et al., *Polysaccharide-Based Hydrogels: Preparation, Characterization, and Drug Interaction Behaviour*. *Biomacromolecules*, 2008. **9**(4): p. 1195-1199.
73. Cheng, N. and X. Cao, *Photosensitive chitosan to control cell attachment*. *Journal of Colloid and Interface Science*, 2011. **361**(1): p. 71-78.
74. Yamaguchi, R., et al., *Preparation of partially N-succinylated chitosans and their cross-linked gels*. *Carbohydrate Research*, 1981. **88**(1): p. 172-175.
75. Freier, T., et al., *Controlling cell adhesion and degradation of chitosan films by N-acetylation*. *Biomaterials*, 2005. **26**(29): p. 5872-5878.
76. Monteiro Jr, O.A.C. and C. Airoidi, *Some studies of crosslinking chitosan-glutaraldehyde interaction in a homogeneous system*. *International Journal of Biological Macromolecules*, 1999. **26**(2-3): p. 119-128.
77. Mi, F.L., H.W. Sung, and S.S. Shyu, *Synthesis and characterization of a novel chitosan-based network prepared using naturally occurring crosslinker*. *Journal of Polymer Science Part a-Polymer Chemistry*, 2000. **38**(15): p. 2804-2814.
78. Zhong, C., et al., *Synthesis, characterization and cytotoxicity of photo-crosslinked maleic chitosan-polyethylene glycol diacrylate hybrid hydrogels*. *Acta Biomaterialia*, 2010. **6**(10): p. 3908-3918.
79. Hern, D.L. and J.A. Hubbell, *Incorporation of adhesion peptides into nonadhesive hydrogels useful for tissue resurfacing*. *Journal of Biomedical Materials Research*, 1998. **39**(2): p. 266-276.
80. Pelham, R.J. and Y.-l. Wang, *Cell locomotion and focal adhesions are regulated by substrate flexibility*. *Proceedings of the National Academy of Sciences*, 1997. **94**(25): p. 13661-13665.
81. Wang, Y.L. and R.J. Pelham, *Preparation of a flexible, porous polyacrylamide substrate for mechanical studies of cultured cells*. *Molecular Motors and the Cytoskeleton*, Pt B, 1998. **298**: p. 489-496.
82. Zainuddin, et al., *PHEMA Hydrogels Modified through the Grafting of Phosphate Groups by ATRP Support the Attachment and Growth of Human Corneal Epithelial Cells*. *Journal of Biomaterials Applications*, 2008. **23**(2): p. 147-168.
83. Pokharna, H.K., et al., *Copolymers of Hydroxyethyl Methacrylate with Quadrol Methacrylate and with Various Aminoalkyl Methacrylamides as Fibroblast Cell Substrata*. *Journal of Bioactive and Compatible Polymers*, 1990. **5**(1): p. 42-52.
84. Temenoff, J.S., et al., *Thermally Cross-Linked Oligo(poly(ethylene glycol) fumarate) Hydrogels Support Osteogenic Differentiation of Encapsulated Marrow Stromal Cells In Vitro*. *Biomacromolecules*, 2003. **5**(1): p. 5-10.
85. Oh, J.K., D.I. Lee, and J.M. Park, *Biopolymer-based microgels/nanogels for drug delivery applications*. *Progress in Polymer Science*, 2009. **34**(12): p. 1261-1282.
86. Stasko, J., et al., *Poly(vinyl alcohol) hydrogels*. *Polüvinüülalkoholi hüdrogeelid.*, 2009. **58**(1): p. 63-66.
87. Schmedlen, R.H., K.S. Masters, and J.L. West, *Photocrosslinkable polyvinyl alcohol hydrogels that can be modified with cell adhesion peptides for use in tissue engineering*. *Biomaterials*, 2002. **23**(22): p. 4325-4332.

88. Martens, P., T. Holland, and K.S. Anseth, *Synthesis and characterization of degradable hydrogels formed from acrylate modified poly(vinyl alcohol) macromers*. *Polymer*, 2002. **43**(23): p. 6093-6100.
89. Mawad, D., et al., *The effect of redox polymerisation on degradation and cell responses to poly (vinyl alcohol) hydrogels*. *Biomaterials*, 2007. **28**(6): p. 947-955.
90. Chirila, T.V., et al., *Poly(2-hydroxyethyl methacrylate) sponges as implant materials: in vivo and in vitro evaluation of cellular invasion*. *Biomaterials*, 1993. **14**(1): p. 26-38.
91. Casadio, Y.S., et al., *Biodegradation of Poly(2-hydroxyethyl methacrylate) (PHEMA) and Poly{(2-hydroxyethyl methacrylate)-co-[poly(ethylene glycol) methyl ether methacrylate]} Hydrogels Containing Peptide-Based Cross-Linking Agents*. *Biomacromolecules*, 2010. **11**(11): p. 2949-2959.
92. Ferruti, P., M.A. Marchisio, and R. Barbucci, *Synthesis, physico-chemical properties and biomedical applications of poly(amidoamine)s*. *Polymer*, 1985. **26**(9): p. 1336-1348.
93. Jacchetti, E., et al., *Biomimetic poly(amidoamine) hydrogels as synthetic materials for cell culture*. *Journal of Nanobiotechnology*, 2008. **6**(1): p. 14.
94. Lopez, A.I., et al., *Antibacterial activity and cytotoxicity of PEGylated poly(amidoamine) dendrimers*. *Molecular BioSystems*, 2009. **5**(10): p. 1148-1156.
95. Chen, J., C. Wu, and D. Oupický, *Bioreducible Hyperbranched Poly(amidoamine)s for Gene Delivery*. *Biomacromolecules*, 2009. **10**(10): p. 2921-2927.
96. Emilietri, E., et al., *Novel amphoteric cystine-based poly(amidoamine)s responsive to redox stimuli*. *Macromolecules*, 2007. **40**(14): p. 4785-4793.
97. Ferruti, P., et al., *Novel Agmatine-Containing Poly(amidoamine) Hydrogels as Scaffolds for Tissue Engineering*. *Biomacromolecules*, 2005. **6**(4): p. 2229-2235.
98. Fusco, S., A. Borzacchiello, and P.A. Netti, *Perspectives on: PEO-PPO-PEO Triblock Copolymers and their Biomedical Applications*. *Journal of Bioactive and Compatible Polymers*, 2006. **21**(2): p. 149-164.
99. Bromberg, L.E. and E.S. Ron, *Temperature-responsive gels and thermogelling polymer matrices for protein and peptide delivery*. *Advanced Drug Delivery Reviews*, 1998. **31**(3): p. 197-221.
100. Lindman, B. and P. Alexandridis, *Amphiphilic block copolymers self-assembly and applications*. 2000, Amsterdam; New York: Elsevier.
101. Cohn, D., et al., *PEO-PPO-PEO-based poly(ether ester urethane)s as degradable reverse thermo-responsive multiblock copolymers*. *Biomaterials*, 2006. **27**(9): p. 1718-1727.
102. Neff, J.A., K.D. Caldwell, and P.A. Tresco, *A novel method for surface modification to promote cell attachment to hydrophobic substrates*. *Journal of Biomedical Materials Research*, 1998. **40**(4): p. 511-519.
103. Vanderhooft, J.L., B.K. Mann, and G.D. Prestwich, *Synthesis and Characterization of Novel Thiol-Reactive Poly(ethylene glycol) Cross-Linkers for Extracellular-Matrix-Mimetic Biomaterials*. *Biomacromolecules*, 2007. **8**(9): p. 2883-2889.

104. Ruoslahti, E., *RGD and other recognition sequences for integrins*. Annual Review of Cell and Developmental Biology, 1996. **12**: p. 697-715.
105. Hölig, P., et al., *Novel RGD lipopeptides for the targeting of liposomes to integrin-expressing endothelial and melanoma cells*. Protein Engineering Design and Selection, 2004. **17**(5): p. 433-441.
106. Ford, M.C., *A macroporous hydrogel for the coculture of neural progenitor and endothelial cells to form functional vascular networks in vivo*. Proceedings of the National Academy of Sciences, 2006. **103**(8): p. 2512-2517.
107. Williams, C.G., et al., *Variable cytocompatibility of six cell lines with photoinitiators used for polymerizing hydrogels and cell encapsulation*. Biomaterials, 2005. **26**(11): p. 1211-1218.
108. Tse, J.R. and A.J. Engler, *Preparation of Hydrogel Substrates with Tunable Mechanical Properties*, in *Current Protocols in Cell Biology*. 2001, John Wiley & Sons, Inc.
109. Shibata, H., et al., *Injectable hydrogel microbeads for fluorescence-based in vivo continuous glucose monitoring*. Proceedings of the National Academy of Sciences of the United States of America, 2010. **107**(42): p. 17894-17898.
110. Duan, S.F., et al., *Negative cooperative effect of cytotoxicity of a di-component initiating system for a novel injectable tissue engineering hydrogel*. Chinese Science Bulletin, 2005. **50**(11): p. 1093-1096.
111. Park, H., et al., *Effect of Swelling Ratio of Injectable Hydrogel Composites on Chondrogenic Differentiation of Encapsulated Rabbit Marrow Mesenchymal Stem Cells In Vitro*. Biomacromolecules, 2009. **10**(3): p. 541-546.
112. Wu, D.C., et al., *'Living' Controlled in Situ Gelling Systems: Thiol-Disulfide Exchange Method toward Tailor-Made Biodegradable Hydrogels*. Journal of the American Chemical Society, 2010. **132**(43): p. 15140-15143.
113. Weiss, P., et al., *Self setting hydrogel as an extracellular synthetic matrix for tissue engineering*, in *Bioceramics 16*, M.A.M.F.J.C.R.L.B. Barbosa, Editor. 2004. p. 1107-1110.
114. Fatimi, A., et al., *The rheological properties of silated hydroxypropylmethylcellulose tissue engineering matrices*. Biomaterials, 2008. **29**(5): p. 533-543.
115. Smidsrød, O. and G. Skjak-Brk, *Alginate as immobilization matrix for cells*. Trends in Biotechnology, 1990. **8**: p. 71-78.
116. Whitesides, G.M., J.P. Mathias, and C.T. Seto, *Molecular Self-Assembly and Nanochemistry: A Chemical Strategy for the Synthesis of Nanostructures*. Science, 1991. **254**(5036): p. 1312-1319.
117. Zhang, S., et al., *A self-assembly pathway to aligned monodomain gels*. Nat Mater, 2010. **9**(7): p. 594-601.
118. Salick, D.A., D.J. Pochan, and J.P. Schneider, *Design of an Injectable beta-Hairpin Peptide Hydrogel That Kills Methicillin-Resistant Staphylococcus aureus*. Advanced Materials, 2009. **21**(41): p. 4120-4123.
119. Hirst, A.R., et al., *Biocatalytic induction of supramolecular order*. Nature Chemistry, 2011. **2**(12): p. 1089-1094.

120. Langer, R. and N.A. Peppas, *Advances in biomaterials, drug delivery, and bionanotechnology*. AIChE Journal, 2003. **49**(12): p. 2990-3006.
121. Mc Bath, R.A. and D.A. Shipp, *Swelling and degradation of hydrogels synthesized with degradable poly(beta-amino ester) crosslinkers*. Polymer Chemistry, 2010. **1**(6): p. 860-865.
122. Tasdelen, B., et al., *Swelling and diffusion studies of poly(N-isopropylacrylamide/itaconic acid) copolymeric hydrogels in water and aqueous solutions of drugs*. Journal of Applied Polymer Science, 2004. **91**(2): p. 911-915.
123. Tan, H., et al., *Injectable in situ forming biodegradable chitosan-hyaluronic acid based hydrogels for cartilage tissue engineering*. Biomaterials, 2009. **30**(13): p. 2499-2506.
124. Sidorenko, A., et al., *Reversible Switching of Hydrogel-Actuated Nanostructures into Complex Micropatterns*. Science, 2007. **315**(5811): p. 487-490.
125. Xu, X.D., et al., *Strategy to introduce a pendent micellar structure into poly(N-isopropylacrylamide) hydrogels*. Langmuir, 2007. **23**(8): p. 4231-4236.
126. Braet, F., R. deZanger, and E. Wisse, *Drying cells for SEM, AFM and TEM by hexamethyldisilazane: A study on hepatic endothelial cells*. Journal of Microscopy-Oxford, 1997. **186**: p. 84-87.
127. Xu, C., *Aligned biodegradable nanofibrous structure: a potential scaffold for blood vessel engineering*. Biomaterials, 2004. **25**(5): p. 877-886.
128. Boyde, A. and S.J. Jones, *Back-scattered electron imaging of skeletal tissues*. Metabolic bone disease & related research, 1983. **5**(3): p. 145-50.
129. Boyde, A., L. Lovicar, and J. Zamecnik, *Combining confocal and BSE SEM imaging for bone block surfaces*. European cells & materials, 2005. **9**: p. 33-8.
130. Rocchietta, I., et al., *Bone regenerated via rhPDGF-BB and a deproteinized bovine bone matrix: Backscattered electron microscopic element analysis*. International Journal of Periodontics & Restorative Dentistry, 2007. **27**(6): p. 539-545.
131. Kingsmill, V.J. and A. Boyde, *Mineralisation density of human mandibular bone: quantitative backscattered electron image analysis*. Journal of Anatomy, 1998. **192**: p. 245-256.
132. Pang, X.A. and C.C. Chu, *Synthesis, characterization and biodegradation of poly(ester amide)s based hydrogels*. Polymer, 2010. **51**(18): p. 4200-4210.
133. Zhang, J.X. and P.X. Ma, *Host-guest interactions mediated nano-assemblies using cyclodextrin-containing hydrophilic polymers and their biomedical applications*. Nano Today, 2010. **5**(4): p. 337-350.
134. Mosmann, T., *RAPID COLORIMETRIC ASSAY FOR CELLULAR GROWTH AND SURVIVAL - APPLICATION TO PROLIFERATION AND CYTO-TOXICITY ASSAYS*. Journal of Immunological Methods, 1983. **65**(1-2): p. 55-63.
135. Cory, A.H., et al., *USE OF AN AQUEOUS SOLUBLE TETRAZOLIUM FORMAZAN ASSAY FOR CELL-GROWTH ASSAYS IN CULTURE*. Cancer Communications, 1991. **3**(7): p. 207-212.

136. Lau, T.T., C.M. Wang, and D.A. Wang, *Cell delivery with genipin crosslinked gelatin microspheres in hydrogel/microcarrier composite*. Composites Science and Technology, 2010. **70**(13): p. 1909-1914.
137. Zhang, J., A. Skardal, and G.D. Prestwich, *Engineered extracellular matrices with cleavable crosslinkers for cell expansion and easy cell recovery*. Biomaterials, 2008. **29**(34): p. 4521-4531.
138. Hong, C.-Y., et al., *Thermal Control over the Topology of Cleavable Polymers: From Linear to Hyperbranched Structures*. Journal of the American Chemical Society, 2007. **129**(17): p. 5354-5355.
139. Hunt, N.C., et al., *Encapsulation of fibroblasts causes accelerated alginate hydrogel degradation*. Acta Biomaterialia, 2010. **6**(9): p. 3649-3656.
140. Sahoo, S., et al., *Hydrolytically Degradable Hyaluronic Acid Hydrogels with Controlled Temporal Structures*. Biomacromolecules, 2008. **9**(4): p. 1088-1092.
141. Bueno, E.M. and J. Glowacki, *Cell-free and cell-based approaches for bone regeneration*. Nat Rev Rheumatol, 2009. **5**(12): p. 685-697.
142. El-Ghannam, A., *Bone reconstruction: from bioceramics to tissue engineering*. Expert Review of Medical Devices, 2005. **2**(1): p. 87(15).
143. Wong, V.W., et al., *Tissue Engineering in Plastic Surgery: A Review*. Plastic and Reconstructive Surgery, 2010. **126**(3): p. 858-868.
144. Salinas, C.N. and K.S. Anseth, *Mesenchymal Stem Cells for Craniofacial Tissue Regeneration: Designing Hydrogel Delivery Vehicles*. Journal of Dental Research, 2009. **88**(8): p. 681-692.
145. Bakhtiari, L., et al., *Investigation of biphasic calcium phosphate/gelatin nanocomposite scaffolds as a bone tissue engineering*. Ceramics International, 2010. **36**(8): p. 2421-2426.
146. Guvendiren, M. and J.A. Burdick, *The control of stem cell morphology and differentiation by hydrogel surface wrinkles*. Biomaterials, 2010. **31**(25): p. 6511-6518.
147. Pritchard, C.D., et al., *An injectable thiol-acrylate poly(ethylene glycol) hydrogel for sustained release of methylprednisolone sodium succinate*. Biomaterials, 2011. **32**(2): p. 587-597.
148. Discher, D.E., P. Janmey, and Y.-l. Wang, *Tissue Cells Feel and Respond to the Stiffness of Their Substrate*. Science, 2005. **310**(5751): p. 1139-1143.
149. Mei, Y., et al., *Combinatorial development of biomaterials for clonal growth of human pluripotent stem cells*. Nature Materials, 2010. **9**(9): p. 768-778.
150. Burdick, J.A. and K.S. Anseth, *Photoencapsulation of osteoblasts in injectable RGD-modified PEG hydrogels for bone tissue engineering*. Biomaterials, 2002. **23**(22): p. 4315-4323.
151. Chatterjee, K., et al., *The effect of 3D hydrogel scaffold modulus on osteoblast differentiation and mineralization revealed by combinatorial screening*. Biomaterials, 2010. **31**(19): p. 5051-5062.
152. Ishihara, K., N. Muramoto, and I. Shinohara, *Controlled release of organic substances using polymer membrane with responsive function for amino compounds*. Journal of Applied Polymer Science, 1984. **29**(1): p. 211-217.

153. Alley, S.C., N.M. Okeley, and P.D. Senter, *Antibody–drug conjugates: targeted drug delivery for cancer*. *Current Opinion in Chemical Biology*, 2010. **14**(4): p. 529-537.
154. Chen, J., et al., *pH and Reduction Dual-Sensitive Copolymeric Micelles for Intracellular Doxorubicin Delivery*. *Biomacromolecules*, 2011. **12**(10): p. 3601-3611.
155. Chen, Q., et al., *Cysteine and pH-Responsive Hydrogel Based on a Saccharide Derivative with an Aldehyde Group*. *Langmuir*, 2009. **26**(5): p. 3165-3168.
156. Gao, Y., et al., *Controlled Intracellular Release of Doxorubicin in Multidrug-Resistant Cancer Cells by Tuning the Shell-Pore Sizes of Mesoporous Silica Nanoparticles*. *Acs Nano*, 2011.
157. Oupický, D., A.L. Parker, and L.W. Seymour, *Laterally Stabilized Complexes of DNA with Linear Reducible Polycations: Strategy for Triggered Intracellular Activation of DNA Delivery Vectors*. *Journal of the American Chemical Society*, 2001. **124**(1): p. 8-9.
158. Dirk, S., *Thermo- and pH-responsive polymers in drug delivery*. *Advanced Drug Delivery Reviews*, 2006. **58**(15): p. 1655-1670.
159. Aryal, S., C.-M.J. Hu, and L. Zhang, *Polymer–Cisplatin Conjugate Nanoparticles for Acid-Responsive Drug Delivery*. *Acs Nano*, 2009. **4**(1): p. 251-258.
160. Gerweck, L.E. and K. Seetharaman, *Cellular pH Gradient in Tumor versus Normal Tissue: Potential Exploitation for the Treatment of Cancer*. *Cancer Research*, 1996. **56**(6): p. 1194-1198.
161. Švastová, E., et al., *Hypoxia activates the capacity of tumor-associated carbonic anhydrase IX to acidify extracellular pH*. *FEBS Letters*, 2004. **577**(3): p. 439-445.
162. Neri, D. and C.T. Supuran, *Interfering with pH regulation in tumours as a therapeutic strategy*. *Nat Rev Drug Discov*, 2011. **10**(10): p. 767-777.
163. Ko, J., et al., *Tumoral acidic extracellular pH targeting of pH-responsive MPEG-poly(β -amino ester) block copolymer micelles for cancer therapy*. *Journal of Controlled Release*, 2007. **123**(2): p. 109-115.
164. Saito, H., A.S. Hoffman, and H.I. Ogawa, *Delivery of Doxorubicin from Biodegradable PEG Hydrogels Having Schiff Base Linkages†*. *Journal of Bioactive and Compatible Polymers*, 2007. **22**(6): p. 589-601.
165. Kratz, F., U. Beyer, and M.T. Schütte, *Drug-polymer conjugates containing acid-cleavable bonds*. *Crit Rev Ther Drug Carrier Syst*, 1999. **16**(3): p. 245-88.
166. Deng, G., et al., *Covalent Cross-Linked Polymer Gels with Reversible Sol–Gel Transition and Self-Healing Properties*. *Macromolecules*, 2010. **43**(3): p. 1191-1194.
167. Rogalsky, A.D., H.J. Kwon, and P. Lee-Sullivan, *Compressive stress–strain response of covalently crosslinked oxidized-alginate/N-succinyl-chitosan hydrogels*. *Journal of Biomedical Materials Research Part A*, 2011. **99A**(3): p. 367-375.
168. Toh, E.K.-W., et al., *Succinated chitosan as a gene carrier for improved chitosan solubility and gene transfection*. *Nanomedicine: Nanotechnology, Biology and Medicine*, 2011. **7**(2): p. 174-183.

169. Kuckling, D., et al., *Preparation and characterization of photo-cross-linked thermosensitive PNIPAAm nanogels*. *Macromolecules*, 2006. **39**(4): p. 1585-1591.
170. Bian, W., et al., *Mesoscopic hydrogel molding to control the 3D geometry of bioartificial muscle tissues*. *Nat. Protocols*, 2009. **4**(10): p. 1522-1534.
171. Tanahashi, K., S. Jo, and A.G. Mikos, *Synthesis and Characterization of Biodegradable Cationic Poly(propylene fumarate-co-ethylene glycol) Copolymer Hydrogels Modified with Agmatine for Enhanced Cell Adhesion*. *Biomacromolecules*, 2002. **3**(5): p. 1030-1037.
172. Emilietri, E., E. Ranucci, and P. Ferruti, *New poly(amidoamine)s containing disulfide linkages in their main chain*. *Journal of Polymer Science Part a-Polymer Chemistry*, 2005. **43**(7): p. 1404-1416.
173. Lee, S.a.P., K., *Synthesis and characterization of sol-gel phase-reversible hydrogels sensitive to glucose*. *Journal of Molecular Recognition* 1996. **9**: p. 549-557.
174. Vacanti, J.P., et al., *Selective cell transplantation using bioabsorbable artificial polymers as matrices*. *Journal of Pediatric Surgery*, 1988. **23**(1): p. 3-9.
175. Biaglow, J.E., et al., *A Method for Measuring Disulfide Reduction by Cultured Mammalian Cells: Relative Contributions of Glutathione-Dependent and Glutathione-Independent Mechanisms*. *Analytical Biochemistry*, 2000. **281**(1): p. 77-86.
176. Chen, J., et al., *A cleavable-polycation template method for the fabrication of noncrosslinked, porous polyelectrolyte multilayered films*. *Advanced Materials*, 2007. **19**(7): p. 979-+.
177. Han, S.-C., et al., *Reducible polyethylenimine hydrogels with disulfide crosslinkers prepared by michael addition chemistry as drug delivery carriers: Synthesis, properties, and in vitro release*. *Journal of Polymer Science Part A: Polymer Chemistry*, 2009. **47**(16): p. 4074-4082.
178. Yu, T.T. and M.S. Shoichet, *Guided cell adhesion and outgrowth in peptide-modified channels for neural tissue engineering*. *Biomaterials*, 2005. **26**(13): p. 1507-1514.
179. Jang, J.-H., et al., *Three-Dimensionally-Patterned Submicrometer-Scale Hydrogel/Air Networks That Offer a New Platform for Biomedical Applications*. *Nano Letters*, 2008. **8**(5): p. 1456-1460.
180. Lo, C.-M., et al., *Cell Movement Is Guided by the Rigidity of the Substrate*. *Biophysical Journal*, 2000. **79**(1): p. 144-152.
181. Wang, L.-S., et al., *The role of stiffness of gelatin-hydroxyphenylpropionic acid hydrogels formed by enzyme-mediated crosslinking on the differentiation of human mesenchymal stem cell*. *Biomaterials*, 2010. **31**(33): p. 8608-8616.
182. Kim, R.H., et al., *Characterization of the Human Bone SialoProtein (BSP) Gene and its Promoter Sequence*. *Matrix Biology*, 1994. **14**(1): p. 31-40.
183. Chun, C., et al., *The use of injectable, thermosensitive poly(organophosphazene)-RGD conjugates for the enhancement of mesenchymal stem cell osteogenic differentiation*. *Biomaterials*, 2009. **30**(31).

184. Wang, K.X. and D.T. Denhardt, *Osteopontin: Role in immune regulation and stress responses*. Cytokine & Growth Factor Reviews, 2008. **19**(5–6): p. 333-345.
185. Aschaffenburg, R. and J.E.C. Mullen, 381. *A rapid and simple phosphatase test for milk*. Journal of Dairy Research, 1949. **16**(01): p. 58-67.
186. Sun, S. and A. Wang, *Adsorption properties of N-succinyl-chitosan and cross-linked N-succinyl-chitosan resin with Pb(II) as template ions*. Separation and Purification Technology, 2006. **51**(3): p. 409-415.
187. Kato, Y., H. Onishi, and Y. Machida, *Lactosaminated and intact N-succinyl-chitosans as drug carriers in liver metastasis*. International Journal of Pharmaceutics, 2001. **226**(1-2): p. 93-106.
188. Shen, F., et al., *Quantitation of Doxorubicin Uptake, Efflux, and Modulation of Multidrug Resistance (MDR) in MDR Human Cancer Cells*. Journal of Pharmacology and Experimental Therapeutics, 2008. **324**(1): p. 95-102.
189. Liu, X., X. Jin, and P.X. Ma, *Nanofibrous hollow microspheres self-assembled from star-shaped polymers as injectable cell carriers for knee repair*. Nat Mater, 2011. **10**(5): p. 398-406.
190. Tamesue, S., et al., *Photoswitchable Supramolecular Hydrogels Formed by Cyclodextrins and Azobenzene Polymers*. Angewandte Chemie International Edition, 2010. **49**(41): p. 7461-7464.
191. Anderson, J.M., et al., *Biphasic Peptide Amphiphile Nanomatrix Embedded with Hydroxyapatite Nanoparticles for Stimulated Osteoinductive Response*. Acs Nano, 2011.
192. Luo, Z., et al., *Redox-Responsive Molecular Nanoreservoirs for Controlled Intracellular Anticancer Drug Delivery Based on Magnetic Nanoparticles*. Advanced Materials, 2011: p. n/a-n/a.
193. Yokochi, T. and K.D. Robertson, *Doxorubicin Inhibits DNMT1, Resulting in Conditional Apoptosis*. Molecular Pharmacology, 2004. **66**(6): p. 1415-1420.
194. Häcker, G., *The morphology of apoptosis*. Cell and Tissue Research, 2000. **301**(1): p. 5-17.